Response to reviewers

We would like to thank the reviewers for the in-depth review and constructive comments. Below we provide point-to-point responses to each comment. Reviewer comments are given in italic and responses are given in bold. Manuscript with revisions marked using track changes is also provided.

Comments to reviewer1#

General comments.

1. *This paper provides a description and evaluation of marine biogeochemical simulation of the NESM v3. Given that this model is new to the CMIP community (participating in CMIP6), it is important to provide such description and evaluation paper to discuss the strengths and limitations of the model to help the end users of CMIP6 archives. Below I provide a few general comments, followed by specific comments and editorial corrections, to help improve the presentation of the paper. I believe that the authors can address these concerns.*

Response: Thank you so much for your in-depth review and constructive comments. The following are the point-to-point responses and manuscript with revisions marked using track changes.

2. The motivation of this paper is not clearly stated in the introduction section. I assume it is to evaluate the model performance of marine biogeochemical fields (e.g., P1, L10 and P3, L23), but the authors should describe why doing so is important for this particular model. I think this could be clearly stated by having a paragraph starting with a sentence like "The objective of this paper is to : : :" in the second last paragraph of the Introduction section, and by linking to CMIP6.

Response: Thanks for the comment. We added a paragraph starting with "The objective of this manuscript is …" in the introduction section (P3, L11).

3. *Restructure. I find that the flow of the paper could be improved if all the method stuff goes into the Method section. See my specific comments.*

Response: Thank you for the suggestion. We give the analysis method section in the revised manuscript (Section 2.4, P9, L20).

4. *Concluding paragraph. The very last paragraph of the Discussion and Conclusion section is very weak (P25, L24). Also the two dots ".." at the very end indicates that it is unfinished. Please work on this last paragraph to provide the take-home message of the manuscript.*

Response: Thanks for the comment. The last paragraph of Discussion and Conclusion Section is rewritten (P26, L19).

5. *Model minus observation figures. Some figures can be improved by having a model-minus-observation difference subplots. This is done for Figures 1 and 9, but not for the others. Doing so makes it easy to show where the model has positive and negative biases and by how much, and helps understand the text (for example, it is hard to notice the negative biases mentioned in P24, L7 just by looking at Fig. 5).*

Response: Thanks for the suggestion. We add additional model-observation subplots for figure 3, 5, 6, 7.

Specific comments

1. *Title. I think the acronym NESM v3 should be mentioned in the title if that's the preferred acronym for CMIP6 exercise.*

Response: Thanks for your comment. The title is changed to 'Marine biogeochemical cycling and oceanic CO2 uptake simulated by the NUIST Earth System Model version 3 (NESM v3)'.

2. *Acronyms. All acronyms should be defined for the first time they appear in the text. For example, in the abstract, CO2, CMIP5, 1ptCO2. I suggest the authors to check throughout the manuscript.*

Response: Thanks for your comment. We checked throughout the manuscript.

3. *P3, L8 to L24. I feel that the details of NESM v3 mentioned in these two paragraphs belong to the method section. Instead, provide the objective paragraph here with a very brief introduction of NESM v3. At this point, the readers are not interested in knowing the details of NESM v3, but rather they want to know why NESM v3 is important and deserves an evaluation paper.*

Response: Thanks for the comment. We move these two paragraphs to model description section and add one paragraph to clarify the motivation of this paper (P3, L11).

4. *P5, L1. This sentence sounds to me that salinity of 4 PSU is added into the ocean when ice melting, but is this correct? I think the sea-ice salinity is fixed at 4PSU which is used to calculate the ice-ocean salt flux, which should actually result in dilution of seawater during ice melting (unless the ocean salinity is less than 4 PSU).*

Response: Thanks for the comment. The sentence is rewritten. Salinity of 4 PSU (salt flux) together with the large amount of fresh water (fresh water flux) is added into ocean when ice melting. Therefore, ice melting results in dilution of seawater, and ice formation results in the increase of salinity (P4, L25).

5. *Sec. 2.2. Perhaps not so important for the interpretation of results, but to complete the description, mention the initial and boundary conditions for biogeochemical state variables. Were they initialized to the WOA18, GLODAP v2? Was the river discharge of biogeochemical state variables prescribed?*

Response: Thanks for the comment. The description of initial and boundary conditions for biogeochemical state variables is expanded. The river discharge is prescribed (P6, L18-27).

6. *P7, L9 and L10. Briefly describe what it means by "offline".*

Response: Thanks for the comment. The offline simulation means uncoupled run. We use each component model's PI control run results as the initial conditions for the couple model. It is described in the manuscript (P7, L13-16).

7. *P7, L22. Why follow the protocol of CMIP5 for 1ptCO2 and not that of CMIP6 (one of the DECK experiments)?*

Response: In this manuscript, 1ptCO_2 experiment are used to diagnose carbon-climate and carbon-concentration sensitive parameters. The only differences between the protocol of CMIP5 and CMIP6 for 1ptCO2 experiment, is that CMIP5 only requires 140 years integration, while CMIP6 requires more than 150 years. Considering that we primarily compared 1ptCO_2 experiments with CMIP5 model results, we only conduct 1ptCO_2 for 140 years, e.g., following CMIP5 protocol.

8. *P8, L16. Consider moving this paragraph earlier (at the beginning of the section) to give a broad picture up front.*

Response: Thanks for your suggestion. We moved this paragraph to the beginning of this section (P7, L5-10).

9. *P8, L24. WOA18 gives nutrient concentrations in units of umol/kg. Briefly mention how they were converted to mmol m-3 for model-obs comparison (e.g. Fig.1).*

Response: Thanks for your comments. We assume the density in the model and observations are same. Then the unit is converted from umol/kg to mmol/m^3 by multiplying modeled density (in unit of kg/m^3) (P8, L21-23).

10. *P9, L1. Briefly mention how these products compare or differ. I mean, do they not all incorporate SeaWiFS? Also, GlobColour and OCCCI are both merged products (and they look pretty much the same; Fig. 5), so the readers may be curious to know why these two similar products deserve comparison.*

Response: Thanks for the comment. Both of GlobColour and OCCCI (from Plymouth Marine Laboratory) incorporate SeaWiFS, MERIS, MODIS-AQUA, and VIIRS. The same components make the two products kind of similar. However, the uncertainty information and algorithms are not the same (http://www.globcolour.info/CDR_Docs/GlobCOLOUR_PUG.pdf). The information is added in the manuscript (P9, L2-3).

11. *P9, L21. Suggest to remove this paragraph as it was already mentioned in P8, L20.*

Response: Thanks for your comments. This paragraph is removed from section 3.1.

12. *P10, L4. In addition to these physical processes, iron limitation is another main reason for high macronutrient levels in this region, which should be mentioned here.*

Response: Thank you for your comments. The effect of iron limitation is emphasized in the revised manuscript (P11, L22-23).

13. *P10, L10. Refer to the figure (Fig. 1 c,f,i) at the end of the first sentence.*

Response: Thank you for your comment. The sentence "some noticeable discrepancies…." is referred to Fig. a3, b3, c3 (P12, L2).

14. *P10, L22 to P11, L4. This paragraph belongs to the methods section.*

Response: Thank you for the comment. The paragraph is moved to the analysis method section.

15. *P11, L2 to P12 L3. Again this paragraph belongs to the method section. Also, mention what the half-saturation constant is to set to in the model for each nutrient.*

Response: Thank you for the comment. The paragraph is moved to the methodology section. The coefficient K is not a constant, but parameterized based on minimum half-saturation constant and concentrations of nutrients, phytoplankton, and diatoms. This is mentioned in the revised manuscript and references are added (P10, L11-13).

16. *P12, L21. I don't think the chlorophyll levels are high for the equatorial Pacific and the Southern Ocean. They may be "relatively" high compared to the surrounding seas, but the absolute magnitudes are low.*

Response: Thanks for the comment. The description is revised accordingly (P13, L24-27).

17. *P13, L7. I am not sure what it means by "the intermediate concentration regions". Maybe provide a number?*

Response: Thanks for the comment. Here the intermediate concentration refers to ~0.5 mg Chl m^3. The manuscript is revised accordingly (P13, L24).

18. *P13, L11. Instead of the International Date Line, refer to the longitude coordinate? Not every reader knows the exact location of the date line. This and the next sentence can be easily identified if the model-obs subplots are provided.*

Response: Thanks for the comment. The International Date Line refer to 180°E. Also, the model-obs subplots for figure 5 and 6 are provided (P15, L14-15).

19. *P13, L14. From 1998? Fig. 6 says from 2003.*

Response: Thank you for the comment. The NPP is from 2003 to 2014. The manuscript is revised accordingly (P15, L12).

20. *P13, L25. PAR should be defined earlier in the text, and here just write as PAR.*

Response: Thank you for the comment. PAR is defined in the model description section (P5, L19).

21. *Figure 6. Caption and the figure text do not match. Please check more carefully. In the caption, b = VGPM, c = Eppley-VGPM, d = CbPM, whereas in the figure, b = VGPMMODIS, c = CbPM-MODIS, d = Eppley-MODIS.*

Response: Thank you for the comment. The figure text is right, and the manuscript is revised.

22. *P14, L25. Here and elsewhere, the term "deviation" is used to refer to the model-obs difference. This is a bit confusing because standard deviations are also used in the later analysis (e.g. P16, L2). Perhaps, use "difference" instead of "deviation".*

Response: Thanks for the comment. We use difference and bias instead of deviation to refer to model-obs difference in the revised manuscript.

23. *P15, L10. Again, this is where having the model-obs difference subplot would be helpful to support this sentence.*

Response： Thanks for the comment. The model-obs difference subplot of alkalinity and DIC are added.

24. *P16, L9. "due to the 3-dimensional correction : : :", unclear what this means. Add one or two sentences to explain.*

Response: Thank you for the comment. The 3-dimensional correction refers to that the global inventory of nutrient and alkalinity are restored toward the observations once a year. We add few explanation and related reference (P18, L6-8).

25. *P16, L12. Provide a reference for the observation value quoted here.*

Response: Thank you for the comment. The reference is provided (P18, L10).

26. *Table 1. As noted in the caption, the pre-industrial years between NESM v3 and IPCC AR5 differ by 100 years. Does this explain why the IPCC AR5 value is higher than NESM v3 because the former incorporates additional 100 years for the cumulative quantity? Also, in the caption, describe what the plus/minus values represent. P17, L25. Should this paragraph have its own section? It is beyond oceanic co2 uptake (Sec 3.4).*

Response: Thank you for the comment. The former additional 100 years can only explain very small part of the higher value, because the atmospheric CO_2 concentration change during this period is small. In another simulation started from 1750 (not shown in this manuscript), the total cumulative quantity is 141.7 Pg C.

The plus/minus values are the uncertainty range provided by IPCC AR5 (P39).

We put this paragraph in a new section named "Assessment by Taylor diagram".

27. *P18, L21. ", which is associated : : : deep ocean," this middle block of sentence is not supported by any figure or reference, and also is unnecessary. It can just be removed and simply be stated as "The reduction of mixed layer depth indicates a more stratified upper ocean : : :".*

Response: Thank you for the comment. The manuscript is revised accordingly (P20, L18).

28. *Sec 3.5.1. This section only discusses the results of the FC simulation. Maybe provide some comments on the different simulations (e.g. BC vs RC simulations).*

Response: Thank you for the comment. SAT, MLD, and AMOC changes in RC and FC simulations are almost the same, while those changes in the BC simulation are relative small. We add some comments on the BC and RC simulations in the revised manuscript (Section 3.6.1).

29. *P19, L11. This first paragraph is already mentioned in the previous section, so why repeat here?*

Response: Thank you for the comment. This paragraph is removed from Section 3.6.2 in the revised manuscript.

30. *P21, L21 to P22, L8. This block of paragraphs belongs to the Method section. Having this much of methodological details in the results section breaks the flow of the paper. Please consider moving it to the Method section.*

Response: Thanks for the comment. We move this paragraph to the Method section.

31. *P22, L16. "Therefore, : : :" this sentence is unclear to me. Especially for the carbon climate parameter, which can be both positive and negative as shown in Figure 16d. Do the authors mean that it is negative in the year 2100?*

Response: Thanks for the comment. During the former several decades, the interannual variation of oceanic CO_2 uptake is of the same magnitude of carbon-climate sensitivity resulted oceanic CO_2 uptake. This is why we can see positive carbon-climate parameter in the first several decades in Figure 16d. Here we refer to the parameters in the year 2100. We add "in the year 2100" in the revised manuscript (P23, L11).

32. *P23, L3. This paragraph could move into the Method section and be combined with the block of paragraphs describing the sensitivity parameter derivation. Also, "4xCO2" is unclear.*

Response: Thanks for the comment. We move this paragraph to the method section. 4XCO2 means the atmospheric CO_2 concentration quadrupled, and the description is added.

33. *P24, L12. "Our results suggest : : :" How does your result support that temperature-dependence is necessary?*

Response: Thanks for your comments. We delete this sentence in Conclusion Section, but add a brief explanation in Section 3.2 (P14, L22-25).

Temperature-dependence is necessary to produce the meridional distribution of NPP. When temperature-dependence is considered (NESM v3, CBPM-MODIS, and EPPLEY), we get high level NPP in low-latitude ocean and low level NPP in high-latitude oceans, while it is opposite when temperature-dependence is unconsidered (VGPM).

34. *P25, L1. "The strong : : :", but why does NESM v3 overestimate nutrients? The iron limitation is too strong? Too strong vertical mixing? A few speculations can be helpful.*

Response: Thanks for the comment. Figure 4 indicates the strong iron limitation and the bias of preformed phosphate in Figure 3 indicates a strong vertical mixing. The possible causes for the overestimated nutrients is provided in the revised manuscript (P25, L25-P26, L2).

35. *P25, L10. Why do the results of IPSL-CM5A-LR appear here and not in the results section? Also, why choose this particular CMIP ensemble member over others? I don't really see the point of adding the comparison with IPSL-CM5A-LR.*

Response: Thanks for the comment. We remove the results of IPSL-CM5A-LR from Conclusion Section, but add some comparisons to Section 3.4 (Taylor diagram). Also, a detailed comparison with IPSL-CM5A-LR is provided in the supplementary material.

The atmospheric component and oceanic component of IPSL-CM5A-LR and NESM v3 are both adopted from ECHAM and NEMO. This makes the two model kind of similar, and some readers wonder how different between the simulation results from the two models.

Editorial corrections

P1, L15. "total CO2 uptake" –> Use subscript for "2"

P3, L2. "; 2)" –> "; and 2)"

P3, L4. "the effect of CO2 concentration" –> "the effect of increasing atmospheric CO_2 concentration"

P4, L7. Should "NUIST-CSM-2.0.1" be "NESM v3"?

P4, L16 (and elsewhere). Add a space between 10 and m (10 m instead of 10m).

P5, L18-19. ": nanophytoplankton and diatoms," –> "(nanophytoplankton and diatoms)" and similarly for zooplankton.

P5, L22. "photosynthetic" –> "photosynthetically"

P6, L9. POM is already defined in P5, L25.

P6, L9. "diatoms silicate", should this be "biogenic silica"?

P6, L9. "described by : : : corresponding to" –> "is partitioned into"

P12, L2. "when all nutrients : : : than 0.9." –> "when the annual mean nutrient coefficients are greater than 0.9 for all nutrients."

P12, L14. SeaWiFS should be defined in P9, L1. OCCCI was already defined in P9, L2.

P12, L19. "plankton" –> "phytoplankton"

P14, L23 Add a space between alkalinity and are.

Fig. 7. Superscript for alkalinity units. Also add a space between from and 1985.

P14, L23. Add a space between alkalinity and are.

P15, L9. Add a space between ocean and means.

P16, L2. I don't think SD has been defined previously. If so, define here.

Figure 10. In the figure, the last subplot is labelled as "c) GLODAP v1", which should be "d) GLODAP v1".

P16, L24. "receptively" –> "respectively".

Figure 12. Caption: "statistical patterns" –> "spatial patterns"(?); "carbon-related" –> "biogeochemical"; "upper ocean" –> "upper 100-m ocean". Provide the information on observations for nutrients, DIC, and alkalinity, such as done for NPP and chlorophyll.

P18, L3. "to atmospheric" –>"to increasing atmospheric".

P18, L5-L8. "presented" –> "present" and "compared" –> "compare".

P18, L20. "and acting to mitigate" –> "and".

P18, L21. "MLD is seen decreasing" –> "Modeled MLD decreases".

P18, L24. "is seen in" –> "is projected for".

Figure 15. In the caption "FC-RC-BC" –> "FC-RC+BC"?

Figure 16. Caption "cumulated" –> "cumulative". "atmospheric co2 (c) and : : :" –> "(c) atmospheric co2 and (d) : : :"

P21, L25. ". The" –> ", the". Similarly for P22, L4.

P23, L11. "estimated by CMIP5 models range" –> "estimated for CMIP5 models ranging"

P24, L3. "Mid-Eastern" –> "Eastern"

P24, L20. "nonlinear of " –> "nonlinear response of oceanic"

P25, L16. "precipitation in" –> "precipitation simulated in"

P25, L18. "which would lead" –> "which leads"

P25, L21. "NUIST-CSM", should this be "NESM v3"?

Response: Thank you so much for pointing out these detailed editorial corrections. All above editorial corrections are checked and revised accordingly.

P24, L14. The numbers quoted in this paragraph is inconsistent with the ones appeared in the Results section. Specifically, year 2016 (should this be 2011? Table 1), 149, 150 +/- 20, and 0.8. Please check these numbers with the Results section.

Response: The result from the pre-industrial era (1850) to the year 2011 are compared with IPCC AR5, while the cumulative uptake from 1870 to 2016 are compared with recent results from Le Quéré et al. (2018). We give both comparisons in the manuscript (P18, L14-22).

Comments from reviewer2#

General comments

Dai and co-authors evaluate the ability of their earth system model NESM v3 to represent the carbon cycle (and, particularly, the CO2 uptake) and the representation of several marine biogeochemical tracers (nutrients, alkalinity, DIC, chlorophyll and net primary production). NESM v3 performances are compared with observations and, occasionally, to CMIP5 models. As regional discrepancies are identified, the authors discussed their physical (e.g. weak upwelling in the Indian Ocean, strong convective mixing at high latitudes and more generally, shortcomings in simulated ocean circulation) or biogeochemical (iron limitation in the Southern Ocean, excessive remineralization in the deep Northern Pacific) origins.

2) Relevance of the subject

Such a paper evaluating the limits of a modelling platform can be very useful to the scientific community which is going to use and analyse NESM v3 outputs, especially if the model has contributed to the CMIP6 Intercomparison Project. However I did not really understand from the text if the model described and used in this paper has really been a part of CMIP6: p.3, l.10: "as a registered model of CMIP6" but p.7, l.21: "following the protocol of CMIP5" Maybe the authors may explain why not using the protocol of CMIP6 (to be CMIP6 fully compliant) ?

Response: Thank you for you positive comments on this manuscript. In this study, historical and SSP5-8.5 experiments follow the CMIP6 protocol, of which the parameters are differ from CMIP5 protocol, including solar forcing, aerosol, land use, and so on. Then we compared these results with observations and CMIP5 model results to evaluate the paper.

However, the only differences of 1ptCO2 experiment between the protocol of CMIP5 and CMIP6, is that CMIP5 only requires 140 years integration, while CMIP6 requires more than 150 years. Considering that we compared the carbon feedback parameter diagnosed from the 1ptCO_2 experiment with CMIP5 model results, we only show 1ptCO2 for 140 years in this manuscript, e.g. following CMIP5 protocol.

3) General structure

The readability could be improved by a better structure. Please have a look at Séférian et al. (2019, https://doi.org/10.1029/2019MS001791) which provides an evaluation of CNRM earth system model for CMIP6 by comparing it to observations, as well as to CMIP5 multi-model ensemble, and to an earlier version of the same model. Keeping the introduction in its actual state (i.e. focusing on carbon uptake), I suggest to move the description of NESM v3 found in the introduction (p.3, l11-16) to the dedicated section (2.1.1). But I would rather expect a more focused introduction, relaying previous/other model evaluations of the carbon cycle and uptake. As it is, the scope of the introduction is a bit too wide.

Response: Thank you for the comment. We move the description of NESM v3 to section 2 and clarify our objective in this section (P3, L11-14).

4) Results

I suggest to discuss the magnitude of the nutrient biases obtained in section 3.1 in regard of those obtained with other models like CMIP5 models (maybe a short summary of the published CMIP5 literature on these aspect will

be enough). This would help the reader to know how NESM v3 places itself in the CMIP models diversity. This is also true for the section relative to the Taylor diagram (Fig. 12): please see my specific comment.

Response: Thank you for the comment. The comparison with CMIP5 models are added to section 3.1 and Taylor diagram.

The section 3.5.2 discussing the coupling between the "radiative" (i.e. in this case only atmospheric radiation is affected by changing concentrations of atmospheric CO2) and "biogeochemical" (i.e. in this case only the ocean carbon cycle is affected by changing atmospheric CO2) sensitivity experiments is quite interesting. However if the motivation of this paper is to evaluate model skills in modeling carbon-related biogeochemical species, the study of the non-linearity of their sum appears a bit beyond the lines of the paper. I would recommend that either the authors restructure (a bit) the current draft or clarify the aim of their study.

Response: Thanks for the comment. We clarify the aim of the study in Introduction Section (P3, L11-14).

For oceanic CO_2 uptake, we evaluate both the amount and the sensitivity. In this study, the sensitivity is represented by the two parameters and their nonlinearity. The section 3.6.2 is a bit restructured and we want to show how the sensitivity and nonlinearity of oceanic CO2 uptake distribute and originated in the NESM v3 (P21, L6- P22, L26).

5) Discussion

I would expect of a paper aiming at evaluating a model that the "Discussion and Conclusion section" would give more details of how this model behaves (in terms of modeled carbon cycle and CO2 uptake here) in comparison with other models or in the context of the other CMIP models. If such comparisons are occasionally done in the current draft version, it would be valuable to systematise them.

Response: Thanks for the comments. The Discussion Section is restructured, and the comparison between the NESM v3 and other models is summarized in an individual paragraph (P25, L9-18).

6) Language

I would recommend a careful reading which may easily help to correct the typing errors.

Response: Thanks for the suggestion. We checked throughout the manuscript.

7) Specific comments

p.3, l.19: modes -> models

p.4, l.4: includes -> that includes or including

p.4, l.15: tripole -> tripolar grid

p.9, l.18: the modeled result -> the modeled sea-air CO2 fluxes to a 4◦x5◦ grid.

p.10, l.3: Fig. 11 -> Fig. 1 ?

p.14, l.23: alkalinityare -> alklinity are

p.16, l.11: "," -> "."

p.16, l.24: receptively -> respectively

p.17, l.4: stimulated -> simulated ?

p.18, l.20: MLD is seen decreasing -> "MLD is seen to decrease" sounds to me more correct.

p.21, l.3: "some regions of the Northern Atlantic even appear CO2 outgassing". The formulation sounds weird to me, please check its grammatical correctness.

p.25, l.27: ". . ." -> "."

Response: Thanks for the comments. All the mentioned editorial errors are revised.

p.7-8, l.27, l.1-4: "To separate the effect of atmospheric CO2 and global warming on the ocean carbon cycle, we performed three types of experiments (biogeochemically coupled, radiatively coupled, and fully coupled). These types of simulations were also performed by previous studies that investigated the effect of CO2 and global warming on the global carbon cycle (Friedlingstein et al., 2006; Arora et al., 2013; Schwinger et al., 2014)."

I suggest to slightly reorganize the above paragraph in order to properly introduce the list items that follows. I suggest something like that:

"Following Friedlingstein et al., 2006; Arora et al., 2013; Schwinger et al., 2014, we performed three types of experiments (biogeochemically coupled, radiatively coupled, and fully coupled) to separate the effect of atmospheric CO2 and global warming on the ocean carbon cycle: 1) Biogeochemically coupled (BC). . .."

Response: Thank for the comment. The above paragraph is rewritten accordingly in Section 2.2 (P7, L23).

p.11, l.21-22: why is the ocean circulation so different in IPSL-CM5A-LR and NESM, as both models share the same oceanic model (NEMO) ?

Response: Thanks for the comment. We compared more than 20 different ocean physical climate fields, including temperature, salinity, wind stress, ocean current, and MOC, between NESM v3 and CMIP5 models. The results show some differences between NESM v3 and IPSL-CM5A-LR. I think the differences possibly come from several sources, including different coupler strategy, atmospheric and sea-ice component, and unique modifications in the ocean model of NESM v3. Some of the modifications are mentioned in the Cao et al. (2018).

However, we have not exanimated how these differences affect biogeochemical cycle. We remove this sentence from discussion section.

p.17, l.23: Similar to the vertically integrated inventory (Fig. 10): I suggest to add the figure you are referring to, in order to facilitate the reading. I also suggest to clarify (in the text or, at least, in the caption of Fig. 11) the

period on which DIC has been averaged for computing these vertical sections: I guess that these vertical sections have been averaged between 1985 and 2014 as other vertical sections ? As it gives an indication of the temporal persistence of the bias, I would suggest to mention it. The vertically integrated inventory of Fig. 10 are not representative of the whole period but represent only few years around 2002 or 1994.

Response: Thanks for the comment. The figure referred is added in the manuscript (P19, L22). For figure 12, the vertical sections of anthropogenic DIC are averaged from 2000 to 2004 to get a better comparison with observations, because the observation of DIC in GLODAP v2 is normalized to the year of 2002.

p.17, l.25 : it would be very helpful to add other models data or even CMIP5 ensemble mean on this Taylor diagram for all the biogeochemical fields in order to get an idea of how NESM v3 behaves in the current modeling landscape.

Response: Thanks for the comment. We add simulation results from IPSL-CM5A-LR to the Taylor diagram, and add descriptions of other CMIP5 models' performance by reviewing previous evaluation papers (Section 3.4, P17, L2-18).

p.26, l.15-16: please replace XXX and YYYY by providing publication numbers, or delete the sentence.

Response: Thanks for the comment. This part will be revised in final revision.

8) Figures

p.40, Figure 2: to improve the readability of this figure, I suggest to separate the 3 oceanic regions (Atlantic, Pacific, Global) and to increase the tick labels and titles. You can keep all the 3x6 subplots on the same figure, but at least try to increase the margin below the 6 subplots related to the Atlantic ocean, and also increase the margin below the 6 subplots related to the Pacific ocean following a pattern like:

a0 b0. c0

a1. b1. c1

<- increased margin

a2. b2 c2

a3. b3. c3

<- increased margin

a4. b4. c4

a5 b5. c5

p.41, Figure 3: same recommendation than for Figure 2, please add an increased margin between the cluster of subplots for preformed PO4 and the cluster of subplots showing regenerated PO4. Increase all ticks labels and titles. As the whole analysis of Fig. 3 is based on biases values, it would be very helpful to show these biases on Fig. 3. You could show a first line of vertical sections relative to observations and then a second line with biases (model-obs) rather than model means.

Response: Thanks for the comment. Figure 2 and 3 are revised accordingly.

p.42, Figure 4: please mention the source of these nutrients limitation patterns. Are they diagnosed from NESM v3 model ?

Response: Thanks for the comments. The limitation patterns are diagnosed from fully-coupled simulation of NESM v3. The figure caption is revised accordingly.

P.44, Figure 6: be careful with the mismatch between subplots titles and their name in the legend.

Response: Thanks for the comment. The caption of figure 6 are revised accordingly.

p.46, Figure 8: see recommendations for Figures 2 and 3.

Response: Thanks for the comment. The ticks labels and titles are increased, as well as the margin below the six subplots. We also replace model distribution with the bias map.

p. 51 and 53, Figures 13 and 15: please add units of analysed fields.

Response: Thanks for the comment. The units are added in the figure caption.

9) Bibliography

Séférian, R., Nabat, P., Michou, M., Saint-Martin, D., Voldoire, A., Colin, J., et al (2019). Evaluation of CNRM Earth-System model, CNRM-ESM2-1: role of Earth system processes in present-day and future climate. Journal of Advances in Modeling Earth Systems, 11. https://doi.org/10.1029/2019MS001791

Marine biogeochemical cycling and oceanic CO_2 uptake simulated by the NUIST Earth System Model version 3 (NESM v3)

Yifei Dai[1, 3], Long Cao[2], Bin Wang[1, 3]

[1] Earth System Modeling Center, and Key Laboratory of Meteorological Disaster of Ministry of Education, Nanjing University of Information Science and Technology, Nanjing 210044, China

[2] Department of Atmospheric Sciences, School of Earth Sciences, Zhejiang University, Hangzhou 310027, China

[3] Department of Atmospheric Sciences and Atmosphere-Ocean Research Center, University of Hawaii, Honolulu HI 96822, USA

*Correspondence: Long Cao (longcao@zju.edu.cn)

Abstract. In this study, we evaluate the performance of Nanjing University of Information Science and Technology (NUIST) Earth System Model, version 3 (hereafter NESM v3) in simulating the marine biogeochemical cycle and carbon dioxide (CO_2) uptake. Compared with observations, NESM v3 reproduces reasonably well the large-scale patterns of upper ocean biogeochemical fields, including nutrients, alkalinity, dissolved inorganic, chlorophyll, and net primary production. ~~The model also reasonably reproduces current-day oceanic CO_2 uptake, the total CO2 uptake is 149 PgC from 1850 to 2016. In the 1ptCO_2 experiment, the NESM v3 produced carbon-climate (γ=-7.9 PgC/K) and carbon-concentration sensitivity parameters (β=0.8 PgC/ppm) are comparable with CMIP5 model results.~~ Some~~The nonlinearity of carbon uptake in the NESM v3 accounts for 10.3% of the total carbon uptake, which is within the range of CMIP5 model results (3.6%~10.6%).~~ ~~Some regional~~ discrepancies between model simulations and observations are identified and the possible causes are investigated. In the upper ocean, the simulated biases in biogeochemical fields are mainly associated with the shortcoming in simulated ocean circulation. Weak upwelling in the Indian Ocean suppresses the nutrient entrainment to the upper ocean, therefore reducing the biological activities and resulting in underestimation of net primary production and chlorophyll concentration. In the Pacific and the Southern Ocean, high-nutrient and low-chlorophyll result from the strong iron limitation. Alkalinity shows high biases in high-latitude oceans due to the strong convective mixing. The major discrepancy in biogeochemical fields is ~~seen~~observed in the deep Northern Pacific. The simulated high concentration of nutrients, alkalinity and dissolved inorganic carbon water is too deep due to the excessive deep ocean remineralization. ~~Despite these~~The model~~ observation discrepancies, it~~ also reasonably reproduces current-day oceanic CO_2 uptake. Model-simulated total oceanic CO_2 uptake is 149 PgC from 1850 to 2016, which compares well

with data-based estimates of 150 ± 20 PgC. In the 1% per year CO_2 increase (1ptCO_2) experiment, the NESM v3 produced carbon-climate (γ=-7.9 PgC/K) and carbon-concentration sensitivity parameters (β=0.88 PgC/ppm) are comparable with Coupled Model Intercomparison Project phase 5 (CMIP5) model results. The nonlinearity of carbon uptake in the NESM v3 accounts for 10.3% of the total carbon uptake, which is within the range of CMIP5 model results (3.6%~10.6%). ~~expected that~~Overall, the NESM v3 can be employed as a useful modeling tool to investigate large scale interactions between the ocean carbon cycle and climate change.

1 Introduction

The global carbon cycle plays an important role in the climate system. The increase in atmospheric ~~carbon dioxide (~~CO_2~~)~~ is responsible for a large part of the observed increase in global mean surface temperature (Ciais et al., 2013). From 1750 to 2016, about 645 ±80 PgC (1 PgC =10^{15} gram carbon) of anthropogenic carbon has been emitted to the atmosphere, including 420 ±20 PgC from fossil fuels and industry and 225 ±75 PgC from land-use-change (Le Quéré et al., 2018). This CO_2 emission caused atmospheric CO_2 concentration to increase by 45% from an annual mean pre-industrial (PI) value of ~277 parts per million (ppm) (Joos and Spahni, 2008) to 406.8 ppm in 2017 (NOAA ESRL Global Monitoring Division, 2017). As a large carbon reservoir, the global ocean contains more than 50 times the amount of carbon than the atmosphere (Denman et al., 2007) and plays a key role in anthropogenic CO_2 uptake (Ballantyne et al., 2012; Wanninkhof et al., 2013). Since the year 1870 to 2016, about 25% of anthropogenic CO_2 (about 150 ±20 PgC) has been absorbed by the ocean (Le Quéré et al., 2018). An increase in atmospheric CO_2 perturbs the atmospheric radiative balance and leads to climate change. Changes in atmospheric temperature, precipitation, evaporation, and wind, induce changes in ocean physical properties such as temperature, salinity, and ocean circulation (Gregory et al., 2005; Pierce et al., 2012). These changes in ocean physical properties, in turn, affect the ocean carbon cycle (Sarmiento and Gruber, 2006). ~~For example, increasing sea surface temperature decreases the CO_2 solubility and results in a reduction of oceanic CO_2 uptake (Najjar, 1992; Teng et al., 1996; Cox et al., 2000; Zickfeld et al., 2008). Meanwhile, global warming would lead to a weakening of the global thermohaline circulation and an increase in ocean stratification (Gregory et al., 2005; Goris et al. 2015), which would reduce the exchange of carbon and nutrients between the upper ocean and the ocean interior. Global warming would also increase the amount of light in the mixed-layer, and then affect phytoplankton~~

growth and biologically-mediated CO_2 uptake (Polovina et al., 2008; Luo et al., 2009; Steinacher et al., 2010; Capotondi et al., 2012).

Friedlingstein et al., (2006) proposed that the response of oceanic uptake of atmospheric CO_2 can be represented by the linear sum of two components: 1) carbon-concentration sensitivity, which refers to the response of oceanic CO_2 uptake to increasing atmospheric CO_2; and 2) carbon-climate sensitivity, which refers to the response of oceanic CO_2 uptake to global warming. Adopting this conceptual framework, a number of studies have analyzed the effect of increasing atmospheric CO_2 concentration and global warming on the carbon cycle in terms of the carbon-concentration and carbon-climate sensitivity parameters under different CO_2 emission and concentration scenarios (Gregory et al., 2009; Boer and Arora, 2009; Tjiputra et al., 2010; Roy et al., 2011; Arora et al., 2013).

Given the importance of carbon cycle feedback in current and future global climate change, it is necessary to include the representation of the global carbon cycle in climate system models (Denman et al., 2007). The first and second generations of the NUIST climate system model have good skill in simulating internal climate modes, global monsoon, and projecting future climate change (Li et al., 2018; Yang and Wang, 2018a; Yang et al., 2018b). However, the previous generations of NESM do not include an active ocean biogeochemical model and cannot be used to study the ocean carbon cycle (Cao et al., 2015). Recently, the third version of the NUIST earth system model (NESM v3) was developed as a newly registered model to CMIP phase 6 (CMIP6, Cao et al., 2018), which couples the Pelagic Interactions Scheme for Carbon and Ecosystem Studies (PISCES v2) to represent the ocean biogeochemical processes (Aumont et al., 2015).

The objective of this manuscript is to evaluate the performance of NESM v3 in simulating marine carbon-related biogeochemical tracers and oceanic anthropogenic CO_2 uptake. As a newly developed earth system model and a new member of the CMIP community, it is essential to evaluate the model's ability against observational data. First, we analyze the present-day mean state of macro-nutrients, chlorophyll, net primary production (NPP), sea-air CO_2 flux, dissolved inorganic carbon (DIC), and alkalinity against available observations and observational-based estimates. Then, we evaluate the amount, spatial distribution, and sensitivity parameters of the anthropogenic carbon uptake. The amount and spatial distribution of oceanic anthropogenic carbon uptake during the historical period and future scenarios are compared with observations and CMIP5 model results. The sensitivity parameters and nonlinearity of oceanic CO_2 uptake diagnosed from the NESM v3 are compared with those from CMIP5 models. We also provide a supplementary material that includes comparisons of biogeochemical fields

in the NESM v3 and IPSL-CM5A-LR (hereafter IPSL) that shares the same marine biogeochemical component (PISCES) as used in NESM v3.

The outline of the paper is the following. In Section 2, we describe the NESM v3 with a focus on the ocean carbon cycle component, as well as the setup of model simulations. The results of model simulations are analyzed in Section 3. Conclusions and discussions are presented in Section 4.

2 Methods

2.1 Model

2.1.1 Framework of the NESM v3

Detailed descriptions of the physical components, major improvements, and model tuning procedures of the NESM v3 are documented in Cao et al. (2018). Here we give a brief introduction.

~~. Recently, the third version of the NUIST earth system model was developed as a registered model of CMIP6 (Cao et al., 2018).~~ NESM v3 consists of three main model components, including European Centre Hamburg Atmospheric Model (ECHAM v6.3) (Stevens et al., 2012; Giorgetta et al., 2013), Nucleus for European Modeling of the Ocean version 3.4 (NEMO v3.4-revision 3814) (Madec and NEMO team, 2012) and Los Alamos sea-ice model version 4.1 (CICE v4.1) (~~Hunke et al., 2010). NESM v3 has good skills in simulating internal modes, such as El Ni ño- Southern Oscillation (ENSO), Madden- Julian oscillation (MJO), and monsoon (Li et al., 2018; Yang and Wang, 2018a; Yang et al., 2018b~~Hunke et al., 2010).

~~The *Pelagic Interactions Scheme for Carbon and Ecosystem Studies* (PISCES-v2) is coupled to the ocean circulation component to represent the ocean biogeochemical processes (Aumont et al., 2015). S ťf árian et al. (2013) assessed the ability of PISCES from three earth system modes: IPSL-CM4-LOOP, IPSL-CM5A-LR, and CNRM-CM5.1. The results show that differences in terms of atmospheric component, ocean subgrid-scale physics and resolution would largely influence the marine biogeochemical cycle. Due to the different physical components and multiple non-trivial modifications of physical processes, it is essential to evaluate the performance of the ocean biogeochemical cycle in the NESM v3, i.e. the agreement between simulated and observed fields (Randall et al., 2007).~~

~~The outline of the paper is the following. In Section 2, we describe the NESM v3 with a focus on the ocean carbon cycle component, as well as the setup of model simulations.~~ ~~We evaluate the~~

modeled biogeochemical fields against available observations in Section 3.1. In Section 3.2, we evaluate modeled oceanic uptake of anthropogenic CO_2 during the historical period against data-based estimates. In Section 3.3, we analyze modeled carbon-concentration sensitivity parameters and carbon-climate sensitivity parameters under different CO_2 concentration scenarios and compare our results with CMIP5 model results. Conclusions and discussions are presented in Section 4. We also provide a supplementary material includes comparisons of some biogeochemical fields in the NESM v3 and IPSL-CM5A-LR.

2 Method

2.1 Model

2.1.1 Framework of NUIST-CSM-2.0.1

Detailed model descriptions, major improvements, and tuning are documented in Cao et al. (2018). Here we give a brief introduction.

In this study, we use the low-resolution version of the NESM v3. The atmospheric resolution is T31L31 which has a horizontal resolution of ~ 3.75 °latitude by 3.75 °longitude and 31 layers. The atmospheric model and land surface model are originally adopted from ECHAM v6.3. The detailed information is shown in Stevens et al. (2012) and Giorgetta et al. (2013). The sea-ice componentmodel includes four ice layers and one snow layer with a multi-layer thermodynamic scheme (Hunke et al., 2010; Cao et al., 2018).Cao et al., 2018). Ocean model runs withhas the ORCA2 global ocean configuration, which is a type of tripoletripolar grid. It is based on a 2 degree Mercator mesh and has 31 layers with the thickness of the ocean layer increasing from 10m10 m in the upper ocean to 500m500 m at 5000m5000 m depth. A local transformation is applied in the tropics to refine the resolution to up to 0.5 degree at the equator. In the ocean model, the incoming solar radiation can penetrate to the upper ocean layers as deep as 391m391 m, and a bio-model penetration parameterization scheme is used to calculate the distribution of solar radiation (Lengaigne et al., 2009). In the NESM v3, we modify theThe ocean background vertical diffusivity to replaceis modified in the NESM v3, where the constant value withis replaced by latitude-dependent values (Jochum et al., 2009, Cao et al., 2018).). The parameterization scheme of the vertical diffusivity is detailed in the supplementary, and the global distribution of vertical diffusivity is also shown (Fig. S0S1). Compared to the original vertical diffusivity coefficient constant of 0.12 cm^2/s, the coefficients of the tropical ocean are reduced and that of the middle and high latitude oceans are

increased, especially in the middle latitude oceans (24 ℃N~33 ℃N and 24 ℃S~33 ℃S). Also, ~~we incorporate~~the NESM v3 incorporates the parameterization of brine rejection in the ocean model ~~based on Smith et al (2010). In the NESM v3,~~and the reference sea-ice salinity is set as 4 PSU~~, which means additional salt flux would inject into the ocean during the processes of ice melting.~~ as suggested by Smith et al (2010).

2.1.2 Ocean biogeochemical component

NESM v3 employs the standard PISCES v2 to represent the ocean biogeochemical cycle. The PISCES model is developed from a simple Nutrient-Phytoplankton-Zooplankton-Detritus (NPZD) model (Aumont et al., 2002). It can be used for both regional and global simulations of lower trophic levels of the marine ecosystem and ocean carbon cycle (Bopp et al., 2005; Resplandy et al., 2012; Séférian et al., 2013).

In the current version, there are 24 prognostic tracers in total, including dissolved inorganic and organic carbon, alkalinity, chlorophyll, and nutrients. We use the same biogeochemical parameters as that used in Aumont et al. (2015). The only exception is the advection scheme for passive tracers. Here we use the Total Variance Dissipation (TVD) formulation instead of the Monotone Upstream Scheme for Conservative Laws (MUSCL) formulation to keep the advection scheme to be consistent with the one used in the physical ocean model. Both TVD and MUSCL schemes have good performance in biogeochemical modeling. The MUSCL scheme has better performance in resolving the small scales, while TVD scheme minimizes systematic error through numerical diffusion, and is a better option for coarse-resolution models (Lévy et al., 2001a).

Two different types of phytoplankton: nanophytoplankton and diatoms, and two size classes of zooplankton: mesozooplankton and microzooplankton~~,~~ are presented in the model. The life cycle of phytoplankton is regulated by ~~several~~ processes~~, including~~ of growth, mortality, aggregation, and grazing by zooplankton (Aumont et al., 2015). The growth rate of phytoplankton is determined by temperature, ~~photosynthetic~~photosynthetically active radiation~~,~~ (PAR), and availability of nutrients, including phosphate, nitrate, silicate, iron, and ammonium. The mortality rate of phytoplankton is set as a constant and is identical for nanophytoplankton and diatoms. The aggregations of nanophytoplankton, which transform the dissolved organic carbon (DOC) to the particular organic matter (POM), only depend on the shear rate, ~~which~~as the main driver of aggregation is the local turbulence. In the NESM

v3, this shear rate is set to 1 s^{-1} in the mixed layer and 0.01 s^{-1} below. The same is assumed for diatoms, while the aggregations of diatoms are further enhanced by the nutrients co-limitation. For all species, the phosphate, nitrate, and carbon are linked by a constant Redfield ratio. In NESM v3, the Redfield ratio of C: N: P is set to be 122:16:1 (Takahashi et al., 1985) and the –O/C ratio is set to 1.34 (Kortzinger et al., 2001). In contrast, the Fe / C, chlorophyll / C, and silicon / C ratio are prognostically simulated by the model ~~predicted~~ based on the external concentrations of the limiting nutrients as in the quota-approach (McCarthy, 1980; Droop, 1983; Aumont et al., 2015).

The remineralization of semi-labile ~~dissolved organic carbon (DOC)~~DOC can occur in either oxic water or anoxic water depending on the local oxygen concentration, and their degradation rates are specified and identical for oxic respiration and denitrification. Detritus is represented by different types, including ~~particulate organic matter (~~POM~~),~~, calcite, iron particles, and ~~diatoms silicate.~~biogenic silica. The POM is ~~described by a simple two-compartment scheme, which uses two tracers corresponding to~~partitioned into two size classes: a smaller class (POC: 1-100μm) and a larger class (GOC: 100-500μm). The sinking speed of GOC (50-200 m d^{-1}) increases with depth and is much faster than that of POC (3 m d^{-1}). A fraction of phytoplankton would be turned to the POM through the processes of mortality and aggregation. The fate of mortality and aggregation of nanophytoplankton depends on the proportion of the calcifying organisms. For nanophytoplankton, it is assumed that half of the calcifying organisms are associated with the calcifying organisms. Because the density of the calcite is larger than that of organic matter, 50% of the dying calcifiers are routed to the fast-sinking particles. The same is assumed for the mortality of diatoms, and 50% of the dying diatoms are turned to the POM due to the larger density of biogenic silica compared to that of organic matter. The degradation rate of the POM depends on the local temperature with a Q_{10} factor (temperature dependence ratio) of ~~about~~ 1.9.

The geochemical boundary condition accounts for the external nutrient supply from five different sources, including atmospheric dust deposition of iron and silicon, river recharge of nutrients, dissolved carbon, and alkalinity, atmospheric deposition of nitrogen, and sediment mobilization of sedimentary iron. In the NESM v3, atmospheric deposition and river recharge are prescribed and sediment mobilization is parameterized. At the bottom of the ocean, different sediment parameterization schemes are applied to biogenic silica, POM, and particulate iron. The amount of permanently buried biogenic silica is assumed to balance the external source, and the burial efficiency of POM is determined by the organic carbon sinking rate at the bottom follows the algorithm proposed by Dunne et al. (2007)~~, and all~~.

All the particulate iron would be buried into the sediment once they reach the ocean bottom. The amount of the unburied calcite and biogenic silica would dissolve back into the ocean water instantaneously. In this study, the initial conditions of the biogeochemical model have been adopted from World Ocean Atlas 2009 (WOA09, Garcia, et al., 2010) and Global Ocean Data Analysis Project (GLODAP, Key et al., 2004; Sabine et al., 2004) dataset.

Carbonate chemistry ~~including air-sea CO_2 exchange~~ is formulated based on the Ocean Carbon-Cycle Model Intercomparison Project (OCMIP-2) protocol (more information can be accessed at http://ocmip5.ipsl.jussieu.fr/OCMIP/). The quadratic wind-speed formulation proposed by Wanninkhof (1992) is used to compute the air-sea exchange of carbon and oxygen.

2.2 Simulations

In total, there are eight different simulations in this study, including one fully coupled spin-up simulation for 2000 years, one PI-control run (CTRL) for 251 years, three transient runs driven by forcing conditions from historical observational data and shared socio-economic pathway scenarios (SSP5-8.5) from 1850 to 2100, i.e., fully-coupled (FC), biogeochemically-coupled (BC), and radiatively-coupled (RC), and three idealized 1ptCO_2 runs for 140 years, i.e., FC-1%, BC-1%, and RC-1%. The following is the detailed experimental design.

First, NESM v3 was spun up for 2000 years with all related parameters set to pre-industrial values (the year 1850), including orbital parameters, land use, aerosol, and greenhouse gas (GHGs) concentration (284 ppm for CO_2, 790 ppb for CH_4, 275 ppb for N_2O, and 0 ppt for both CFC_{11} and CFC_{12}). Here, we use PI control simulations of each component model as the initial conditions for the couple model. The atmosphere and sea-ice ~~components~~models use the end of a 550-year ~~offline~~PI control simulation as ~~its~~the initial conditions, and the ocean ~~component~~model uses the end of a 4000-year ~~offline~~PI control simulation as ~~its~~the initial ~~state~~condition. Averaged over the last 100 years of the spin-up simulation, linear drift of globally integrated sea-air CO_2 flux is 0.0006 PgC yr^{-1} per year, indicating that a quasi-equilibrium state has been reached for the global ocean carbon cycle. Global mean sea surface temperature (SST) averaged over the last 100 years of 2000-year spin-up simulation is 13.1 Celsius (℃) with ~~the~~a linear drift of -0.0001 ℃ per year, and ocean mean temperature is 3.5~~℃~~ ℃ with ~~the~~a linear drift of 0.00016~~℃~~ ℃ per year, indicating that the dynamic ocean component has also reached a quasi-equilibrium state.

Following the protocol of CMIP6 historical and ~~the shared socio-economic pathway scenarios experiments~~SSP5-8.5 experiment design (Eyring et al., 2016; Jones et al., 2016), the model is further integrated with changing conditions, including GHGs, ozone, aerosol, land use, and solar forcing from 1850 to 2100. From the year 1850 to 2014, GHGs concentration and other forcing conditions are consistent with observations, and from the year 2015 to 2100, GHGs concentration and forcing conditions are produced based on SSP5-8.5. ~~In addition, following~~Meanwhile, we extended the ~~protocol of CMIP5 (Taylor et al., 2012),~~spin-up by 251 years (1850-2100) as the PI-control simulation.

Also, we performed a similar set of simulations to have a direct comparison with CMIP5 results, i.e., an idealized ~~1%/yr CO_2 run (core 6.1 in CMIP5 experiment design, hereafter~~ 1ptCO_2~~),~~ run, in which atmospheric CO_2 concentration increases at a rate of 1% per year starting from the end state of the pre-industrial simulation with other GHGs concentration remaining at the pre-industrial level. The simulation lasted for 140 years until atmospheric CO_2 concentration has quadrupled. ~~Also, we conducted a 251-year PI-control simulation.~~

~~To separate the effect of atmospheric CO_2 and global warming on the ocean carbon cycle,~~Following Friedlingstein et al., 2006 and Arora et al., 2013, we performed three types of experiments (biogeochemically coupled, radiatively coupled, and fully coupled~~). These types of simulations were also performed by previous studies that investigated~~) for each scenario to separate the effect of atmospheric CO_2 and global warming on the ~~global~~ocean carbon cycle ~~(Friedlingstein et al., 2006; Arora et al., 2013; Schwinger et al., 2014).~~ :

1) ~~Biogeochemically coupled (~~BC~~)~~ simulations in which the code of the ocean carbon cycle sees changing atmospheric CO_2, but the code of atmospheric radiation sees a constant pre-industrial concentration of CO_2. In this way, the ocean carbon cycle is only affected by changing atmospheric CO_2, but no direct effect of CO_2-induced warming;

2) ~~Radiatively coupled (~~RC~~)~~ simulations in which the code of the ocean carbon cycle sees pre-industrial atmospheric CO_2, but the code of atmospheric radiation sees the changing concentrations of atmospheric CO_2. In this way, the ocean carbon cycle is only affected by CO_2-induced warming, but no direct effect of changing atmospheric CO_2.

3) ~~Fully-coupled (~~FC~~)~~ simulations in which both the codes of the ocean carbon cycle and atmospheric radiation see the changing concentrations of atmospheric CO_2. In this way, the ocean carbon cycle is affected by changes in both atmospheric CO2 and CO2-induced warming.

~~In total, there are eight different simulations in this study, including one fully coupled spin-up simulation for 2000 years, one PI-control run (CTRL) for 251 years, three historical+SSP5-8.5 runs (FC, BC, and RC) from 1800 to 2100, and three idealized 1%/yr CO_2 runs (FC-1%, BC-1%, and RC-1%) for 140 years.~~

2.3 ~~Validation~~Evaluation data

~~In this study, we compare the NESM v3 simulated ocean biogeochemical fields, including nutrients, chlorophyll, marine net primary production (NPP), alkalinity, dissolved inorganic carbon (DIC), and oceanic anthropogenic CO_2 inventory with available observations and data-based estimates.~~

~~Data of global ocean distributions~~Global ocean distribution data of nutrients concentrations, including nitrate, phosphate, and silicate, are from the *World Ocean Atlas 2018* (WOA18, Garcia, et al., 2018). In this study, we assume the density of the seawater in the model and observations are the same, and then the unit of observations is converted from umol/kg to mmol/m3 by multiplying the modeled density (in the unit of kg/m3). Geographic distributions of DIC, alkalinity, and anthropogenic carbon is taken from the ~~*Global Ocean Data Analysis Project v2* (~~GLODAP~~)~~ v2 (Key et al., 2015; Lauvset et al., 2016). Both WOA18 and GLODAP v2 data have a horizontal resolution of 1 °×1 °with 33 levels and represent the climatology in recent decades. We ~~compare~~compared modeled chlorophyll in recent decades with the SeaWiFS dataset (NASA Goddard Space Flight Center, 2014), GlobColour merged data (Maritorena, et al., 2010), and Ocean Colour Climate Change Initiative (OCCCI) merged data (http://www.oceancolour.org/). OCCCI and GlobColour incorporate the same datasets, while their uncertainty information and algorithms are not the same.

~~Moderate~~Mode-simulated NPP is compared with moderate Resolution Imaging Spectroradiometer (MODIS) estimated marine ~~net primary production (NPP)~~NPP based on three different algorithms ~~are compared with model simulation in this study~~, including the Standard Vertically Generalized Production Model (VGPM), Eppley-VGPM, and the carbon-based Production Model (CbPM). The datasets can be accessed at http://www.science.oregonstate.edu/ocean.productivity/index.php. In the VGPM and ~~Epply~~Eppley-VGPM, NPP is described as the product of chlorophyll and photosynthetic efficiencies (Behrenfeld and Falkowski, 1997a, 1997b), while the Eppley-VGPM emphasizes the photoacclimation

effect at high SSTs-, i.e., the growth rate is higher at high-temperature regions ((Eppley, 1972; Morel, 1991). In the CbPM, NPP is described as the product of carbon biomass and growth rate (Behrenfeld et al. 2005; Westberry et al. 2008). All three datasets have a horizontal resolution of 1/12 °×1/12 °from 2003 to 2014. The distribution of observed surface ocean sea-air CO_2 flux for the reference year of 2000 is taken from Takahashi et al (2009) and has a spatial resolution of 4 °latitude by 5 °longitude.

To have a direct comparison between the NESM v3 resultsoutput and observations, we interpolated all modeled results and observations to a 1 °×1 °grid using the distance-weighted average remapping method, except for the sea-air CO_2 flux. Due to the low resolution of observational sea-air flux, we interpolated the modeled resultsea-air CO_2 flux to a 4 ° × 5 °grid.

2.4 Analysis method

2.4.1 Nutrient decomposition

To figure out whether the ocean circulation or biogeochemical processes causes the bias of nutrients in the model simulation, we decomposing phosphate to its preformed and regenerated components (Weiss et al., 1970; Duteil et al., 2012). The regenerated phosphate is released through the remineralization processes of organic matter, and the preformed phosphate is the remaining biotically unutilized surface phosphate, which is transported into the ocean interior by ocean circulation. The regenerated and preformed phosphate are computed as:

$$P_{regenerated} = R_{P:-o_2} \times AOU \quad (1)$$

$$P_{preformed} = P - P_{regenerated} \quad (2)$$

Where AOU is the apparent oxygen utilization, which represents the biological consumption of oxygen. It is computed as the difference between oxygen saturation and simulated oxygen concentration. $R_{P:-o_2}$ represents the oxidation ratio of phosphate and oxygen, which is set to 1/163 in the NESM v3. P represents the simulated phosphate concentration.

2.4.2 Nutrient limitation

In the NESM v3, the nutrients limitation coefficient (0~1) is computed from the Michaelis-Menten equation as follow:

$$MM=N / (K+N) \quad (3)$$

Where MM is the Michaelis-Menten coefficient, N is the nutrient concentration, and K is the half-saturation coefficient, which is parameterized based on half-saturation constant and concentrations of nutrients, phytoplankton, and diatoms (Aumont et al., 2015).

We calculated the annual mean nutrient limitation coefficient of each nutrient (phosphate, nitrate, silicate, and iron) and then considered the nutrient with the lowest limitation coefficient as the most limiting factor. Temperature and light are assumed to be the most limiting factor when the annual mean nutrient coefficients are greater than 0.9 for all nutrients (Moore et al., 2013).

2.4.3 Carbon-concentration and carbon-climate sensitivity parameters

Following Arora et al. (2013), we diagnose the carbon-climate and carbon-concentration sensitivity parameters from two types of experiments performed by a subset of CMIP5 models, i.e., BC simulations and RC simulations.

In the biogeochemically-coupled simulations where the ocean carbon uptake is only affected by changing atmospheric CO_2, the relationship between atmospheric CO_2 concentration and sea-air CO_2 flux can be simplified as:

$$\int_0^t F' \, dt \approx \beta \Delta C_A \quad (5)$$

Where F' represents oceanic carbon uptake change in the biogeochemically coupled simulation. In the radiatively-coupled simulations where the oceanic carbon uptake is only affected by temperature change, the relationship between temperature and sea-air CO_2 flux can be simplified as:

$$\int_0^t F' \, dt \approx \gamma \Delta T \quad (6)$$

Where F' represents oceanic carbon uptake change in the radiatively coupled simulation.

3 Results

3.-1 Nutrients

~~In this section, we compare model-simulated ocean biogeochemical fields, including nutrients, chlorophyll, alkalinity, dissolved inorganic carbon (DIC), and net primary production (NPP), against available observations and data-based estimates.~~

Nutrients play vital roles in the ocean biogeochemical cycle. A lack of nutrients would limit the growth of phytoplankton. Figure 1 compares the model simulated annual mean spatial distributions of ~~average~~ nutrients ~~concentrations (nitrate,~~concentration, including phosphate~~,~~ (PO_4^{3-}), nitrate (NO_3^-), and silicate~~)~~ ~~in~~ (SiO_4^{2-}), averaged over the top ~~100m~~100 m depth from 1985 to 2014 with the WOA18 observations. The model reproduces reasonably well the large-scale ~~pattern~~patterns of upper ocean mean nutrients concentrations~~. The~~ with pattern correlation coefficients (PCCs) larger than 0.8 and variability similar to the observations. The PCCs of nitrate, phosphate, and silicate between model simulation and WOA18 are respectively 0.93, 0.91, and 0.83, ~~respectively. The~~ and the normalized standard deviations (SDs, normalized to the respective observed standard deviations) of nitrate, phosphate, and silicate are respectively 1.05, 1.06, and 1.22~~, respectively (Fig. 11). Phosphate~~. The spatial distributions of nutrients in the NESM v3 with high concentrations in the Southern Ocean and low concentrations in the subtropical Pacific are generally consistent with other CMIP5 models results (Ilyina et al., 2013; Moore et al., 2013; Séférian et al., 2013; Tjiputra et al., 2013). As shown in the supplement, PCCs of nutrients between the NESM v3 and IPSL simulations are all over 0.9.

For both the NESM v3 simulation and observations, phosphate, nitrate, and silicate in the Southern Ocean have the highest nutrient concentrations ~~of ~1.8, ~25 and ~60 mmol/m^3, respectively~~. Strong vertical mixing and upwelling bring nutrient-rich deep water to the surface (Whitney, 2011). ~~The relative~~ Also, the strong iron limitation (Fig. 4) that reduces the biological uptake of the macro-nutrients is one of the main causes of the high nutrients ~~concentration, about 50% of the values~~level in the Southern Ocean~~, are found~~. The relatively high concentration of nutrients is simulated in the subarctic Pacific Ocean, and the mid-eastern Pacific Ocean, which is about 50% of the concentration in the Southern Ocean. Relatively low ~~concentrations~~concentration of nutrients, less than 20% of the ~~values~~concentration in the Southern Ocean, ~~are found~~is simulated in subtropical regions ~~where the vertical mixing~~. Some noticeable discrepancies between ~~the surface~~model simulations and observations are also found (Fig. a3, b3, c3). Phosphate and nitrate are overestimated in the Southern Ocean and the Pacific Ocean but are underestimated in the Indian Ocean, Subarctic Pacific, and Middle-low latitude

Atlantic. ~~the deep~~Except for the Indian Ocean and Subarctic Pacific, silicate is overestimated over all of the global ocean ~~is weak.~~, resulting in the high global mean concentration (50% higher than the WOA18 observations).

~~Some noticeable discrepancies between model simulations and observations are found. Phosphate and nitrate are overestimated in the Southern Ocean and the Pacific Ocean but are underestimated in the Indian Ocean, Subarctic Pacific, and Middle-low latitude Atlantic. Silicate is overestimated nearly over the global ocean, except the Indian Ocean and Subarctic Ocean.~~

Figure 2 shows the ~~recent 30 years~~ zonal mean latitudinal-depth distributions of nutrients from the FC simulation and WOA18 observations in the Pacific, the Atlantic, and the global ocean~~.~~ from 1985 to 2014. Nutrients distributions are reproduced well in the Atlantic. The deepest penetration of relatively low-nutrients water to a ~~1000m~~1000 m depth is simulated in the middle latitude regions. The high concentration of nutrients is found in the Atlantic south of 45 ℃S, and phosphate and nitrate are equator-ward transported by the Antarctic Intermediate Water at near ~~1000m~~1000 m depth. In the Pacific, the spatial patterns of nutrients broadly agree with observations, but with noticeable positive biases in the deep Northern Pacific. The simulated centers of phosphate and nitrate-rich water are too deep.

To further analyze the possible reasons for discrepancies in nutrients ~~distribution~~distributions, we decompose phosphate to its preformed and regenerated components ~~(Weiss et al., 1970; Duteil et al., 2010)~~(Weiss et al., 1970; Duteil et al., 2012) and compare the results with the WOA18 observations (Fig. ~~3).~~3). ~~The regenerated phosphate is released through the remineralization processes of organic matter, and the preformed phosphate is the remaining biotically unutilized surface phosphate, which is transported into the ocean interior by ocean circulation. The regenerated and preformed phosphate are computed as:~~

~~$P_{regenerated} = R_{P:O_2} \times AOU$~~

~~(1)~~

~~$P_{preformed} = P \quad P_{regenerated}$~~

~~(2)~~

~~Where AOU is the apparent oxygen utilization, which represents the biological consumption of oxygen. It is computed as the difference between oxygen saturation and simulated oxygen concentration. $R_{P:O_2}$~~

~~represents the oxidation ratio of phosphate and oxygen, which is set to 1/163 in the NESM v3. *P* represents the simulated phosphate concentration.~~

For the global, Atlantic, and Pacific Ocean, the preformed phosphate diagnosed from the model accounts for 51%, 47%, and 57% of the total phosphate inventory, and the result diagnosed from the WOA18 is 57%, 55%, and 64%, respectively. A relatively small percentage of the preformed phosphate indicates stronger biological activities in the model. Compared to observations, the model simulates a larger depletion of preformed phosphate (bias is about 0.2 mmol /m^3) in the North Atlantic, which indicates too active biological processes in the upper ocean. In the Pacific Deep Ocean, the preformed phosphate concentrations are between 1.3 to 1.5 mmol/m^3 ~~from~~for both model simulation and observations.

The ~~regenerated phosphate concentrations have larger variations than~~ NESM v3 simulates a dipole pattern of preformed phosphate ~~concentration.~~bias above 1500 m depth, which is probably associated with the overestimated vertical mixing that brings too much nutrient-rich water from the intermediate ocean to the surface (Fig. a2, a4, and a6). The noticeable positive biases of regenerated phosphate are found in the deep Northern Pacific. ~~The~~In the model simulation, the high regenerated phosphate water in the North Pacific is ~~simulated~~ too deep, and the biases resemble the difference found in latitudinal-depth distributions of nutrients.

In the deep ocean, preformed phosphate is only affected by ocean circulation, while regenerated phosphate is affected by both circulation and remineralization. ~~The~~In the deep ocean, the NESM v3 simulates the preformed phosphate well but overestimates the regenerated phosphate ~~in the deep ocean~~, suggesting that the overestimated nutrients in the North Pacific deep ocean are mainly caused by biological processes. ~~Another evidence is that overestimation of nutrients has also been found in other PISCES models, such as IPSL-CM5A-LR (Séférian et al., 2013), while the simulated ocean circulations in IPSL and NESM are different.~~

~~We next~~Next, we present the ~~model~~NESM v3-simulated ~~pattern~~patterns of nutrient limitation. ~~In the model, the nutrients limitation coefficient (0~1) is computed from the Michaelis-Menten equation as follow:~~

~~MM=N / (K+N)~~
~~(3)~~

~~Where MM is the Michaelis-Menten coefficient, N is the nutrient concentration, and K is the half-saturation constant.~~

~~We calculated the annual mean nutrient limitation coefficient of each nutrient (phosphate, nitrate, silicate, and iron) and then considered the nutrient with the lowest limitation coefficient as the most limiting factor.~~ ~~Temperature and light are assumed to be the most limiting factor when all nutrients are sufficient for phytoplankton growth and all nutrient limitation coefficients are greater than 0.9.~~ As shown in figure 4, the limiting patterns of nanophytoplankton and diatoms are similar in the mid-low latitude oceans. Iron is the most limiting nutrient for both nanophytoplankton and diatoms in the equatorial Pacific Ocean and the Southern Ocean. Nitrate is the most limiting factor in the subtropical Pacific Ocean, and phosphate is the most limiting factor in the Indian Ocean and middle-low latitude of the Atlantic Ocean. At high latitude oceans, nanophytoplankton is mostly limited by the available light and temperature, while diatoms are mostly limited by silicate. The NESM v3 simulated limiting pattern is generally consistent with the results diagnosed from IPSL-CM4A-LOOP (Schneider et al., 2008), except that the iron limitation diagnosed from the NESM v3 is stronger in the Pacific and the Southern Ocean.

3.~~-~~2 Biological Production

Figure 5 shows the modeled spatial distribution of annual mean surface chlorophyll concentration from 1998 to 2014 compared with ~~Sea-Viewing Wide Field-of-View Sensor (~~SeaWiFS~~)~~ observational data ~~(Behrenfeld and Falkowski, 1997a, 1997b),~~, GlobColour merged data, and ~~Ocean Colour Climate Change Initiative (~~OCCCI~~)~~ merged data.

In the NESM v3, chlorophyll in both nanophytoplankton and diatoms are parameterized based on the photo-adaptive model (Geider et al., 1997) in which chlorophyll is regulated by the chlorophyll-to-carbon ratio, growth of ~~plankton~~phytoplankton biomass, mortality, aggregation, and the grazing by zooplankton. The large-scale pattern of simulated ocean chlorophyll concentration broadly agrees with observations with high levels of chlorophyll in the subarctic Pacific Ocean~~,~~ and North Atlantic~~, equatorial Pacific, and the Southern Ocean~~ (>1 mg Chl m^3) and ~~low~~intermediate levels of chlorophyll in the Southern Ocean (~0.5 mg Chl m^3). Also, the relatively high chlorophyll concentration in the equatorial Pacific (~0.3 mg Chl m^3) surrounded by low chlorophyll concentration seawater over the subtropical oceans (<0.1 mg Chl m^3) are reproduced. The relatively high chlorophyll concentrations

along the extratropical coastal regions are reproduced, but the model generally underestimates chlorophyll concentration in the tropical coastal regions, especially in the tropical Indian Ocean, maritime continent, and the tropical Atlantic Ocean. This underestimation is partly associated with the deficiencies in modeled coastal dynamics, which is usually not represented well by the relatively coarse global ocean models (Aumont et al., 2015). It is reported that the observed chlorophyll distribution is better reproduced when PISCES is coupled to a higher resolution ocean circulation model (Lee et al., 2000; Hood et al., 2003; Kone et al., 2009). Also, we ~~can see~~inspect an underestimation of chlorophyll over the ~~entire~~ Northern Indian Ocean. This is associated with the underestimation of nutrients over the Indian Ocean (Fig. 1) that ~~increase~~increases nutrients limitation and ~~inhibit~~inhibits growth.

In the Southern Ocean where the seawater is typically characterized by high nutrients and low chlorophyll (Lin et al., 2016), noticeable discrepancies are seen among different observational datasets that are associated with different algorithms used for ~~different~~these products. For example, in ~~the intermediate concentration regions such as~~ the Southern Ocean, chlorophyll derived from reflectance by standard algorithms tend to be underestimated by a factor of about 2 to 2.5 (Kahru and Mitchell, 2010). In the Southern Ocean, the NESM v3 overestimates the chlorophyll concentration ~~in~~to the east of 150 ℃ and underestimates it near the International Date Line~~.~~ (180 ℃). In the Atlantic part of the Southern Ocean, the modeled chlorophyll concentration is within the range of observational estimates, higher than the SeaWiFS but lower than the GlobColour and OCCCI.

Figure 6 shows the annual mean climatology of vertically integrated NPP from ~~1998~~2003 to 2014. Three different algorithms, including VGPM, ~~Epply~~Eppley-VGPM, and CbPM, are used to estimate the NPP based on the MODIS ~~observation data. Both VGPM and Epply-VGPM are chlorophyll-based algorithms in which NPP is calculated as a function of chlorophyll, available light, and the photosynthetic efficiency. The only difference between VGPM and Epply-VGPM is the description of photosynthetic efficiency (Behrenfeld and Falkowski, 1997a, 1997b). The Eppley-VGPM emphasizes the effect of SST, i.e. growth rate is higher at high temperature regions (Eppley, 1972). Therefore, compared~~observations. Similar to the ~~VGPM, the Eppley-VGPM estimates more NPP in low latitude oceans and less at high latitude oceans (Fig. 6b and 6d). NPP in the~~ CbPM ~~is described as the product of carbon biomass and growth rate (Behrenfeld et al. 2005; Westberry et al. 2008). In~~, the NESM v3~~, the NPP is~~ also ~~described~~simulates the NPP as the product of phytoplankton biomass and growth rate~~, although~~. However, the calculation of growth rate in the NESM v3 is more complex than that in CbPM, which

involves chlorophyll, nutrients availability, temperature, respiration, and ~~the photosynthetically active radiation (~~PAR~~). Compared to the three products, the~~.

There are significant differences between the NESM v3 simulated NPP and VGPM because the formulation of growth rate in the NESM v3 follows Eppley (1972), i.e., the growth rate is higher at high-temperature regions. Therefore, the NESM v3 estimates more NPP in low latitude oceans and less at high latitude oceans than that in the VGPM (Fig. 6e). The climatology of the NESM v3 simulated vertically integrated NPP resembles ~~Epply~~Eppley-VGPM and CbPM estimates~~. High level of NPP (more than 250 g C/m^2/year)~~ (Fig. 6a, c, d). The main observed spatial pattern of high concentrations of NPP in the eastern equatorial Pacific and middle-latitude oceans ~~around 40 °S and 40 °N and the~~and low ~~level~~concentration of NPP ~~(less than 100 g C/m^2/year)~~ in the middle-low latitude oceans, the Southern Ocean, and high latitude oceans ~~is~~are reproduced~~.~~ by the NESM v3. Also, the NESM v3 reproduced the high ~~level~~concentrations of NPP ~~(more than 325 g C/m^2/year)~~ in low~~ -~~latitude coastal regions ~~is reproduced~~ to some extent. Comparison between three observational data-based estimates and the NESM v3 also suggests that temperature-dependence is important to produce the meridional distribution pattern of marine NPP with the high level of NPP over the high-latitude oceans and low level of NPP over the low-latitude oceans.

Although the global pattern of NPP broadly agrees with the observational estimates, PCC between model simulation and ~~Epply~~Eppley-VGPM is only 0.5, indicating that some local features are not well described in the NESM v3. Compared to CbPM and ~~Epply~~Eppley-VGPM, the NESM v3 significantly underestimates the NPP in the Indian Ocean. The NESM v3 also underestimates the NPP in the eastern coastal areas of the United States and the Arctic coastal areas.

Averaged from 2003 to 2014, the globally integrated ocean NPP from the NESM v3 simulation is 45.1 PgC yr^{-1}, compared with the data-based estimates of 37 to 67 PgC yr^{-1}. The large range of data-based estimates of global NPP is a result of different satellite observations and different algorithms for the NPP estimation (Longhurst et al., 1995; Antoine et al., 1996; Behrenfeld and Falkowski, 1997b; Behrenfeld et al., 2005). Global NPP simulated by CMIP5 models also shows a wide range of values from 30.9 to 78.7 PgC yr^{-1} (Bopp et al., 2013). NESM v3 simulated global NPP is within the range of data-based estimates and current CMIP5 model estimates. Of the NESM v3 simulated global ocean NPP, 20% is contributed by diatoms, and 80% is contributed by nanophytoplankton. For comparison, from the data-based estimate, 7% to 32% of the total NPP is associated with diatoms (Uitz et al.,2010;

Hirata et al., 2011), while ocean biogeochemical models estimate that 15% to 30% global NPP is from diatoms (Aumont et al., 2003; Dutkiewicz et al., 2005; Yool et al., 2011).

3.~~-~~3 Dissolved inorganic carbon and alkalinity

Figures 7 and 8 display the modeled and observed alkalinity and DIC averaged over the upper ocean (0-~~100m~~100 m) and along zonally averaged section in the Pacific Ocean, Atlantic Ocean, and the global ocean. The model's ~~skills~~skill in simulating ~~alkalinityare~~alkalinity is moderate (PCC = 0.56). The observed global spatial pattern of alkalinity is generally simulated by the NESM v3. The model reproduced the observed high alkalinity in the subtropical surface oceans and low alkalinity near the maritime continent ~~are simulated~~, and the modeled global upper ocean mean alkalinity only has a minor negative bias of 0.45%. The major discrepancies are seen in the Southern Ocean and the subarctic Pacific with a positive bias of more than 80 mmol/m^3. In high-latitude oceans, convective mixing of alkalinity-rich deep water is an important factor of changing upper ocean alkalinity, and SST can be used as a proxy of the convective mixing change (Lee et al., 2006). An underestimation of SST of 1ºC is simulated at high latitude oceans (figures not shown), indicating a stronger convective mixing, which may explain the overestimated alkalinity at high latitude oceans. The alkalinity has a negative bias of more than 60 mmol/m^3 near the maritime continent, where the alkalinity concentration is usually related to salinity (Lee et al., 2006). ~~Cao et al. (2018)~~Cao et al. (2018) found that the NESM v3 simulates excessive precipitation over the maritime continent, which results in an underestimation of ~~surface~~the salinity of 2 PSU ~~is caused by excessive precipitation in this region.~~ .

NESM v3 simulates well the large-scale pattern of the observed DIC (PCC = 0.78) with high DIC ~~concentrations~~concentration in the middle-high latitude Atlantic and low DIC concentrations in the middle-low latitude Pacific and the ~~entire~~ Indian Ocean. The model simulated global upper ~~oceanmeans~~ocean means DIC only has a minor positive ~~deviation~~bias of 0.27%. Although the global pattern of DIC is different from alkalinity, their ~~deviation~~bias patterns (model simulation relative to observation) are similar~~. A~~ (Fig. 7e, f). The largest positive DIC bias of more than 80 mmol C/m^3 is ~~seen~~simulated in the Southern Ocean and Subarctic Pacific, and a negative bias of more than ~~40~~80 mmol C/m^3 is ~~seen~~simulated in the maritime continent.

The large-scale patterns of the zonal averaged latitudinal-depth distribution of both DIC and alkalinity are simulated well in the Atlantic Ocean. Apparent biases of DIC and alkalinity are seen in the deep

Northern Pacific. One noticeable pattern of the observed DIC and alkalinity ~~distributions~~ is that their maximum concentrations are around 2000-~~3000m~~3000 m of the North Pacific Ocean, which the model fails to reproduce. The model also overestimates DIC storage in the deep Pacific Ocean. The mismatches between model simulation and observations, i.e. underestimation of DIC and alkalinity concentrations in the upper ~~1000m~~1000 m depth and overestimation of their concentrations in the deep ocean, resemble those of nitrate and phosphate. It indicates that ~~model data~~modeled discrepancies of alkalinity and DIC may also be attributed to excessive deep and active remineralization processes, which ~~would release a~~releases the large amount of dissolved carbon in the deep ocean.

3.4 Assessment of biogeochemical fields by Taylor diagram

Figure 9 respectively compares the spatial patterns of the NESM v3 and IPSL simulated biogeochemistry-related fields with corresponding observations using a Taylor diagram (Taylor, 2001). In summary, model-simulated statistical patterns of the upper ocean nutrients compare well with observations, while the simulated spatial patterns of chlorophyll, primary production, and alkalinity show larger discrepancies from observations. It is noted that chlorophyll and NPP are not directly observed but diagnosed from the observation-based data, and thus their estimations are subject to considerable uncertainties. Compared with biogeochemical fields in IPSL, the NESM v3 has comparable skill in reproducing spatial distributions of nutrients and chlorophyll, but less skill in reproducing DIC and alkalinity with relatively larger SDs.

We also examine other CMIP5 models results that documented in previous studies (Moore et al., 2013; Anav et al., 2013; Tjiputra et al., 2013; S ́ef ́erian et al., 2013). The skill of the models are different according to the biogeochemical fields examined. For example, PCCs between nutrients and observations in Community Earth System Model (CESM) are about 0.8, which is lower than that in the NESM v3, but CESM has a better representation of chlorophyll distribution (Moore et al., 2013). A further study is needed to rank those models, which is beyond the scope of this study. Nevertheless, the NESM v3 shows comparable skill in simulating upper ocean biogeochemical fields in the present-day with other CMIP5 models.

3.5 Oceanic anthropogenic CO_2 uptake during the historical period

In this section, we compare the NESM v3 simulated anthropogenic carbon uptake during the historical period (FC) against available ~~observations.~~observational data-based estimates.

First, we compare the NESM v3 simulated sea-air CO_2 flux against available observations for the reference year of 2000 ~~(Takahashi et al., 2009).~~(Takahashi et al., 2009). As shown in Fig. ~~9~~10, the NESM v3 realistically reproduces the large-scale pattern of observed sea-air CO_2 flux with CO_2 outgassing in the equatorial oceans and uptake in the mid-to-high latitude oceans (PCC=0.71 and ~~SD~~SDs =1.04). For both observation and model results, strong CO_2 uptake is found in the North Atlantic where sea surface temperature is low and the formation of deep water is active. Compared to the data-based estimates, ~~there are overestimates of~~ modeled sea-air CO_2 flux is overestimated in the tropical Pacific, ~~near 45 °S oceans~~the Southern ocean, and the Northern Pacific (near 30 °N ~~oceans, and~~), while the strongest underestimates of modeled sea-air CO_2 flux are seen in the high-latitude oceans (Fig. 9c and 9d). The globally integrated ocean uptake flux from observation is ~~2.~~1.6 ±0 ~~±0.7~~.9 PgC per year in the year 2000 ~~(Takahashi et al., 2009),~~(Takahashi et al., 2009), while the value is 2.8 ~~Pg C~~PgC per year from the model simulation. The ~~deviation~~difference between model and observation is mainly originated from positive bias (~1 PgC yr^{-1}) in the pre-industrial steady-state oceanic CO_2 uptake due to the 3-dimensional correction of nutrient and alkalinity in the PISCES model ~~(Séférian et al., 2015; Aumont et al., 2015),~~(Séférian et al., 2013). The 3-dimensional correction refers to that the global inventory of nutrient and alkalinity are restored toward the observations every January 1 (Aumont et al., 2015). In the NESM v3, the pre-industrial steady-state of total oceanic CO_2 uptake is 1.0 Pg C per year, compared with the observation value of 0.4 ±0.2 Pg C per year~~.~~ (Takahashi et al., 2009). Taking the pre-industrial steady-state into consideration, the total ocean anthropogenic CO_2 uptake flux in the year 2000 is 1.8 PgC from the model simulation, while it is estimated to be 2.0±1.0 PgC from the observation (Takahashi et al., 2009).

We compared the NESM v3 simulated anthropogenic CO_2 budget with the data-based estimate provided by the ~~Intergovernmental Panel on Climate Change~~ Fifth Assessment Report of IPCC (IPCC AR5) (Table 1). The model-simulated ocean uptake of anthropogenic CO_2 is slightly lower than that from the IPCC AR5 but within the estimated uncertainty range. From the pre-industrial time to the year 2011, NESM v3 simulated cumulative oceanic CO_2 uptake is 137.2 PgC, compared with IPCC data-based estimates of 155 ±30 PgC~~.~~ (Ciais et al., 2013). The ~~decade average~~decadal mean oceanic anthropogenic CO_2 uptake diagnosed from the FC run increases from 1.7 to 2.3 PgC yr^{-1} from 1980 to 2009, while the observation ranges from 2.0±0.7 to 2.4±0.7 PgC yr^{-1}. Also, compared ~~to~~with recent ~~results (Le Quéré et al., 2018),~~estimates, from the year 1870 to 2016, the modeled cumulative CO_2 uptake of 149 PgC is within the observational range of 150 ±20 PgC~~.~~ (Le Quéré et al., 2018).

The vertically integrated column inventory of modeled ocean storage of anthropogenic DIC (i.e. FC ~~minus~~relative to CTRL simulation) from 2000 to 2004 (Fig. ~~10a~~11a) and from 1992 to 1996 (Fig. ~~10c~~11c) are compared with GLODAP v2 (Fig. ~~10b~~11b) and GLODAP v1 (Fig. ~~10d), receptively~~11d), respectively. NESM v3 reasonably captures the large-scale data-based distribution of anthropogenic DIC. The largest inventory in the 2000s of more than 100 mol C m^{-2} is simulated in the Northern Atlantic where SST is low and deep water formation is active. In the model simulation, the North Atlantic stores 20.8% of the global oceanic anthropogenic carbon, while it is 17.6% in the observation (Fig. 11a and 11b). In other oceans, the large inventory is mainly found in the middle-latitude areas near 30 ℃N and 30 ℃S. In the Southern Hemisphere Oceans, 58.9% of the global oceanic anthropogenic DIC inventory is simulated, compared to the value of 62.6% in the observation.

The most noticeable discrepancy between the GLODAP v2 and model simulation around 2002 is found in the south of 50 ℃S. Only 8.3% of the global oceanic anthropogenic DIC inventory is ~~stimulated~~simulated, while the value is 15.5% in the observation. However, we noticed that the vertically integrated anthropogenic DIC concentration is also low in the southern ocean south of 50 ℃S in the GLODAP v1 and only 9.9% of the global inventory is stored in this region. ~~The oceanic anthropogenic DIC storage is the cumulative result of the air-sea CO_2 exchange. Takahashi et al. (2009) found the CO_2 outgassing amount of about 1 mol C m^{-2} yr^{-1} in the Southern Ocean south of 45 ℃S. In this aspect, the storage in this region should be as small as that in the GLODAP v1 and the simulated results.~~ It is noted that anthropogenic DIC in the GLODAP is diagnosed by a ~~relative~~ crude application of the transit time distribution method, and thus the results are subject to considerable uncertainties (Lauvset et al., 2016).

Figure ~~11~~12 shows the ~~zonal mean~~ latitudinal-depth ~~distribution~~distributions of anthropogenic DIC concentration in the Atlantic, Pacific, and the global Ocean from the NESM v3 FC simulation and GLODAP v2. The anthropogenic CO_2 invades the ocean in the air-sea interface and then penetrates downward. The observed highest concentrations (more than 51 mmol C m^{-3}) in near-surface waters and the observed low concentration (less than 3 mmol C m^{-3}) in most of the deep ocean (the Pacific and the middle-low latitude Atlantic) are simulated. For both data-based estimates and model simulations, a substantial amount of anthropogenic CO_2 has penetrated down to the ocean interior as deep as 1000 m depth with two penetration tongues near 30 ℃N and 40 ℃S and the deepest penetration of anthropogenic DIC is found in the Northern Atlantic. Deep penetration of anthropogenic DIC is typically associated

with convergence zones at temperate latitudes and high latitude oceans where vertical mixing is strong (Sabine et al., 2004). Similar to the vertically integrated inventory~~,~~ of anthropogenic DIC (Fig. 11), the major discrepancy of anthropogenic DIC in the latitudinal-depth distribution is also found in the Southern Atlantic south of 50 ℃.

~~Figure 12 compares the spatial pattern of the NESM v3 simulated biogeochemistry-related fields with corresponding observations using a Taylor diagram (Taylor, 2001). In summary, model-simulated statistical patterns of the upper ocean nutrients compare well with observations, while the simulated spatial patterns of chlorophyll, primary production, and alkalinity show larger deviations from observations. It is noted that chlorophyll and NPP are not directly observed but diagnosed from the observation-based data, and thus their estimations are subject to considerable uncertainties.~~

3.~~ 5 Response~~6 Sensitivity of the oceanic CO_2 uptake to increasing atmospheric CO_2 and global warming

The ocean carbon cycle is regulated by changes in atmospheric CO_2 and physical climate (Doney et al., 2004). Increasing atmospheric CO_2 affects oceanic CO_2 uptake directly. Meanwhile, global warming also affects the ocean carbon cycle via changes in climatic fields ~~such as temperature and ocean circulation.~~(Gregory et al., 2005; Pierce et al., 2012). In this section, we first presented the NESM v3 simulated physical climate change and oceanic CO_2 uptake under the historical and SSP5-8.5 scenario. Then, we ~~presented~~present NESM v3 simulated ~~oceanic CO_2 uptake and~~ carbon cycle sensitivity parameters and their nonlinearity in the SSP5-8.5 and 1ptCO_2 runs ~~and compared the simulated results with that from CMIP5 models~~.

3.~~ 5.~~ 6.1 NESM v3 simulated physical climate change under historical and SSP5-8.5 scenario

Figure 13 shows the NESM v3 simulated changes (~~minus~~relative to control simulation) in global annual mean surface air temperature (SAT), mixed layer depth (MLD), and the intensity of Atlantic meridional overturning circulation (AMOC) ~~at 30 ºN~~ from 1850 to 2100 under the historical and SSP5-8.5 ~~scenario.~~scenarios. Changes of SAT, MLD, and AMOC in RC and FC simulations are almost the same, while those changes in the BC simulation are rather small. In the FC simulation, the annual global mean SAT anomaly averaged ~~over the period of~~from 2080 to 2100 (relative to the period of 1986-2005) is 4.6 K, which is at the higher end of the CMIP5 model results (2.6 ~ 4.7 K) under the RCP 8.5 scenario (Collins and Knutti, 2013; Knutti and Sedláček, 2013). It is noted that the CMIP6 input forcing is used

in this study and the atmospheric CO_2 concentration at the end of the 21st century in SSP5-8.5 is about 10% higher than the concentration in the ~~CMIP5~~ RCP 8.5 scenario. In the year 2100, SAT change is 6.3 (6.7 and 0.8) K in the FC (RC and BC) simulation. With the increasing atmospheric temperature, the global ocean also becomes warmer in FC and RC simulations, reducing CO_2 solubility and ~~acting to mitigate~~ oceanic CO_2 uptake.

Modeled MLD ~~is seen decreasing~~decreases since the 1980s. In the year 2100, the MLD change is -8.5 (-8 and -1) meter in the FC (RC and BC) simulation. The reduction of mixed layer depth~~, which is associated with a relatively faster warming of the surface ocean and a slower response of the deep ocean,~~ indicates a more stratified upper ocean ~~with global warming (Held et al., 2010).~~. A substantial weakening of AMOC intensity in the ~~RC and~~ FC ~~simulations~~simulation is ~~seen in~~projected for the 21st century, which is associated with ocean surface warming and increased freshwater input into the North Atlantic (Gregory et al., 2005). In the pre-industrial period, the model-simulated AMOC index at 30 ℃N is 17.5 Sv (1Sv =10^6 m^3 s^{-1}), within the range ~~from~~of 14 to 31 Sv from CMIP5 models (Weaver et al., 2012). The modeled annual mean of AMOC transport at 30 ℃N averaged from 2004 to 2011 is 17.1 Sv, while the observation record during the same period from RAPID/MOCHA (Rapid Climate Change programme / Meridional Ocean Circulation and Heatflux Array) is 17.5 ±3.8 Sv (Rhein et al., 2013). By the year 2100, the simulated intensity of AMOC declines to 8.0 Sv. ~~The~~ In the FC simulation, the simulated 54% weakening of AMOC by the end of this century is at the higher end of what is simulated by CMIP5 models that range from 15% to 60% under the RCP 8.5 scenario (Cheng et al., 2013). The higher atmospheric CO_2 concentration at the end of 2100 in the SSP5-8.5 may partly explain the larger AMOC change in this study. Also, Cao et al. (2018) pointed out that the equilibrium climate sensitivity to CO_2 forcing in the NESM v3 is about 10% higher than the CMIP5 ensemble.

3.~~ 5.~~ 6.2 NESM v3 simulated oceanic CO_2 ~~uptake~~uptakes under historical and SSP5-8.5 scenario

~~The ocean carbon cycle is regulated by changes in atmospheric CO_2 and physical climate (Doney et al., 2004).~~ ~~In the FC simulation, weakening of the vertical ocean mixing, as indicated by the reduced mixed layer depth, will reduce the vertical transport of CO_2 from the upper ocean to ocean interior, and the weakening of AMOC would significantly reduce the oceanic CO_2 uptake in the Northern Atlantic (Roy et al., 2011). A warmer surface ocean would reduce CO_2 solubility, also reducing oceanic CO_2 uptake.~~

Figure 14 shows the time evolution of the oceanic CO_2 uptake from the BC, RC, FC, and the linear sum of BC and RC. In the BC simulation, the global ocean absorbed a total amount of 662 PgC of anthropogenic CO_2 from the atmosphere by the year 2100. In the RC simulation, the increased sea surface temperature, enhanced ocean stratification, and the weakened AMOC all act to decrease CO_2 uptake. (Cox et al., 2000; Zickfeld et al., 2008; Roy et al., 2011; Goris et al. 2015). As a result, global warming alone causes the ocean to release CO_2 into the atmosphere. by reducing CO_2 solubility, enhancing the oceanic pCO_2 and altering biological rates (Steinacher et al., 2010; Olonscheck et al., 2013; Lewandowska et al., 2014; Cao et al. 2017). By the year 2100, the modeled cumulative CO_2 uptake is -35.9 PgC. In the FC simulation, oceanic CO_2 uptake is affected by both the increase in atmospheric CO_2 and global warming. By the end of the 21st century, simulated cumulative oceanic CO_2 uptake since the pre-industrial era is 567 PgC, which is within the ranges from 420 PgC to 600 Pg C from CMIP5 models results under the RCP 8.5 scenario (Jones et al., 2013).

The sum of the simulated oceanic CO_2 uptake from the BC and RC simulations (626 PgC) is larger than that from the FC run (567 PgC), indicating that the effect of increasing atmospheric CO_2 (carbon-concentration sensitivity) and the effect of global warming (carbon-climate sensitivity) on the oceanic CO_2 uptake isare not exactly additive. This nonlinearity was also found in previous studies (Boer and Arora, 2009; Gregory et al., 2009; Schwinger et al., 2014). The NESM v3 simulated nonlinearity (i.e., BC+RC-FC) is 59 PgC by the end of the 21st century. This nonlinearity is about 10.4% of the total ocean uptake, and it, which is larger than the absolute value of the radiative effect on oceanoceanic carbon uptake (-35.9 PgC).

To better understand oceanic CO_2 uptake in response to changing atmospheric CO_2 and global warming in model simulation, Figure 15 shows the spatial distribution of anthropogenic sea-air CO_2 flux at the end of the 21st century (averaged over the year 2091 to 2100) under the SSP5-8.5 scenario from FC, RC, and BC simulations, and the difference between FC simulation and the sum of RC and BC simulations.

In the BC simulation, the total oceanic anthropogenic CO_2 uptake is 8.0 Pg C per year at the end of the 21st century. The ocean absorbs atmospheric CO_2 in most regions except for a few scattered grid points at the mid-latitudes with slight CO_2 outgassing. The strongest CO_2 uptake of about 150 g C m^{-2} yr^{-1} is found in the North Atlantic, subarctic Pacific, and the Southern Ocean between 45 °S and 60 °S.. Results from the RC simulation show CO_2 outgassing in large parts of the global ocean as a result of global warming that reduces the CO_2 solubility and increases the oceanic pCO_2. The total CO_2 outgassing in

~~the RC simulation is 0.67 Pg C, less than 10% of the amount of CO_2 uptake in the BC simulation. The warming also has a direct impact on the marine biological processes by altering metabolic, photosynthesis, and respiration rates of plankton. As a consequence, the changes in biological production and the subsequent export of organic matter and $CaCO_3$ changes may further affect the oceanic CO_2 uptake by altering the DIC, alkalinity, and biological pump (Olonscheck et al., 2013; Lewandowska et la., 2014). Plattner et al. (2001) found that the biologically mediated changes enhance ocean CO_2 uptake at the high latitude, and reduce ocean CO_2 uptake at the low latitude. Cao et al. (2017) found that 20% of warming reduced cumulative oceanic CO_2 uptake is associated with the change in marine biological rates. However, this result has a large model dependency, and the net biological effect on CO_2 uptake is uncertain because of the complex interaction among biological activities. In the Arctic Ocean, warming induces a net uptake of CO_2 of 0.07 PgC yr^{-1} (~6 g C m^{-2} yr^{-1}).~~ In the Arctic Ocean, warming induces a net uptake of CO_2 of 0.07 PgC yr^{-1} because the reduced sea-ice extent under global warming allows more open seawater to absorb atmospheric CO_2. In the Northern Atlantic, the capacity of the ocean uptakes CO_2 is significantly suppressed due to the reduced AMOC.

The FC simulation shows the combined ~~effect~~effects of the increasing atmospheric CO_2 and global warming ~~on the oceanic CO_2 uptake~~ (Fig. 14c). Oceanic CO_2 uptake is simulated in most regions with the strongest uptake in the Southern Ocean, indicating the dominant role of the increasing atmospheric CO_2 ~~on the oceanic carbon uptake. Similar to the BC simulation, the strongest CO_2 uptake is simulated in the Southern Ocean. Due to the reduced AMOC, the capacity of the Northern Atlantic uptakes CO_2 is significantly suppressed. Thus, some regions of the Northern Atlantic even appear CO_2 outgassing. Also,~~. CO_2 outgassing is seen in the subtropical Pacific, indicating that the radiative effect dominates the ~~biogeochemical effect~~response of oceanic CO_2 uptake in this region.

~~Figure 15d shows the spatial distribution of differences in sea-air CO_2 flux between the FC simulation and the sum of the BC and RC simulations during the 2090s.~~ The ~~differences represent the~~ nonlinearity ~~between~~of oceanic carbon ~~climate~~ uptake sensitivity ~~and carbon-concentration sensitivity~~during the 2090s is shown in Figure 15d. In the NESM v3, a relatively large nonlinearity is simulated in the Northern Atlantic north of 45 ℃N (19.8% of the total nonlinearity) and the Southern Ocean south of 40 ℃S (35.3% of the total nonlinearity), which is consistent with the findings of previous studies (Zickfeld et al., 2011; Schwinger et al., 2014). The background simulation effects can partly explain the nonlinearity. Compared with the ~~radiatively coupled~~RC simulation, more carbon is subject to the impact of climate

change in ~~fully-coupled simulations.~~the FC simulation. As a consequence, in ~~fully-coupled simulations~~the FC simulation, the increased temperature would have a larger effect on CO_2 solubility and buffer factor (Yi et al., 2001). Also, reduced ocean circulation and increased ocean stratification would slow down the transport of anthropogenic CO_2 from the surface to the deep ocean. Thus, compared to the BC simulation, slowing ocean ventilation in the FC simulation would cause a larger reduction in oceanic CO_2 uptake. The oceanic carbon uptake in the ~~fully-coupled simulations~~FC simulation is lower than the sum of the BC and RC simulations, which is consistent with other CMIP5 models (Schwinger et al., 2014). The above results also indicate that oceanic CO_2 uptake in high-latitude oceans is more sensitive to both the increasing atmospheric CO_2 concentration and global warming than low-latitude oceans, as well as their nonlinear interactions.

3. ~~5.~~ 6.3 carbon-concentration and carbon-climate sensitivity parameters diagnosed from the ~~NESM v3~~SSP5-8.5.

In this section, we ~~investigate~~investigated oceanic CO_2 uptake under the framework of the carbon-concentration and carbon-climate sensitivity parameters.

~~Arora et al. (2013) diagnosed these two parameters from two types of experiments performed by a subset of CMIP5 models, i.e., BC simulations and RC simulations.~~

~~In the biogeochemically-coupled simulations where the ocean carbon uptake is only affected by changing atmospheric CO_2. The relationship between atmospheric CO_2 concentration and sea-air CO_2 flux can be simplified as:~~

~~$$\int_0^t F' \, dt \approx \beta \Delta C_A \quad (5)$$~~

~~Where F' represents oceanic carbon uptake change in the biogeochemically coupled simulation. In the radiatively-coupled simulations where the oceanic carbon uptake is only affected by temperature change. The relationship between temperature and sea-air CO_2 flux can be simplified as:~~

~~$$\int_0^t F' \, dt \approx \gamma \Delta T \quad (6)$$~~

~~Where F' represents oceanic carbon uptake change in the radiatively coupled simulation.~~

~~In this study, we estimate the strengths of sensitivity parameters of carbon-concentration and carbon-climate sensitivities, using equations (5) and (6).~~ Figure 16 shows the change in ocean carbon storage

against the change in the atmospheric CO_2 concentration (Fig. 16a) and the global annual mean surface temperature (Fig. 16b), respectively. The derived evolution of the carbon-concentration sensitivity parameter β as a function of atmospheric CO_2 concentration and carbon-climate sensitivity parameter γ as a function of the change in temperature is shown in Fig. 16c and 16d, respectively.

As shown in Fig. 16, in the BC and RC simulations, modeled ocean storage of anthropogenic CO_2 scales roughly linearly with atmospheric CO_2 and changes in global mean surface temperature. Increasing atmospheric CO_2 alone increases oceanic CO_2 uptake whereas increasing temperature alone decreases CO_2 uptake. ~~Therefore~~In the year 2100, the carbon-climate parameter γ is negative of -5.4 Pg C/K while the carbon-concentration parameter β is positive~~. In the year 2100, the carbon-climate parameter is -5.4 Pg C/K and the carbon-concentration parameter is~~ of 0.79 Pg C/ppm. From 1850 to 2100, the carbon-climate parameter decreases with the increasing temperature change, indicating that with enhanced warming, each degree increase of surface temperature ~~increase~~ would induce more CO_2 outgassing from the ocean (Fig. 16d). The Carbon-concentration parameter initially increases with atmospheric CO_2 and then decreases (Fig. 16c). The decreasing trend of β is consistent with the slowdown of the increasing trend of the oceanic CO_2 uptake at the end of the 21st century as a result of decreased oceanic buffer ability due to the increasing DIC concentration. Similar trends of carbon-climate and carbon-concentration sensitivity parameters are also found in ~~previous studies~~CMIP5 models (Arora et al., 2013). The increased sensitivity of CO_2 outgassing to temperature and the decreased sensitivity of CO_2 uptake to atmospheric CO_2 concentration indicate that the ocean's ability to absorb atmospheric CO_2 would be weakened with increasing atmospheric CO_2 and global warming.

3. ~~5~~6. 4 Carbon-concentration and carbon-climate sensitivity parameters from 1ptCO_2 runs.

~~Arora et al., (2013) analyzed carbon-concentration and carbon-climate sensitivity parameters from CMIP5 models using the benchmark simulations in which atmospheric CO_2 is assumed to increase at a rate of 1% per year for 140 years to reach 4×CO_2. It is reported that the carbon feedback parameters of β and γ are sensitive to CO_2 scenarios (Gregory et al., 2009; Arora et al., 2013). To have a direct comparison with CMIP5 results, we performed a similar set of simulations.~~

In this section, we compared the carbon sensitivity parameters diagnosed from the 1ptCO_2 experiment between the NESM v3 and CMIP5 models. The total CO_2 uptake during the 140 years in FC-1% is 636 Pg C, while the results from CMIP5 models range from 533 to 676 Pg C. The sum of the total CO_2

uptake in the RC-1% and the BC-1% is 65.7 Pg C, which is larger than that in the FC-1%. The simulated nonlinearity (i.e. BC-1% + RC-1% - FC-1%) is about 10.3% of the total CO_2 uptake in the FC-1%, which is at the higher end of the nonlinearity estimated ~~by~~for CMIP5 models ~~range~~ranging from 3.6%-10.6% (Schwinger et al., 2014).

Then, we compare NESM v3 simulated β and γ parameters with those of CMIP5 results. Figure 17 shows the simulated β and γ parameters in the 1ptCO_2 runs. At the end of 1ptCO_2 runs, the diagnosed value of β from CMIP5 models ranges from 0.69 to 0.91 PgC/ppm with a multi-model mean value of 0.80 PgC/ppm. For comparison, the β diagnosed from the NESM v3 simulations is 0.88 PgC/ppm at the end of the simulation. The declining trend in β is found after ~~550ppm~~550 ppm, later than in Hist+RCP8.5 experiments (~400 ppm), which is consistent with the results in CMIP5 models. Compared with β, the γ ~~parameter~~ from CMIP5 models has a much larger range, and the value at the end of the simulations ranges from -2.4 to -12.1 PgC/K. The larger spread of γ is associated with the spread of the model-simulated climate change and the dependency of carbon cycle processes on climate change. For comparison, our simulated γ parameter is -7.9 PgC/K.

4 Discussion and conclusion

In this study, we ~~evaluated~~evaluate the performance of the ~~NUIST Earth System Model (~~NESM v3~~)~~ in simulating the present-day ocean biogeochemical cycle and historical and future oceanic carbon uptake. We also investigated the response of oceanic CO_2 uptake to the individual and combined effect of increasing atmospheric CO_2 and CO_2-induced global warming under SSP5-8.5 and 1ptCO_2 scenarios. The strengths and limitations of the NESM v3 are analyzed and documented.

The ~~model~~NESM v3 simulates reasonably well the large-scale patterns of upper ocean nutrients ~~with~~ (PCCs>0.8 and SDs close to 1.0). The high nutrient concentrations in the ~~Mid-~~Eastern Pacific, subarctic Pacific, and the Southern Ocean~~. The NESM v3~~ are reproduced in the model. Also, the simulated global patterns of ~~upper ocean~~ alkalinity ~~and~~, DIC~~-~~, chlorophyll, and NPP broadly agree with observations ~~with~~and data-based estimates with their main features reproduced (PCCs: 0.5~0.8; SDs: 0.5~1.6). For example, the high alkalinity concentration in the middle-latitude oceans ~~and~~, the high DIC and chlorophyll concentration in the high-latitude oceans~~.~~

~~Chlorophyll is reproduced in the model with~~ , and the high ~~concentrations in the high-latitude ocean, but there are noticeable negative biases in the Indian Ocean and maritime continent. The vertically~~

~~integrated NPP in the model broadly agrees with observational~~ NPP ~~diagnosed by Epply-VGPM and CbPM with high NPP concentrations~~concentration in the low-latitude oceans~~.~~ are reproduced by the NESM v3. The global mean concentration of DIC and alkalinity in the upper ocean only has a bias of 0.27% and 0.45%. The integrated global ocean NPP from 2003 to 2014 simulated by the NESM v3 is 45.1 PgC yr^{-1}, which is comparable with observation-based estimates ~~and CMIP5 model-simulated results of 30.9-78.7 PgC yr^{-1}. Our results suggest that temperature-dependence is necessary to be considered when estimating marine NPP~~of 37-67 PgC yr^{-1}.

~~The~~ Compared with observational data-based estimates, the NESM v3 ~~simulates reasonably well the~~ does a good job in simulating oceanic CO_2 uptake. The observed global pattern of sea-air CO_2 flux~~.~~ is reproduced in the model. In the year 2000, the oceanic anthropogenic CO_2 uptake flux is 1.8 PgC in the NESM v3 simulation, whereas it is 2.0 ±1.0 PgC in the observations. The model-simulated cumulative anthropogenic CO_2 uptake from the ~~pre-industrial time to the~~ year 1870 to 2016 is 149 PgC, which compares well with data-based estimates of 150 ± 20 PgC~~.~~ (Le Quéré et al., 2018).

The behavior of the NESM v3 is also comparable with CMIP5 models in the historical period and future projection. The skills of the models in simulating biogeochemical fields are different according to the variables examined. The integrated global ocean NPP simulated by the NESM v3 (45.1 Pg C) is within the range of CMIP5 models from 30.9 to 78.7 PgC yr^{-1}. At the end of the 21st century of the SSP5-8.5 future scenario, the NESM v3 simulated the total amount of oceanic CO_2 (567 PgC) is at the higher end of CMIP5 results (420~600 PgC). The sensitivity of oceanic CO_2 uptake strongly depends on scenarios. In the 1ptCO_2 ~~run, by year 140~~experiment, the NESM v3 simulated sensitivities of oceanic CO_2 uptake, i.e., carbon-concentration sensitivity ~~parameter is~~(β = 0.~~8~~88 PgC/ppm~~, and the~~), carbon-climate sensitivity ~~parameter is~~(γ = -7.9 PgC/K~~, indicating that increasing atmospheric CO_2 alone increases oceanic CO_2 uptake while global warming alone decreases oceanic CO_2 uptake. These estimated sensitivity parameters are comparable with those estimated by CMIP5 models. The nonlinear of CO_2 uptake is mainly simulated in the high-latitude oceans~~), and ~~is associated with equilibrium climate sensitivity (ECS). The ECS in the NESM v3 is about 10% higher than the CMIP5 ensemble (Cao et al., 2018), and thus results in a relatively larger~~the nonlinearity ~~of oceanic CO_2 uptake. In this study, the~~ (10.3%), compare well with those diagnosed from CMIP5 models (β: 0.69 to 0.91 PgC/ppm, γ: -2.4 to -12.1 PgC/K, and nonlinearity ~~accounts for about~~: 3.6% to 10~~% of the total oceanic CO_2 uptake.~~.6%).

The model captures many aspects of the spatial ~~structure~~structures of biogeochemical fields and their responses to climate change. However, ~~some defects~~model-observation discrepancies and their underlying causes should also be emphasized, which are useful to users of the NESM v3 and also helpful to future model development. In general, the simulated biases in biogeochemical fields in the upper ocean are associated with the shortcoming in simulated ocean circulation, while the discrepancies in the deep ocean are primarily attributed to excessive remineralization.

~~Slight~~In the upper ocean, slight overestimations of nutrients are found in the Pacific and the Southern Ocean (Fig. ~~1), where the~~1). In our simulations, the regions of overestimated nutrients (Fig.1) in general corresponds to regions with strong iron limitation ~~is simulated~~ (Fig. ~~5~~4). The strong iron limitation in these areas limits biological activities, therefore reducing the uptake of nutrients by phytoplankton. Also, the overestimated nutrients are probably associated with strong vertical mixing in the Pacific and the Atlantic, which is indicated by the dipole pattern of preformed phosphate bias above 1500 m depth (Fig. 3). In the Indian Ocean, the underestimation of nutrients is associated with the weak upwelling (figures not shown) that suppresses the nutrient entrainment to surface water. The low-level nutrients in the Indian Ocean reduce the biological activities and then result in ~~negative biases~~underestimation of NPP and chlorophyll. Also, in a relatively coarse resolution model, the ~~negative biases~~underestimation of NPP and chlorophyll in the Indian Ocean could be associated with the poor descriptions of mesoscale and submesoscale processes (McGillicuddy et al., 1998; Lévy et al., 2001b). The underestimation of alkalinity is simulated near the maritime continent, where the model underestimates the surface salinity due to excessive precipitation. In the high-latitude ocean, the model underestimates SST of about 1 ℃, indicating stronger convective mixing, which leads to the overestimation of alkalinity.

~~The~~As for vertical profiles of the biogeochemical field, the latitudinal-depth distribution of nutrients broadly agrees with observations, but the simulated high-concentration centers in the Northern Pacific are too strong and too deep (Fig. 2). ~~The same problem is also found in the IPSL-CM5A-LR simulated nutrients (figures in the supplement). By decomposing phosphate into its preformed and regenerated components (Fig. 3), then comparing them with the total phosphate distribution, we found that excessive~~Excessive remineralization ~~in the deep ocean~~ is the main cause of the overestimated nutrients in the Northern Deep Pacific~~.~~

~~The negative deviations of alkalinity of ~60 mmol / m^3 and DIC of ~40 mmol C / m^3 are simulated near the maritime continent, where the model underestimates the surface salinity of ~ 2 PSU. Cao et al.~~

~~(2018) found that this underestimation of surface salinity is caused by excessive precipitation in this region. In the high-latitude ocean, the model underestimates SST of about 1 ℃, indicating stronger convective mixing, which would lead~~ according to the ~~overestimation of alkalinity.~~results of nutrients decomposition (Fig. 3). Similar to the ~~latitudinal-depth~~vertical distributions of nutrients, the model-simulated high concentration centers of alkalinity and DIC are also too strong and too deep in the Northern Pacific. Excessive remineralization in the deep ocean consumes a large amount of oxygen and releases dissolved organic carbon and nutrients. To better evaluate the ~~NUIST-CSM~~NESM v3 simulated ocean dynamics and the ocean carbon cycle, the simulation of natural and bomb ^{14}C will be implemented in future versions of NESM.

~~It is expected that an improved representation of physical circulation would result in an improved representation of the marine biogeochemical cycle. Overall, NESM v3 can be applied in the future~~Overall, compared with both observations and CMIP5 models, the NESM v3 does a good job in simulating ocean biogeochemical fields and oceanic carbon uptake. Despite these model-observation discrepancies, it is expected that NESM v3 can be used as a useful modeling tool to study interactive feedbacks between the ocean carbon cycle and climate change and the underlying mechanisms.~~...~~

Code and data availability.

The source code of NESM v3, together with all input data are saved in one compressed file, which can be downloaded from: https://doi.org/10.5281/zenodo.3524938 after registration. Also, a user guide describing the installation instructions, driver scripts, and software dependencies can be found in the repository at the same link. The simulation results illustrated in this study can be made available upon request to the authors.

Author contributions. Yifei Dai and Long Cao performed the simulations, analyzed the experiments, and made the figures. The NUIST ESM team led by Bin Wang provided the code of NESM v3 used in this study and Bin Wang provided helpful discussions. Yifei Dai, Long Cao, and Bin Wang all contributed to the writing of the manuscript.

Acknowledgement

Long Cao is supported by the National Natural Science Foundation of China (41675063; ~~41422503~~41975103). Bin Wang acknowledges the support by the Nanjing University of Information

Science and Technology through funding the joint China-US Atmosphere-Ocean Research Center at the University of Hawaii. Yifei Dai acknowledges the support by the China Scholarship Council by providing a scholarship under the State Scholarship Fund. This is the ESMC publication number XXX and IPRC publication number YYYY.

Reference

Anav, A., Friedlingstein, P., Kidston, M., Boop, L., Ciais, P., Cox, P., Jones, C., Jung, M., Myneni, R., and Zhu, Z.: Evaluating the Land and Ocean Components of the Global Carbon Cycle in the CMIP5 Earth System Models. Journal of Climate, 26(18), 6801–6843, 2013.

Antoine, D., André, J.M., and Morel, A.: Oceanic primary production: 2. Estimation at global scale from satellite (Coastal Zone Color Scanner) chlorophyll. Global Biogeochemical Cycles, 10(1), 57-69, 1996.

Arora, V.K., Boer, G.J., Friedlingstein, P., Eby, M., Jones, C.D., Christian, J.R., Bonan, G., Bopp, L., Brovkin, V., Cadule, P., Hajima, T., Ilyina, T., Lindsay, K., Tjiputra, J.F., and Wu, T.: Carbon–concentration and carbon–climate feedbacks in CMIP5 Earth system models. Journal of Climate, 26(15), 5289-5314, 2013.

Aumont, O., Belviso, S., and Monfray, P.: Dimethylsulfoniopropionate (DMSP) and dimethylsulfide (DMS) sea surface distributions simulated from a global three‐dimensional ocean carbon cycle model. Journal of Geophysical Research: Oceans, 107(C4), 2002.

Aumont, O., Maier-Reimer, E., Blain, S., and Monfray, P.: An ecosystem model of the global ocean including Fe, Si, P colimitations. Global Biogeochemical Cycles, 17(2), 1060, 2003.

Aumont, O., Éthé, C., Tagliabue, A., Bopp, L., and Gehlen, M.: PISCES-v2: an ocean biogeochemical model for carbon and ecosystem studies. Geoscientific Model Development, 8(8), 2465-2513, 2015.

Ballantyne, A.P., Alden, C.B., Miller, J.B., Tans, P.P., and White, J.W.C.: Increase in observed net carbon dioxide uptake by land and oceans during the past 50 years. Nature, 488(7409), 70-72, 2012.

Behrenfeld, M.J., and Falkowski, P. G.: Photosynthetic rates derived from satellite-based chlorophyll concentration. Limnology and Oceanography, 42(1), 1-20, 1997a.

Behrenfeld, M. J., and Falkowski P G.: A consumer's guide to phytoplankton primary productivity models. Limnology and Oceanography, 42(7), 1479-1491, 1997b.

Behrenfeld, M.J., Boss, E., Siegel, D.A., and Shea, D.M.: Carbon-based ocean productivity and phytoplankton physiology from space. Global Biogeochemical Cycles, 19, GB1006, 2005.

Boer, G.J., and Arora, V.: Temperature and concentration feedbacks in the carbon cycle. Geophysical Research Letters, 36, L02704, 2009.

Bopp, L., Aumont, O., Cadule, P., Alvain, S. and Gehlen, M.: Response of diatoms distribution to global warming and potential implications: A global model study. Geophysical Research Letters, 32, L19606, 2005.

Bopp, L., Resplandy, L., Orr, J.C., Doney, S.C., Dunne, J.P., Gehlen, M., Halloran, P., Heinze, C., Ilyina, T., Seferian, R., Tjiputra, J., and Vichi, M.: Multiple stressors of ocean ecosystems in the 21st century: projections with CMIP5 models. Biogeosciences, 10, 6225-6245, 2013.

Cao, J., Wang, B., Xiang, B., Li, J., Wu, T., Fu, X., Wu, L., and Min, J.: Major modes of short-term climate variability in the newly developed NUIST Earth System Model (NESM), Adv. Atmos. Sci., 32, 585–600, https://doi.org/10.1007/s00376-014-4200-6, 2015.

Cao, J, Wang, B., Yang, Y.-M., Ma, L., Li, J., Sun, B., Bao, Y., He, J., Zhou, X., and Wu, L.: The NUIST Earth System Model (NESM) version 3: Description and preliminary evaluation, Geosci. Model Dev. 11(7), 2975-2993, 2018.

Cao, L., and Zhang, H.: The role of biological rates in the simulated warming effect on oceanic CO_2 uptake. Journal of Geophysical Research: Biogeosciences, 122(5), 1098-1106, 2017.

Capotondi, A., Alexander, M.A., Bond, N.A., Curchitser, E.N., and Scott, J. D.: Enhanced upper ocean stratification with climate change in the CMIP3 models. Journal of Geophysical Research: Oceans, 117, C04031, 2012.

Ciais, P., Sabine, C., Bala, G., Bopp, L., Brovkin, V., Canadell, J., Chhabra, A., DeFries, R., Galloway, J., Heimann, M., Jones, C., Le Quéré, C., Myneni, R.B., Piao, S., and Thornton, P.: Carbon and Other Biogeochemical Cycles. In: Climate Change 2013: The Physical Science Basis. Contribution of Working Group I to the Fifth Assessment Report of the Intergovernmental Panel on Climate Change [Stocker, T.F., D. Qin, G.-K. Plattner, M. Tignor, S.K. Allen, J. Boschung, A. Nauels, Y. Xia, V. Bex

and P.M. Midgley (eds.)]. Cambridge University Press, Cambridge, United Kingdom and New York, NY, USA, 2013.

Collins, M., Knutti, R., Arblaster, J., Dufresne, J.-L., Fichefet, T., Friedlingstein, P., Gao, X., Gutowski, W.J., Johns, T., Krinner, G., Shongwe, M., Tebaldi, C., Weaver, A.J., and Wehner, M.: Long-term Climate Change: Projections, Commitments and Irreversibility. In: Climate Change 2013: The Physical Science Basis. Contribution of Working Group I to the Fifth Assessment Report of the Intergovernmental Panel on Climate Change. Stocker, T.F., D. Qin, G.-K. Plattner, et al., Eds., Cambridge University Press, Cambridge, United Kingdom and New York, NY, USA, 2013.

Cox, P.M., Betts, R.A., Jones, C.D., Spall, S.A., and Totterdell, I.J.: Acceleration of global warming due to carbon-cycle feedbacks in a coupled climate model. Nature, 408(6809), 184-187, 2000.

Cheng, W., Chiang, J.C., and Zhang, D.: Atlantic meridional overturning circulation (AMOC) in CMIP5 models: RCP and historical simulations. Journal of Climate, 26(18), 7187-7197, 2013.

Denman, K.L., G. Brasseur, A. Chidthaisong, P. Ciais, P.M. Cox, R.E. Dickinson, D. Hauglustaine, C. Heinze, E. Holland, D. Jacob, U. Lohmann, S Ramachandran, P.L. da Silva Dias, S.C. Wofsy, and X. Zhang,: Couplings Between Changes in the Climate System and Biogeochemistry. In: Climate Change 2007: The Physical Science Basis. Contribution of Working Group I to the Fourth Assessment Report of the Intergovernmental Panel on Climate Change [Solomon, S., D. Qin, M. Manning, Z. Chen, M. Marquis, K.B. Averyt, M.Tignor and H.L. Miller (eds.)]. Cambridge University Press, Cambridge, United Kingdom and New York, NY, USA, 2007.

Doney, S.C., Lindsay, K., Caldeira, K., Campin, J.M., Drange, H., Dutay, J.C., Follows, M., Gao, Y., Gnanadesikan, A., Gruber, N., Ishida, A., Joos, F., Madec, G., Maier-Reimer, E., Marshall, J.C., Matear, R.J., Monfray, P., Mouchet, A., Naijar, R., Orr, J.C., Plattner, G.-K., Sarmiento, J., Schlitzer, R., Slater, R., Totterdell, I.J., Weirig, M.-F., Yamanaka, Y., and Yool, A.: Evaluating global ocean carbon models: The importance of realistic physics. Global Biogeochemical Cycles, 18, GB3017, 2004.

Droop, M. R.: 25 years of algal growth kinetics, Bot. Mar., 26, 99–112, 1983.

Dunne, J.P., Sarmiento, J.L., and Gnanadesikan, A.: A synthesis of global particle export from the surface ocean and cycling through the ocean interior and on the seafloor. Global Biogeochemical Cycles, 21, GB4006, 2007.

Duteil, O., Koeve, W., Oschlies, A., Aumont, O., Bianchi, D., Bopp, L., Galbraith, E., Matear, R., Moore, J.K., Sarmiento, J.L., and Segschneider, J.: Preformed and regenerated phosphate in ocean general circulation models: can right total concentrations be wrong? Biogeosciences, 9(5), 1797-1807, 2012.

Dutkiewicz, S., Follows, M.J., and Parekh, P.: Interactions of the iron and phosphorus cycles: A three-dimensional model study. Global Biogeochemical Cycles, 19, GB1021, 2005.

Eppley, R.W.: Temperature and phytoplankton growth in the sea. Fish. Bull, 70(4), 1063-1085, 1972.

Eyring, V., Bony, S., Meehl, G. A., Senior, C. A., Stevens, B., Stouffer, R. J., and Taylor, K. E.: Overview of the Coupled Model Intercomparison Project Phase 6 (CMIP6) experimental design and organization, Geosci. Model Dev., 9, 1937-1958, 2016.

Friedlingstein, P., Cox, P., Betts, R., Bopp, L., von Bloh, W., Brovkin, V., Cadule, P., Doney, S., Eby, M., Fung, I., Bala, G., John, J., Jones, C., Joos, F., Kato, T., Kawamiya, M., Knorr, W., Lindsay, K., Matthews, H.D., Raddatz, T., Rayner, P., Reick, C., Roeckner, E., Schnitzler, K.-G., Schnur, R., Strassmann, K., Weaver, A.J., Yoshikawa, C., and Zeng, N.: Climate–carbon cycle feedback analysis: results from the C4MIP model intercomparison. Journal of Climate, 19(14), 3337-3353, 2006.

~~Garcia, C.A.E., Garcia, V.M.T., and McClain, C.R.: Evaluation of SeaWiFS chlorophyll algorithms in the Southwestern Atlantic and Southern Oceans. Remote Sensing of Environment, 95(1), 125-137, 2005.~~

Garcia, H., Locarnini, R., Boyer, T., Antonov, J., Zweng, M., Baranova, O. and Johnson, D.: World Ocean Atlas 2009, vol. 4, Nutrients (Phosphate, Nitrate, Silicate), edited by: Levitus, S. NOAA Atlas NESDIS, US Gov. Printing Office, Wash., DC, 2010.

Garcia, H. E., K. Weathers, C. R. Paver, I. Smolyar, T. P. Boyer, R. A. Locarnini, M. M. Zweng, A. V. Mishonov, O. K. Baranova, D. Seidov, and J. R. Reagan.: World Ocean Atlas 2018, Volume 4: Dissolved Inorganic Nutrients (phosphate, nitrate and nitrate+nitrite, silicate). A. Mishonov Technical Ed,: NOAA Atlas NESDIS 84, 35 pp, 2018.

Geider, R.J., MacIntyre, H.L. and Kana, T.M.: Dynamic model of phytoplankton growth and acclimation: responses of the balanced growth rate and the chlorophyll a: carbon ratio to light, nutrient-limitation and temperature. Marine Ecology Progress Series, 148, 187-200, 1997.

Giorgetta, M. A., Roeckner, E., Mauritsen, T., Bader, J., Crueger, T., Esch, M., Rast, S., Kornblueh, L., Schmidt, H., Kinne, S., Hohenegger, C., Möbis, B., Krismer, T., Wieners, K.-H., and Stevens, B.: The Atmospheric General Circulation Model ECHAM6: Model Description, Tech. rep., Max Planck Institute for Meteorology, Hamburg, Germany, 2013.

Goris, N., Tjiputra, J., Schwinger, J., and Heinze, C.: Responses of carbon uptake and oceanic pCO_2 to climate change in the North Atlantic: A model study with the Bergen Earth System Model, Global Biogeochem. Cycles, 29(10), 1567-1583, 2015.

Gregory, J.M., Dixon, K.W., Stouffer, R.J., Weaver, A.J., Driesschaert, E., Eby, M., Fichefet, T., Hasumi, H., Hu, A., Jungclaus, J.H., Kamenkovich, I.V., Levermann, A., Montoya, M., Murakami, S., Nawrath, S, Oka, A., Sokolov, A.P., and Thorpe, R.B.: A model intercomparison of changes in the Atlantic thermohaline circulation in response to increasing atmospheric CO2 concentration. Geophysical Research Letters, 32, L12703, 2005.

Gregory, J.M., Jones, C.D., Cadule, P., and Friedlingstein, P.: Quantifying carbon cycle feedbacks. Journal of Climate, 22(19), 5232-5250, 2009.

~~Held, I.M., Winton, M., Takahashi, K., Delworth, T., Zeng, F., and Vallis, G.K.: Probing the fast and slow components of global warming by returning abruptly to preindustrial forcing. Journal of Climate, 23(9), 2418-2427, 2010.~~

Hirata, T., Hardman-Mountford, N.J., Brewin, R.J.W., Aiken, J., Barlow, R., Suzuki, K., Isada, T., Howell, E., Hashioka, T., Noguchi-Aita, M., and Yamanaka, Y.: Synoptic relationships between surface Chlorophyll-a and diagnostic pigments specific to phytoplankton functional types. Biogeosciences, 8(2), 311-327, 2011.

Hood, R.R., Kohler, K.E., McCreary, J.P. and Smith, S.L.: A four-dimensional validation of a coupled physical–biological model of the Arabian Sea. Deep Sea Research Part II: Topical Studies in Oceanography, 50(22-26), 2917-2945, 2003.

Hunke, E.C., Lipscomb, W.H., Turner, A.K., Jeffery, N. and Elliott, S.: CICE: the Los Alamos Sea Ice Model Documentation and Software User's Manual Version 4.1 LA-CC-06-012. T-3 Fluid Dynamics Group, Los Alamos National Laboratory, Los Alamos N.M, 2010.

Ilyina, Tatiana, Katharina D. Six, Joachim Segschneider, Ernst Maier-Reimer, Hongmei Li, and Ismael Nunez-Riboni: Global ocean biogeochemistry model HAMOCC: Model architecture and performance as component of the MPI-Earth system model in different CMIP5 experimental realizations. Journal of Advances in Modeling Earth Systems, 5, 287-315, 2013.

Jochum, M.: Impact of latitudinal variations in vertical diffusivity on climate simulations. Journal of Geophysical Research: Oceans, 114, C01010, 2009.

Jones, C., Robertson, E., Arora, V., Friedlingstein, P., Shevliakova, E., Bopp, L., Brovkin, V., Hajima, T., Kato, E., Kawamiya, M. Liddicoat, S., Lindsay, K., Reick, C. H., Roelandt, C., Segschneider, J., and Tjiputra, J.: Twenty-first-century compatible CO2 emissions and airborne fraction simulated by CMIP5 earth system models under four representative concentration pathways. Journal of Climate, 26(13), 4398-4413, 2013.

Jones, C.D., Arora, V., Friedlingstein, P., Bopp, L., Brovkin, V., Dunne, J., Graven, H., Hoffman, F., Ilyina, T., John, J.G. and Jung, M.: C4MIP–The Coupled Climate–Carbon Cycle Model Intercomparison Project: experimental protocol for CMIP6. Geoscientific Model Development, 9(8), 2853-2880, 2016.

Joos, F., and Spahni, R.: Rates of change in natural and anthropogenic radiative forcing over the past 20,000 years. Proceedings of the National Academy of Sciences, 105(5), 1425-1430, 2008.

Kahru, M., and Mitchell, B.G.: Blending of ocean colour algorithms applied to the Southern Ocean. Remote Sensing Letters, 1(2), 119-124, 2010.

Key, R. M., Kozyr, A., Sabine, C. L., Lee, K., Wanninkhof, R., Bullister, J. L., Feely, R. A., Millero, F. J., Mordy, C., and Peng, T.-H.: A global ocean carbon climatology: Results from Global Data Analysis Project (GLODAP). Global Biogeochemical Cycles, 18(4), 357-370, 2004.

Key, R.M., A. Olsen, S. van Heuven, S. K. Lauvset, A. Velo, X. Lin, C. Schirnick, A. Kozyr, T. Tanhua, M. Hoppema, S. Jutterström, R. Steinfeldt, E. Jeansson, M. Ishi, F. F. Perez, and T. Suzuki.: Global Ocean Data Analysis Project, Version 2 (GLODAPv2), ORNL/CDIAC-162, NDP-P093. Carbon

Dioxide Information Analysis Center, Oak Ridge National Laboratory, US Department of Energy, Oak Ridge, Tennessee. 2015.

Knutti, R., and Sedláček, J.: Robustness and uncertainties in the new CMIP5 climate model projections. Nature Climate Change, 3(4), 369-373, 2013.

Koné, V., Aumont, O., Lévy, M., and Resplandy, L.: Physical and biogeochemical controls of the phytoplankton seasonal cycle in the Indian Ocean: A modeling study. Indian Ocean Biogeochemical Processes and Ecological Variability, 185, 147-166, 2009.

Körtzinger, A., Hedges, J.I., and Quay, P.D.: Redfield ratios revisited: Removing the biasing effect of anthropogenic CO2. Limnology and Oceanography, 46(4), 964-970, 2001.

Lauvset, S. K, R. M. Key, A. Olsen, S. van Heuven, A. Velo, X. Lin, C. Schirnick, A. Kozyr, T. Tanhua, M. Hoppema, S. Jutterström, R. Steinfeldt, E. Jeansson, M. Ishii, F. F. Pérez, T. Suzuki and S. Watelet.: A new global interior ocean mapped climatology: the 1 °x1 °GLODAP version 2, Earth System Science Data, 8, 325-340, 2016.

Le Quéré, C., ., Andrew, R. M., Friedlingstein, P., Sitch, S., Pongratz, J., Manning, A. C., Korsbakken, J. I., Peters, G. P., Canadell, J. G., Jackson, R. B., Boden, T. A., Tans, P. P., Andrews, O. D., Arora, V. K., Bakker, D. C. E., Barbero, L., Becker, M., Betts, R. A., Bopp, L., Chevallier, F., Chini, L. P., Ciais, P., Cosca, C. E., Cross, J., Currie, K., Gasser, T., Harris, I., Hauck, J., Haverd, V., Houghton, R. A., Hunt, C. W., Hurtt, G., Ilyina, T., Jain, A. K., Kato, E., Kautz, M., Keeling, R. F., Klein Goldewijk, K., Körtzinger, A., Landschützer, P., Lefèvre, N., Lenton, A., Lienert, S., Lima, I., Lombardozzi, D., Metzl, N., Millero, F., Monteiro, P. M. S., Munro, D. R., Nabel, J. E. M. S., Nakaoka, S.-I., Nojiri, Y., Padin, X. A., Peregon, A., Pfeil, B., Pierrot, D., Poulter, B., Rehder, G., Reimer, J., Rödenbeck, C., Schwinger, J., Séférian, R., Skjelvan, I., Stocker, B. D., Tian, H., Tilbrook, B., Tubiello, F. N., van der Laan-Luijkx, I. T., van der Werf, G. R., van Heuven, S., Viovy, N., Vuichard, N., Walker, A. P., Watson, A. J., Wiltshire, A. J., Zaehle, S., and Zhu, D.: Global Carbon Budget 2017, Earth Syst. Sci. Data, 10, 405-448, 2018.

Lee, C.M., Jones, B.H., Brink, K.H., and Fischer, A.S.: The upper-ocean response to monsoonal forcing in the Arabian Sea: seasonal and spatial variability. Deep Sea Research Part II: Topical Studies in Oceanography, 47(7-8), 1177-1226, 2000.

Lee, K., L. T. Tong, F. J. Millero, C. L. Sabine, A. G. Dickson, C. Goyet, G. H. Park, R. Wanninkhof, R. A. Feely, and R. M. Key: Global relationships of total alkalinity with salinity and temperature in surface waters of the world's oceans, Geophys. Res. Lett., 33, L19605, 2006.

Lengaigne, M., Madec, G., Bopp, L., Menkes, C., Aumont, O. and Cadule, P.: Bio-physical feedbacks in the Arctic Ocean using an Earth system model. Geophysical Research Letters, 36, L21602, 2009.

Lewandowska, A.M., Boyce, D.G., Hofmann, M., Matthiessen, B., Sommer, U. and Worm, B.: Effects of sea surface warming on marine plankton. Ecology Letters, 17(5), 614-623, 2014.

Lévy, M., Estublier, A., and Madec, G.: Choice of an advection scheme for biogeochemical models. Geophysical Research Letters, 28(19), 3725-3728, 2001a.

Lévy, M., Klein, P., and Treguier, A.M.: Impact of sub-mesoscale physics on production and subduction of phytoplankton in an oligotrophic regime. Journal of Marine Research, 59(4), 535-565, 2001b.

Li, J., Y.M. and Wang, B.: Evaluation of NESMv3 and CMIP5 Models' Performance on Simulation of Asian-Australian Monsoon. Atmosphere, 9(9), 327, 2018.

Lin, H., Kuzminov, F.I., Park, J., Lee, S., Falkowski, P.G., and Gorbunov, M.Y.: The fate of photons absorbed by phytoplankton in the global ocean. Science, p.aab2213, 2016.

Longhurst, A., Sathyendranath, S., Platt, T., and Caverhill, C.: An estimate of global primary production in the ocean from satellite radiometer data. Journal of Plankton Research, 17(6), 1245-1271, 1995.

~~Luo, Y., Liu, Q., and Rothstein, L.M.: Simulated response of North Pacific Mode Waters to global warming. Geophysical Research Letters, 36(23), 2009.~~

Madec, G.: NEMO ocean engine. Note du pôle de modélisation, No. 27, Institut Pierre-Simon Laplace (IPSL), France, 2012.

Maritorena, S., d'Andon, O.H.F., Mangin, A. and Siegel, D.A.: Merged satellite ocean color data products using a bio-optical model: Characteristics, benefits and issues. Remote Sensing of Environment, 114(8), 1791-1804, 2010.

McCarthy, J. J.: The kinetics of nutrient utilization, Can. B. Fish. Aquat. Sci., 210, 211–233, 1980.

McGillicuddy Jr, Robinson, A.R., Siegel, D.A., Jannasch, H.W., Johnson, R., Dickey, T.D., Mcneil, J., Michaels, A.F., and Knap, A.H.: Influence of mesoscale eddies on new production in the Sargasso Sea. Nature, 394(6690), 263-266, 1998.

Moore, J. K., Lindsay, K., Doney, S. C., Long, M. C., and Misumi, K.: Marine Ecosystem Dynamics and Biogeochemical Cycling in the Community Earth System Model [CESM1(BGC)]: Comparison of the 1990s with the 2090s under the RCP4.5 and RCP8.5 Scenarios. Journal of Climate, 26, 9291-9312, 2013.

Morel, A: Light and marine photosynthesis: a spectral model with geochemical and climatological implications. Progress in oceanography, 26(3), 263-306, 1991.

Najjar, R.G.: Marine biogeochemistry, in Climate System Modeling, edited by K.E. Trenberth. Cambridge Univ. Press, New York, 1992.

NASA Goddard Space Flight Center, Ocean Ecology Laboratory, Ocean Biology Processing Group: Sea-viewing Wide Field-of-view Sensor (SeaWiFS) Ocean Color Data, NASA OB.DAAC, 2014.

NOAA ESRL Global Monitoring Division: Atmospheric Carbon Dioxide Dry Air Mole Fractions from quasi-continuous measurements at Mauna Loa, Hawaii. Compiled by K.W. Thoning, D.R. Kitzis, and A. Crotwell. National Oceanic and Atmospheric Administration (NOAA), Earth System Research Laboratory (ESRL), Global Monitoring Division (GMD): Boulder, Colorado, USA. Version 2018-10, 2017. http://dx.doi.org/10.7289/V54X55RG.

Olonscheck, D., Hofmann, M., Worm, B. and Schellnhuber, H.J.: Decomposing the effects of ocean warming on chlorophyll a concentrations into physically and biologically driven contributions. Environmental Research Letters, 8(1), p.014043, 2013.

Plattner, G.K., Joos, F., Stocker, T.F. and Marchal, O.: Feedback mechanisms and sensitivities of ocean carbon uptake under global warming. Tellus B: Chemical and Physical Meteorology, 53(5), 564-592, 2001.

Polovina, J.J., Howell, E.A., and Abecassis, M.: Ocean's least productive waters are expanding. Geophysical Research Letters, 35, L03618, 2008.

Pierce, D.W., Gleckler, P.J., Barnett, T.P., Santer, B.D., and Durack, P.J.: The fingerprint of human-induced changes in the ocean's salinity and temperature fields. Geophysical Research Letters, 39, L21704, 2012.

~~Randall DA, Wood RA, UK.: Climate models and their evaluation. Climate change 2007: the physical science basis. Contribution of working group I to the fourth assessment report of the intergovernmental panel on climate change, Cambridge University Press, Cambridge, UK, New York, NY, USA, 1–74, 2007.~~

Resplandy, L., Levy, M., Bopp, L., Echevin, V., Pous, S., Sarma, V.V.S.S., and Kumar, D.: Controlling factors of the oxygen balance in the Arabian Sea's OMZ. Biogeosciences, 9, 5095-5109, 2012.

Rhein, M., Rintoul, S.R., Aoki, S., Campos, E., Chambers, D., Feely, R.A., Gulev, S., Johnson, G.C., Josey, S.A., Kostianoy, A., Mauritzen, C., Roemmich, D., Talley, L.D., and Wang, F.: Observations: Ocean. In: Climate Change 2013: The Physical Science Basis. Contribution of Working Group I to the Fifth Assessment Report of the Intergovernmental Panel on Climate Change [Stocker, T.F., D. Qin, G.-K. Plattner, M. Tignor, S.K. Allen, J. Boschung, A. Nauels, Y. Xia, V. Bex and P.M. Midgley (eds.)]. Cambridge University Press, Cambridge, United Kingdom and New York, NY, USA, 2013.

Roy, T., Bopp, L., Gehlen, M., Schneider, B., Cadule, P., Frölicher, T.L., Segschneider, J., Tjiputra, J., Heinze, C., and Joos, F.: Regional impacts of climate change and atmospheric CO2 on future ocean carbon uptake: A multimodel linear feedback analysis, J. Clim., 24(9), 2300– 2318, 2011.

Sabine, C.L., Feely, R.A., Gruber, N., Key, R.M., Lee, K., Bullister, J.L., Wanninkhof, R., Wong, C.S.L., Wallace, D.W., Tilbrook, B., Millero, F.J., Peng, T.-H., Kozyr, A., Ono, T., and Rios, A.F.: The oceanic sink for anthropogenic CO2. Science, 305(5682), 367-371, 2004.

Sarmiento, J. l., and N. Gruber.: Ocean Biogeochemical Dynamics. Princeton University Press, Princeton, NJ, USA, 2006.

Schneider, B., Bopp, L., Gehlen, M., Segschneider, J., Frölicher, T.L., Cadule, P., Friedlingstein, P., Doney, S.C., Behrenfeld, M.J., and Joos, F.: Climate-induced interannual variability of marine primary and export production in three global coupled climate carbon cycle models. Biogeosciences, 5(2), 597-614, 2008.

Schwinger, J., Tjiputra, J. F., Heinze, C., Bopp, L., Christian, J.R., Gehlen, M., Ilyina, T., Jones, C.D., y Média, D.S., Segschneider, J., Séférian, R., and Totterdell, I.: Nonlinearity of ocean carbon cycle feedbacks in CMIP5 Earth system models. Journal of Climate, 27(11), 3869-3888, 2014.

Séférian, Roland, Laurent Bopp, Marion Gehlen, James C. Orr, Christian Ethé, Patricia Cadule, Olivier Aumont, David Salas y Média, Aurore Voldoire, and Gurvan Madec.: Skill assessment of three earth system models with common marine biogeochemistry. Climate Dynamics, 40(9-10), 2549-2573, 2013.

Smith, R., Jones, P., Briegleb, B., Bryan, F., Danabasoglu, G., Dennis, J., Dukowicz, J., Eden, C., Fox-Kemper, B., Gent, P., Hecht, M., Jayne S., Jochum M., Large W., Lindsay K., Maltrud M., Norton N., Peacock S., Vertenstein M., and Yeager S.: The parallel ocean program (POP) reference manual ocean component of the community climate system model (CCSM) and community earth system model (CESM). Rep. LAUR-01853, 141, 1-140, 2010.

Steinacher, M., Joos, F., Frölicher, T.L., Bopp, L., Cadule, P., Cocco, V., Doney, S.C., Gehlen, M., Lindsay, K., Moore, J.K., and Schneider, B.: Projected 21st century decrease in marine productivity: a multi-model analysis. Biogeosciences, 7(3), 979-1005, 2010.

Stevens, B., Giorgetta, M., Esch, M., Mauritsen, T., Crueger, T., Rast, S., Salzmann, M., Schmidt, H., Bader, J., Block, K., Brokopf, R., Fast, I., Kinne, S., Kornblueh, L., Lohmann, U., Pincus, R., Reichler, T., and Roeckner, E.: The atmospheric component of the MPI-M Earth System Model: ECHAM6, J. Adv. Model. Earth Syst., 5, 46–172, 2012.

~~Stocker, T.F., and Wright, D.G.: Rapid changes in ocean circulation and atmospheric radiocarbon. Paleoceanography, 11(6), 773-795, 1996.~~

Takahashi, T., Broecker, W.S., and Langer, S.: Redfield ratio based on chemical data from isopycnal surfaces. Journal of Geophysical Research: Oceans, 90(C4), 6907-6924, 1985.

Takahashi, T., Sutherland, S.C., Wanninkhof, R., Sweeney, C., Feely, R.A., Chipman, D.W., Hales, B., Friederich, G., Chavez, F., Sabine, C., Watson, A., Bakker, D.C.E., Schuster, U., Metzl, N., Yoshikawa-Inoue, H., Ishii, M., Midorikawa, T., Nojiri, Y., Kortzinger, A., Steinhoff, T., Hoppema, M., Olafsson, J., Arnarson, T.S., Tilbrook, B., Johannessen, T., Olsen, A., Bellerby, R., Wong, C.S., Delille, B., Bates, N.R., and de Baar, H.J.W.: Climatological mean and decadal change in surface

ocean pCO2, and net sea–air CO2 flux over the global oceans. Deep Sea Research Part II: Topical Studies in Oceanography, 56(8-10), 554-577, 2009.

Taylor, K.E.: Summarizing multiple aspects of model performance in a single diagram. Journal of Geophysical Research: Atmospheres, 106(D7), 7183-7192, 2001.

~~Taylor, K.E., Stouffer, R.J., and Meehl, G.A.: An overview of CMIP5 and the experiment design. Bulletin of the American Meteorological Society, 93(4), 485-498, 2012.~~

~~Teng, H., Masutani, S.M., Kinoshita, C.M., and Nihous, G.C.: Solubility of CO2 in the ocean and its effect on CO2 dissolution. Energy Conversion and Management, 37(6-8), 1029-1038, 1996.~~

Tjiputra, J. F., Assmann, K., Bentsen, M., Bethke, I., Otterå, O.H., Sturm, C., and Heinze, C.: Bergen Earth system model (BCM-C): model description and regional climate-carbon cycle feedbacks assessment. Geoscientific Model Development, 3(1), 123-141, 2010.

Tjiputra, J. F., Roelandt, C., Bentsen, M., Lawrence, D. M., Lorentzen, T., Schwinger, J., Seland, Ø., and Heinze, C.: Evaluation of the carbon cycle components in the Norwegian Earth System Model (NorESM). Geoscientific Model Development, 6, 301-325, 2013.

Uitz, J., Claustre, H., Gentili, B., and Stramski, D.: Phytoplankton class-specific primary production in the world's oceans: seasonal and interannual variability from satellite observations. Global Biogeochemical Cycles, 24, GB3016, 2010.

Wanninkhof, R.: Relationship between wind speed and gas exchange over the ocean. Journal of Geophysical Research: Oceans, 97(C5), 7373-7382, 1992.

Wanninkhof, R., Park, G.H., Takahashi, T., Sweeney, C., Feely, R.A., Nojiri, Y., Gruber, N., Doney, S.C., McKinley, G.A., Lenton, A., Le Quere, C., Heinze, C., Schwinger, J., Graven, H., and Khatiwala, S.: Global ocean carbon uptake: magnitude, variability and trends. Biogeosciences, 10, 1983-2000, 2013.

Weaver, A. J., Sedláček, J., Eby, M., Alexander, K., Crespin, E., Fichefet, T., Philippon‐Berthier, G., Joos, F., Kawamiya, M., Matsumoto, K., Steinacher, M., Tachiiri, K., Tokos, K., Yoshimori, M., and Zickfeld, K.: Stability of the Atlantic meridional overturning circulation: A model intercomparison. Geophysical Research Letters, 39, L20709, 2012.

Weiss, R.F.: August. The solubility of nitrogen, oxygen and argon in water and seawater. In Deep Sea Research and Oceanographic Abstracts, 17(4), 721-735, 1970.

Westberry, T., Behrenfeld, M.J., Siegel, D.A. and Boss, E.: Carbon-based primary productivity modeling with vertically resolved photoacclimation. Global Biogeochemical Cycles, 22, GB2024, 2008.

Whitney F A.: Nutrient variability in the mixed layer of the subarctic Pacific Ocean, 1987–2010. Journal of Oceanography, 67(4), 481-492, 2011.

Yang, Y.M., and Wang, B.: Improving MJO simulation by enhancing the interaction between boundary layer convergence and lower tropospheric heating. Climate Dynamics, 1-23, 2018a.

Yang, Y.M., Wang, B. and Li, J.: Improving Seasonal Prediction of East Asian Summer Rainfall Using NESM3. 0: Preliminary Results. Atmosphere, 9(12), 487, 2018b.

Yi, C., Gong, P., Xu, M., and Qi, Y.: The effects of buffer and temperature feedback on the oceanic uptake of CO2. Geophysical Research Letters, 28(5), 751-754, 2001.

Yool, A., Popova, E.E., and Anderson, T. R.: Medusa-1.0: a new intermediate complexity plankton ecosystem model for the global domain. Geoscientific Model Development, 4(2), 381-417, 2011.

Zickfeld, K., Eby, M., and Weaver, A.J.: Carbon-cycle feedbacks of changes in the Atlantic meridional overturning circulation under future atmospheric CO2. Global Biogeochemical Cycles, 22, GB3024, 2008.

Zickfeld, K., Eby, M., Matthews, H.D., Schmittner, A., and Weaver, A.J.: Nonlinearity of carbon cycle feedbacks. Journal of Climate, 24(16), 4255-4275, 2011.

Table 1. Global ocean anthropogenic CO_2 uptake simulated by NESM v3 during different periods compared against data-based ~~estimate~~estimates (Ciais et al., 2013~~) (it~~). (The uncertainty ranges are given after ±) (It is noted that the pre-industrial time in this study represents the year 1850 while it represents 1750 in IPCC AR5).

	Pre-industrial-2011 Cumulative PgC	1980-1989 PgC yr^{-1}	1990-1999 PgC yr^{-1}	2000-2009 PgC yr^{-1}	2002-2011 PgC yr^{-1}
IPCC AR5	155 ±30	2.0 ±0.7	2.2 ±0.7	2.3 ±0.7	2.4 ±0.7
NESM v3	137.2	1.7	2.0	2.3	2.3

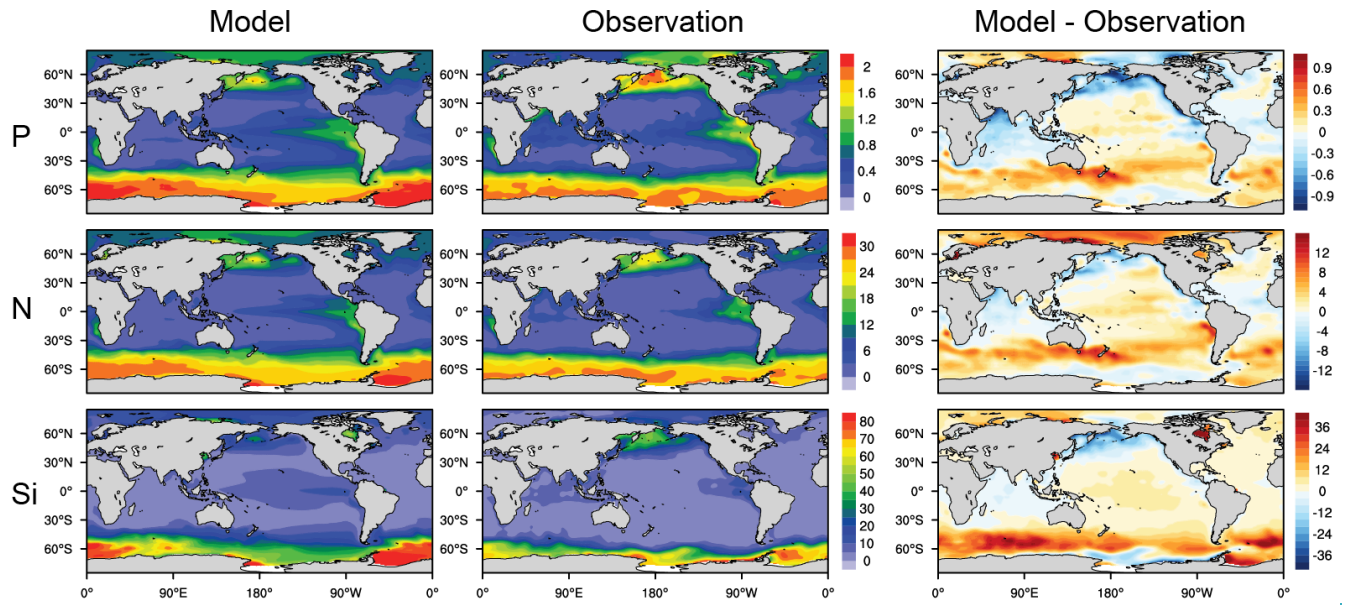
Model
Observation
Model - Observation
P
N
Si
60°N
30°N
0°
30°S
60°S
0°
90°E
180°
90°W
0°
2
1.6
1.2
0.8
0.4
0
0.9
0.6
0.3
0
-0.3
-0.6
-0.9
30
24
18
12
6
0
12
8
4
0
-4
-8
-12
80
70
60
50
40
30
20
10
0
36
24
12
0
-12
-24
-36

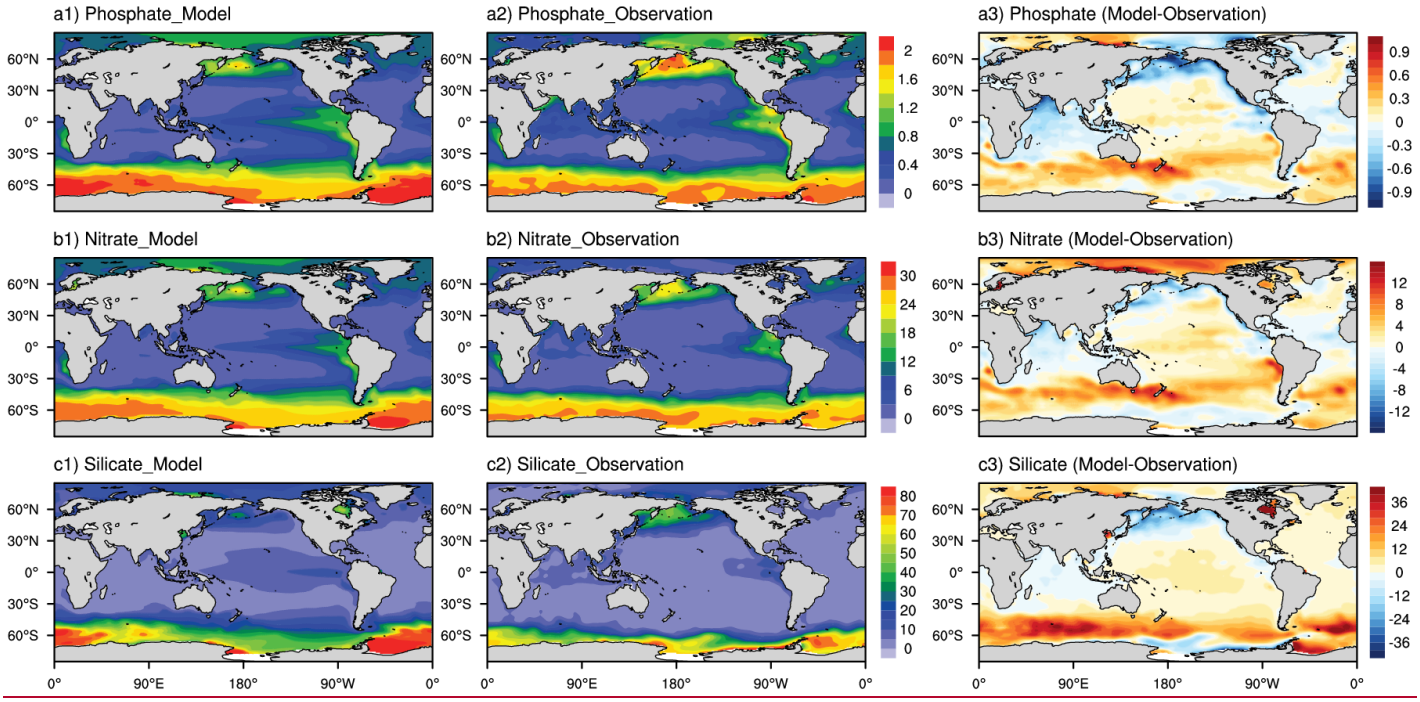
a1) Phosphate_Model
a2) Phosphate_Observation
a3) Phosphate (Model-Observation)
b1) Nitrate_Model
b2) Nitrate_Observation
b3) Nitrate (Model-Observation)
c1) Silicate_Model
c2) Silicate_Observation
c3) Silicate (Model-Observation)
60°N
30°N
0°
30°S
60°S
0°
90°E
180°
90°W
0°
2
1.6
1.2
0.8
0.4
0
0.9
0.6
0.3
0
-0.3
-0.6
-0.9
30
24
18
12
6
0
12
8
4
0
-4
-8
-12
80
70
60
50
40
30
20
10
0
36
24
12
0
-12
-24
-36

Figure 1. Annual mean (averaged over 1985 to 2004) upper ocean (averaged in the upper ~~100m~~100 m) distribution of phosphate (~~PO_4^{3-}),~~a1, a2), nitrate (~~NO_3^-),~~b1, b2) and silicate (~~SiO_4^{2-}) from 1985 to 2014~~c1, c2) from the NESM v3 simulations (FC) and the WOA18 observation dataset (in the unit of mmol~~/m^3).~~ m^{-3}). The difference between model simulation and observation are also shown (a3, b3, and c3)

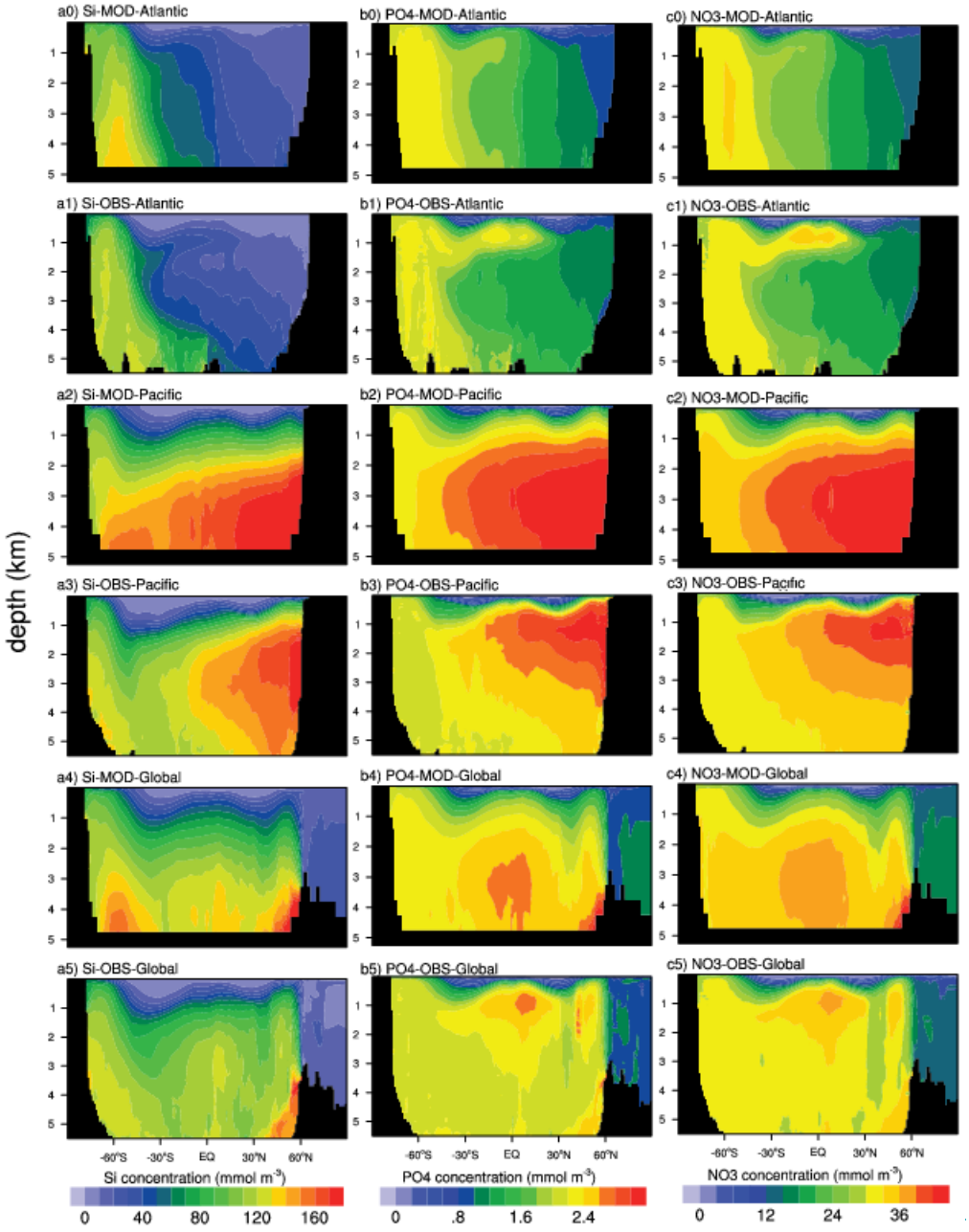

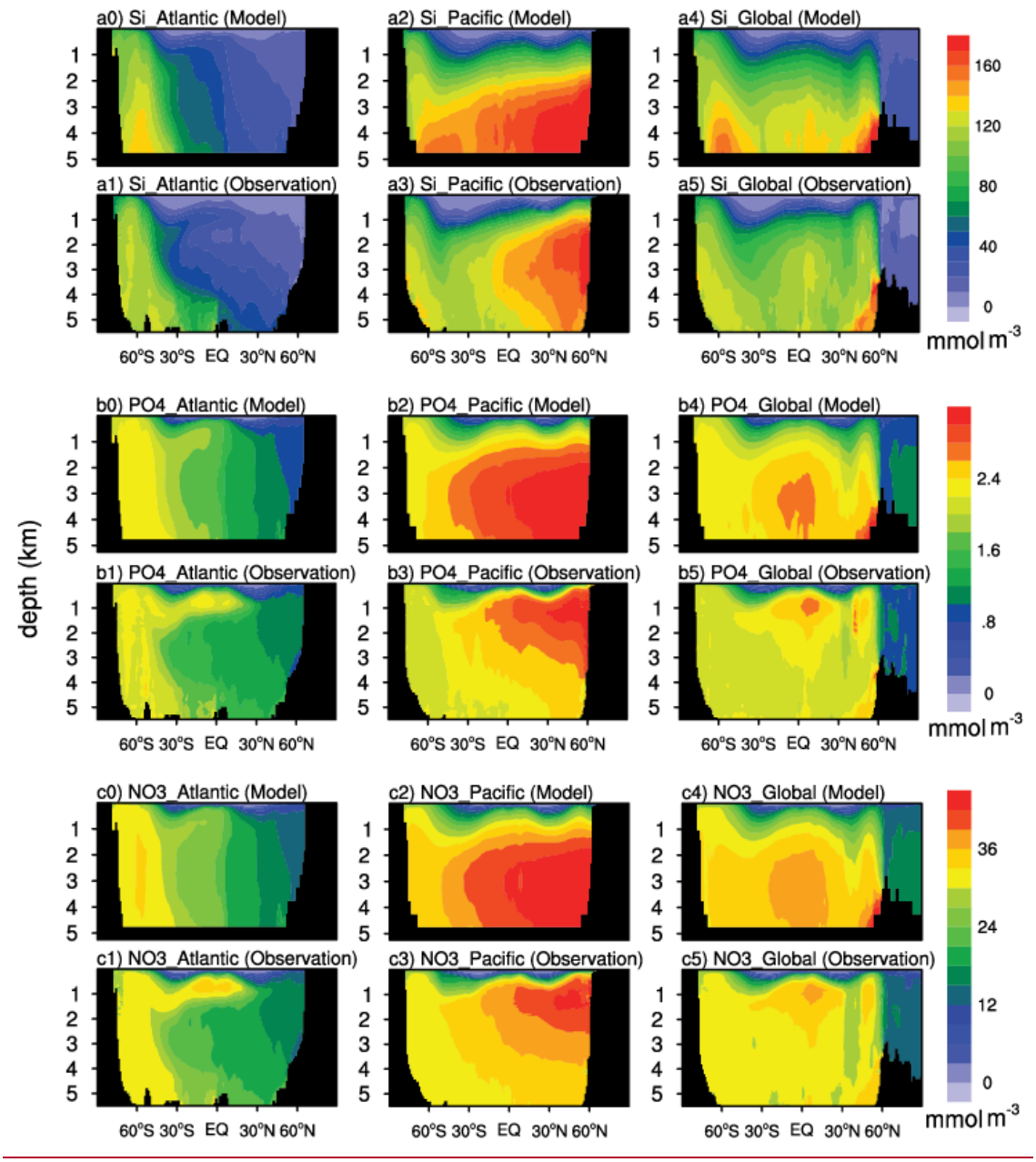

Figure 2. The latitude-depth distribution of silicate (a), phosphate (b), and nitrate (c) averaged from 1985 to 2014 from the NESM v3 simulation (FC) ~~compared with~~and the WOA18 observation dataset (with a unit of mmol m^{-3}). a, b, and c represent the silicate, phosphate, and nitrate, respectively. ~~0~~a1, a2, b1, b2, c1, and ~~1~~c2 represent the distributions in the Pacific Ocean, ~~2~~a3, a4, b3, b4, c3, and ~~3~~c4 represent the distributions in the Atlantic Ocean, and ~~4~~a5, a6, b5, b6, c5, and ~~5~~c6 represent the distributions in the Global Ocean.

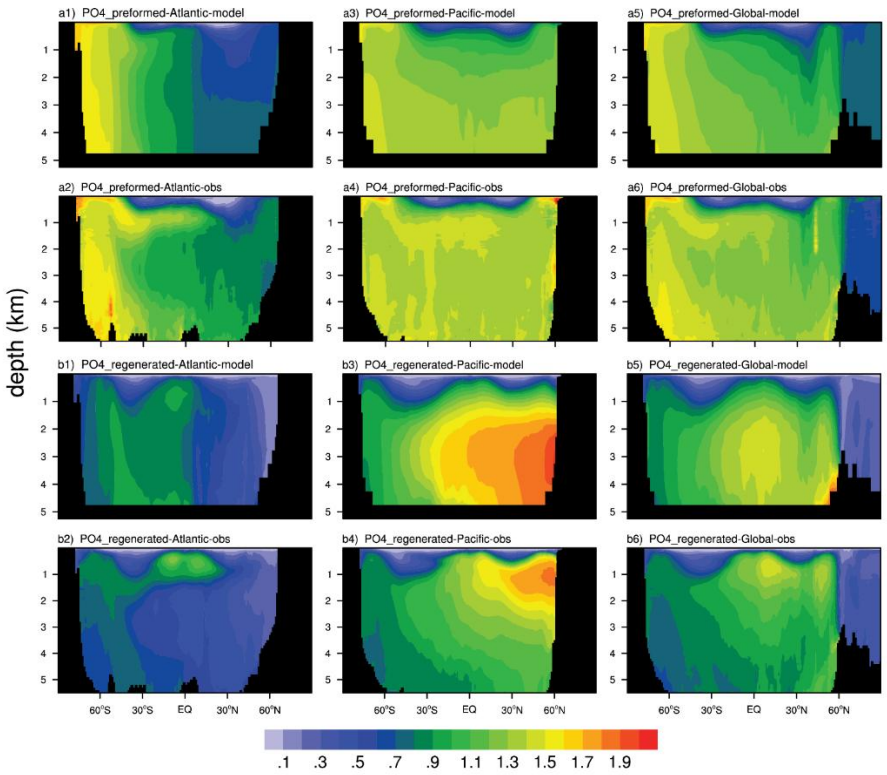
a1) PO4_preformed-Atlantic-model
a3) PO4_preformed-Pacific-model
a5) PO4_preformed-Global-model
a2) PO4_preformed-Atlantic-obs
a4) PO4_preformed-Pacific-obs
a6) PO4_preformed-Global-obs
b1) PO4_regenerated-Atlantic-model
b3) PO4_regenerated-Pacific-model
b5) PO4_regenerated-Global-model
b2) PO4_regenerated-Atlantic-obs
b4) PO4_regenerated-Pacific-obs
b6) PO4_regenerated-Global-obs
depth (km)
1
2
3
4
5
60°S
30°S
EQ
30°N
60°N
.1
.3
.5
.7
.9
1.1
1.3
1.5
1.7
1.9

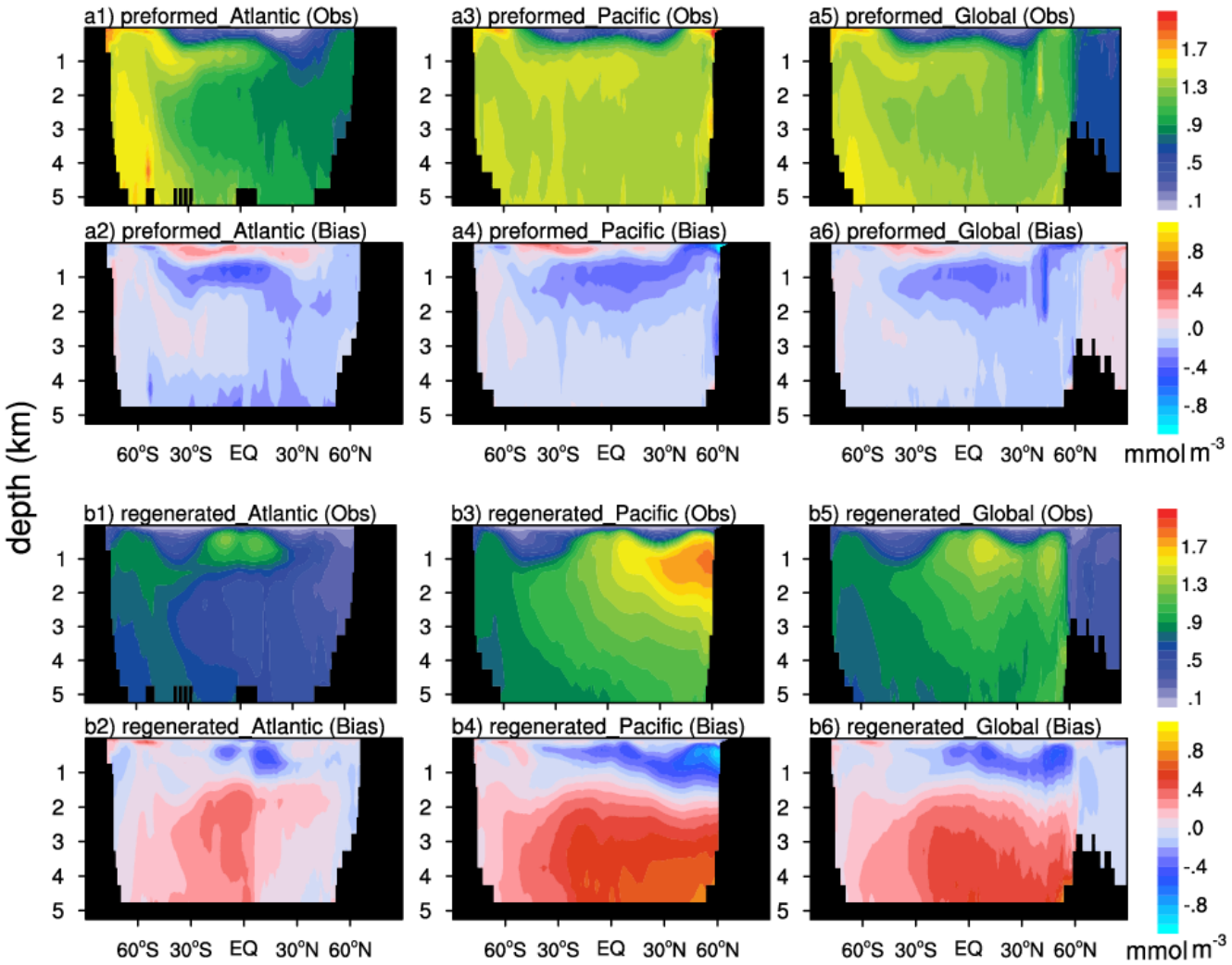

Figure 3. ~~The latitude~~Latitude-depth distribution of preformed and regenerated phosphate concentration (mmol m^{-3}) ~~simulated by the model and analyzed from WOA18 observation dataset~~ in the Pacific, Atlantic, and global Ocean~~.~~ averaged over 1985 to 2014. The results diagnosed from the WOA18 observation dataset are shown in the first and third rows (a1, a3, a5, b1, b3, and b5). The difference (model minus observation) between NESM v3 simulations and observation are shown in the second and the last rows (a2, a4, a6, b2, b4, and b6). The panels from a1 to a6 show the preformed component, ~~while~~and the panels from b1 to b6 show the regenerated component.

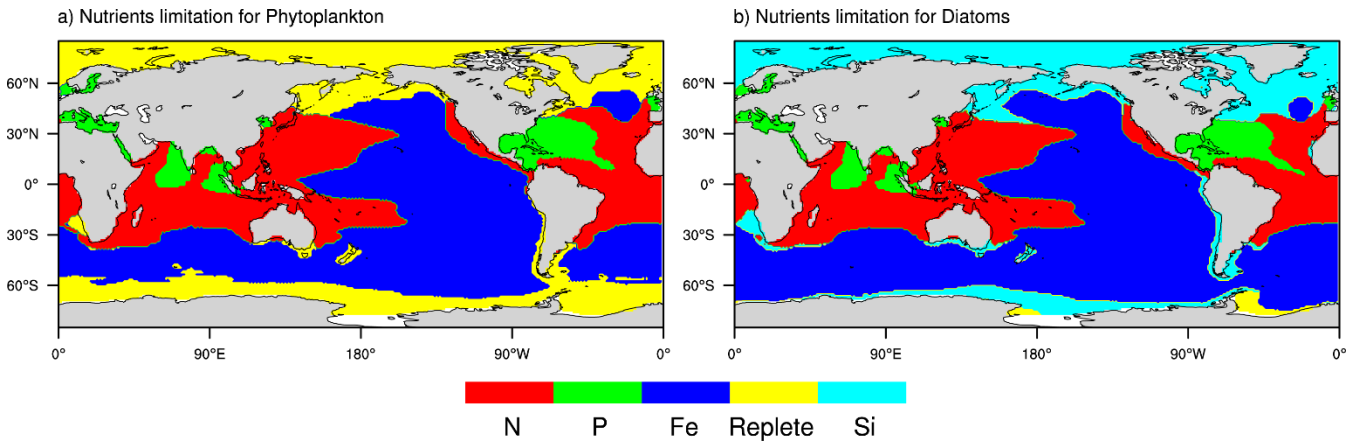

Figure 4. ~~Diagnosed~~The diagnosed pattern of nutrients limitation from the NESM v3 simulation (FC). The limitation maps are shown over the annual time scale ~~for nanophytoplankton and from~~ averaged over 1985 to 2014 ~~in the FC simulation. Shade of each color indicate~~for phytoplankton (a) and diatoms (b). Different colors represent the factor that most limits growth. Replete means nutrient concentrations are sufficient for the phytoplankton growth (growth rate is greater than 90% of their maximal growth rate).

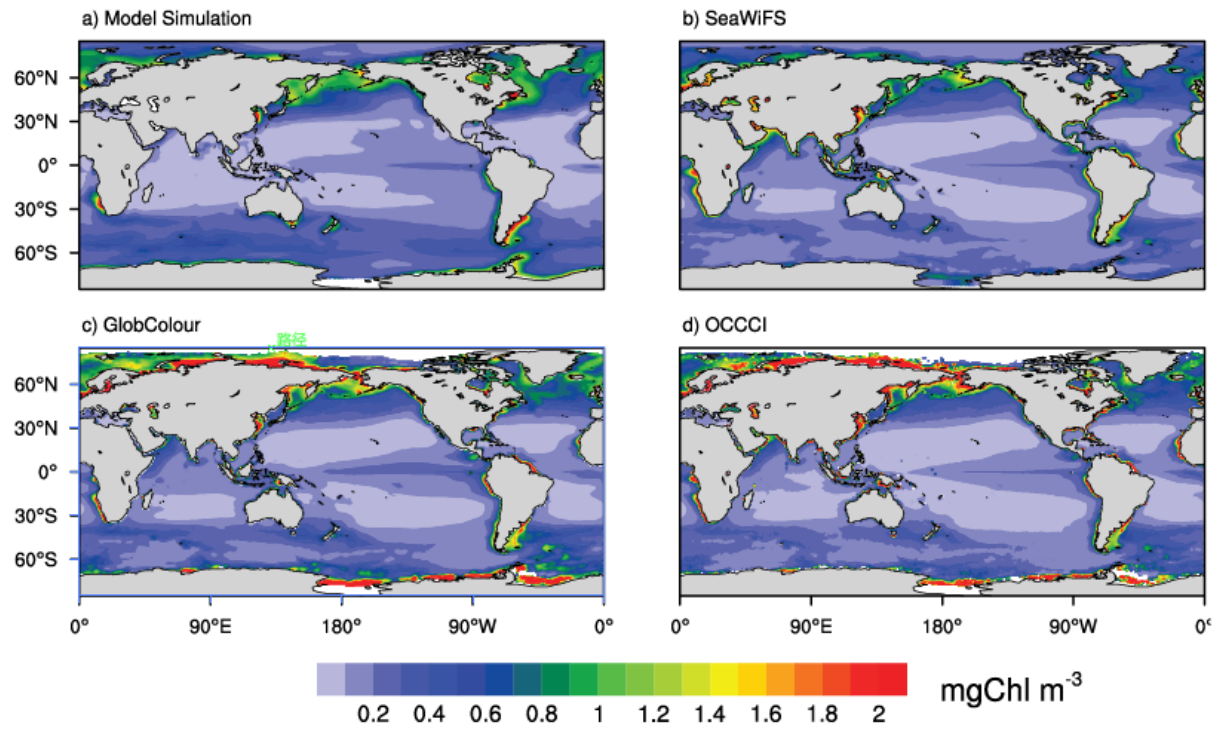
a) Model Simulation
b) SeaWiFS
c) GlobColour
d) OCCCI
60°N
30°N
0°
30°S
60°S
0°
90°E
180°
90°W
0.2
0.4
0.6
0.8
1
1.2
1.4
1.6
1.8
2
mgChl m-3

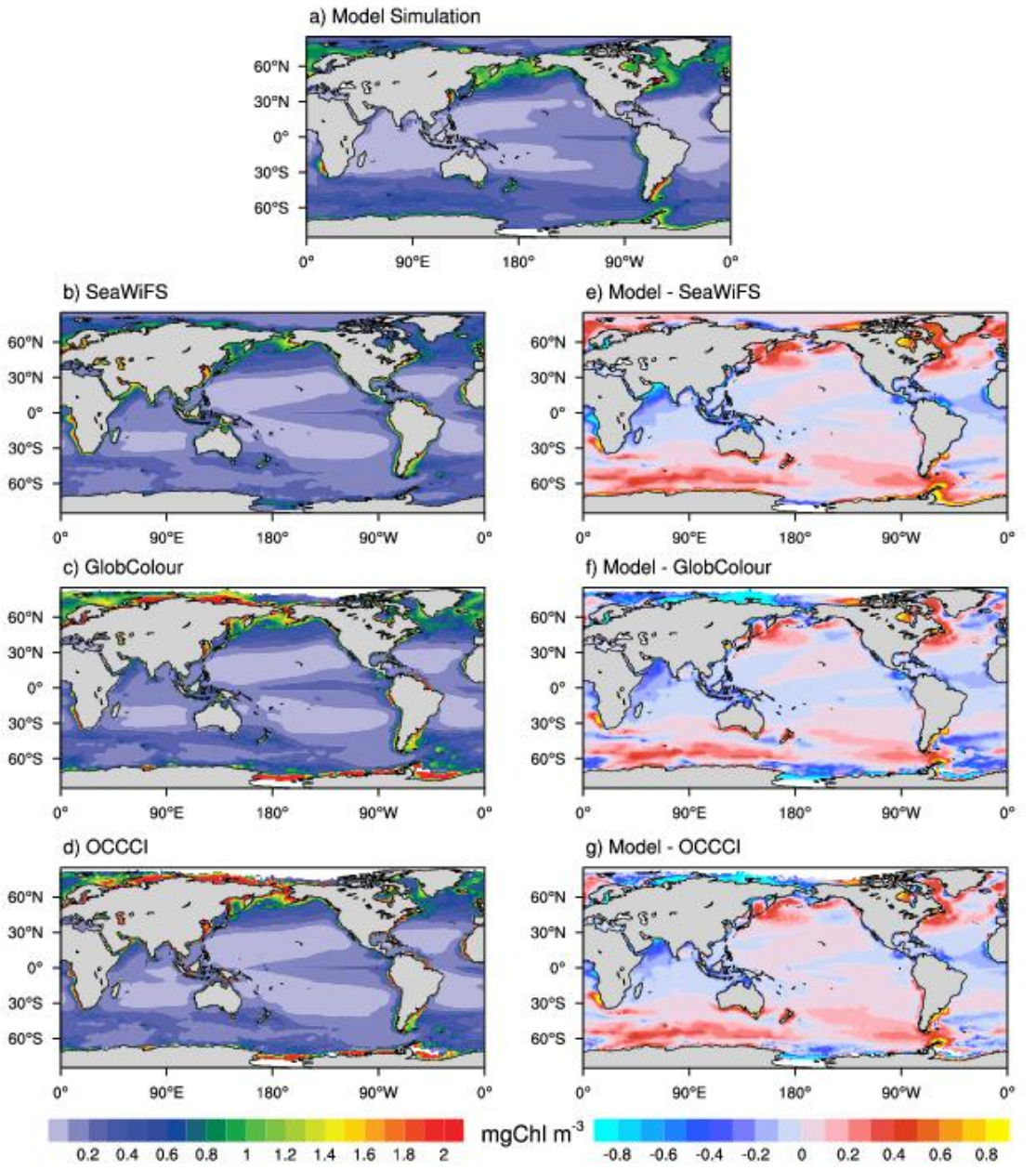

Figure 5. Annual mean surface chlorophyll concentration (mg Chl m^{-3}) from the NESM v3 FC simulations (a; ~~from~~averaged over 1998 to 2014), the SeaWiFS dataset (b; ~~from~~averaged over 1998 to 2010), the GlobColour merged dataset (c; ~~from~~averaged over 1998 to 2014), and OCCCI merged dataset (d; ~~from~~averaged over 1998 to 2014). The biases between the NESM v3 simulation and observations are shown in the e, f, and g.

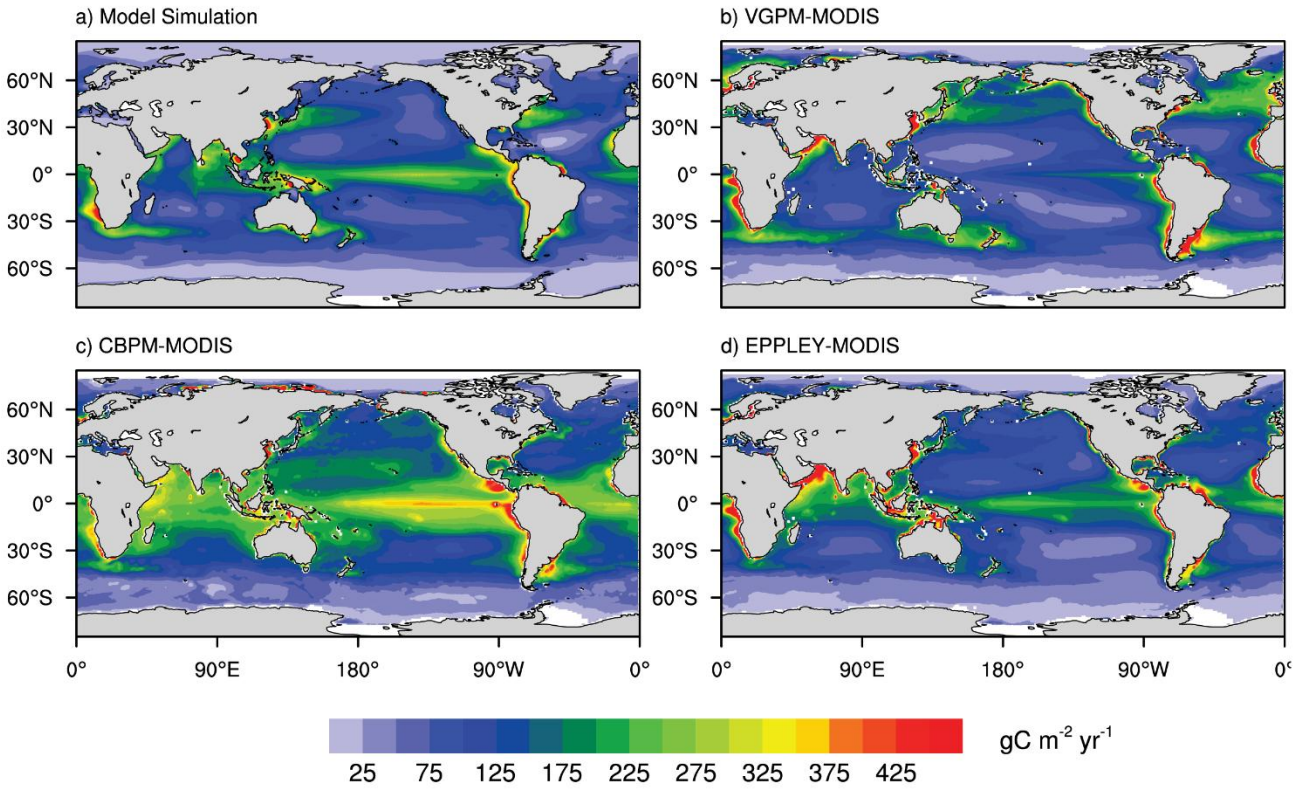
a) Model Simulation
b) VGPM-MODIS
c) CBPM-MODIS
d) EPPLEY-MODIS
60°N
30°N
0°
30°S
60°S
0°
90°E
180°
90°W
25
75
125
175
225
275
325
375
425
gC m-2 yr-1

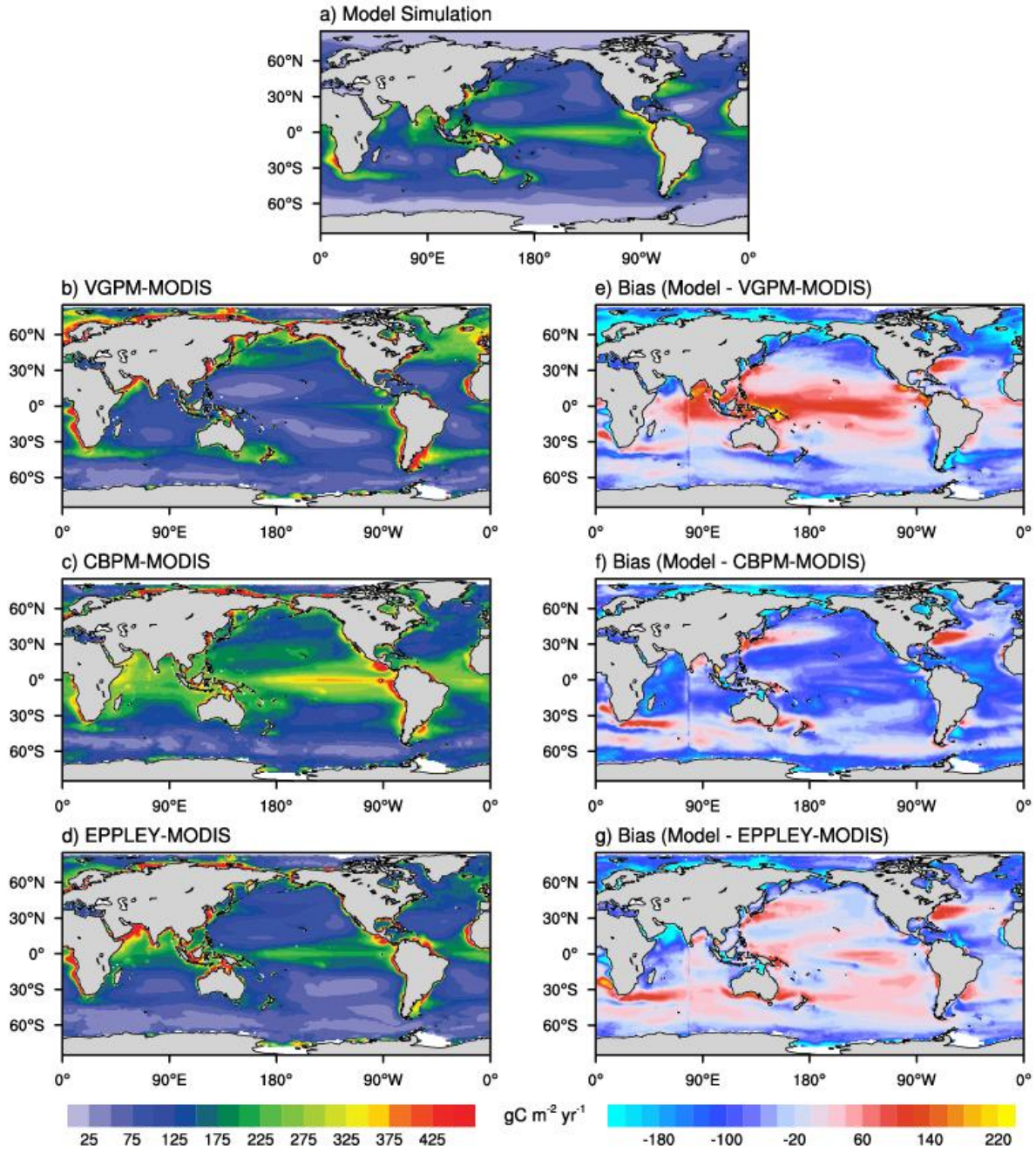

Figure 6. Annual mean distribution of vertically integrated net primary production (g C m^{-2} yr^{-1}) averaged from 2003 to 2014 from the NESM v3 FC simulations (a) and MODIS observation-based estimates (b: VGPM~~; c: Epply-VGPM; d: CbPM~~-MODIS; c: CBPM-MODIS; d: Eppley-MODIS). The bias of model simulations and observations are shown in the right three panels (e, f, g).

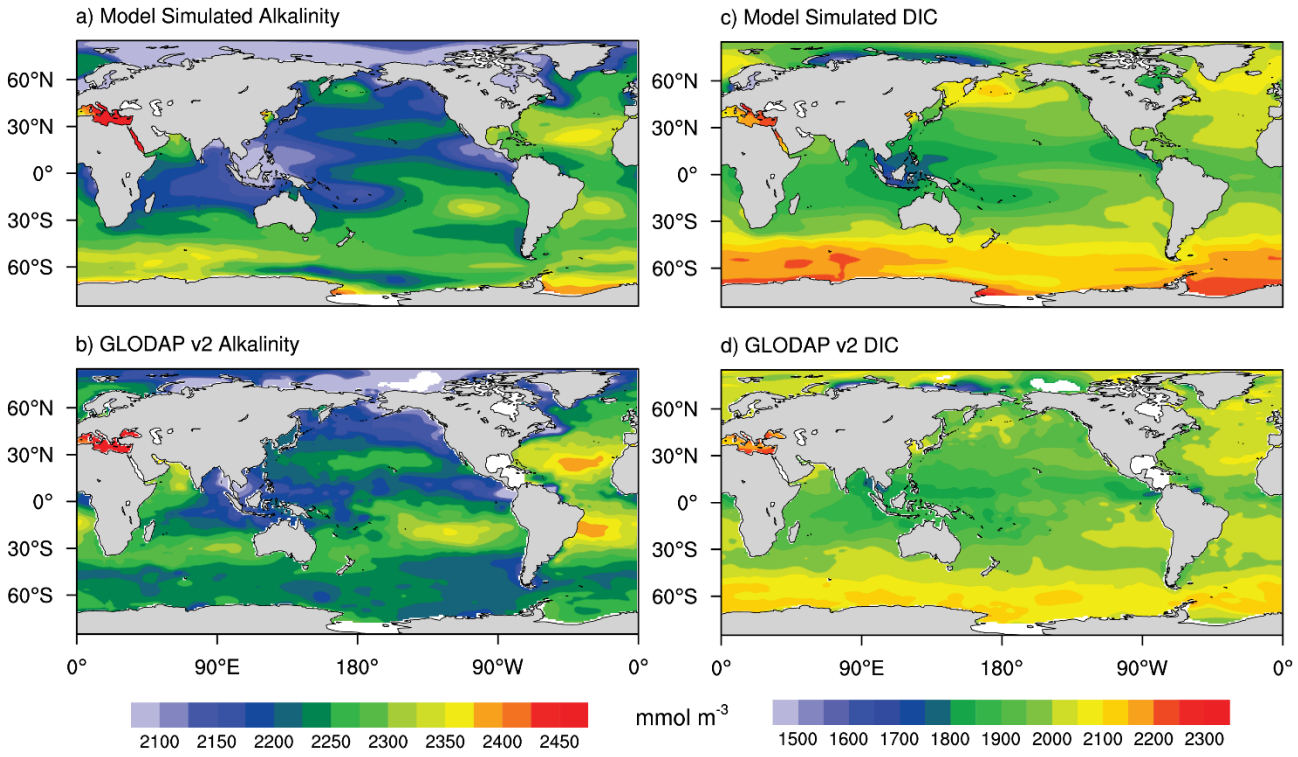
a) Model Simulated Alkalinity
c) Model Simulated DIC
b) GLODAP v2 Alkalinity
d) GLODAP v2 DIC
60°N
30°N
0°
30°S
60°S
0°
90°E
180°
90°W
0°
2100 2150 2200 2250 2300 2350 2400 2450
mmol m-3
1500 1600 1700 1800 1900 2000 2100 2200 2300

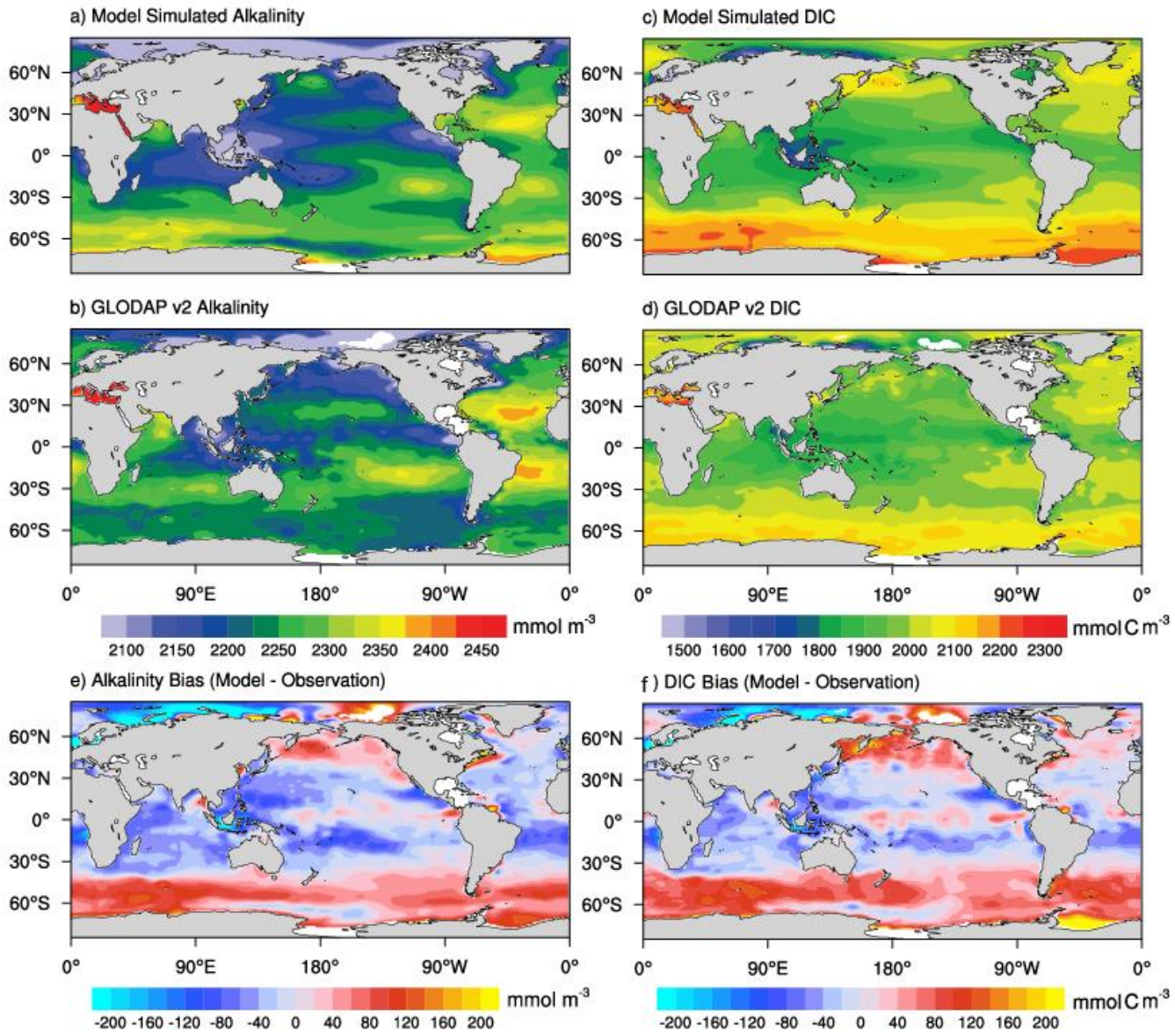

Figure 7. Annual mean distributions of upper ocean mean (0-~~100m~~100 m) alkalinity (mmol m^{-3}) (a, b) and DIC (~~mol~~mmol C m^{-3}) (c, d) averaged ~~from1985~~from 1985 to 2014 from the NESM v3 ~~EC~~ simulations (a, c) and GLODAP v2 (b, d). The bias of the NESM v3 simulations and observations are shown in the last two panels (e, f).

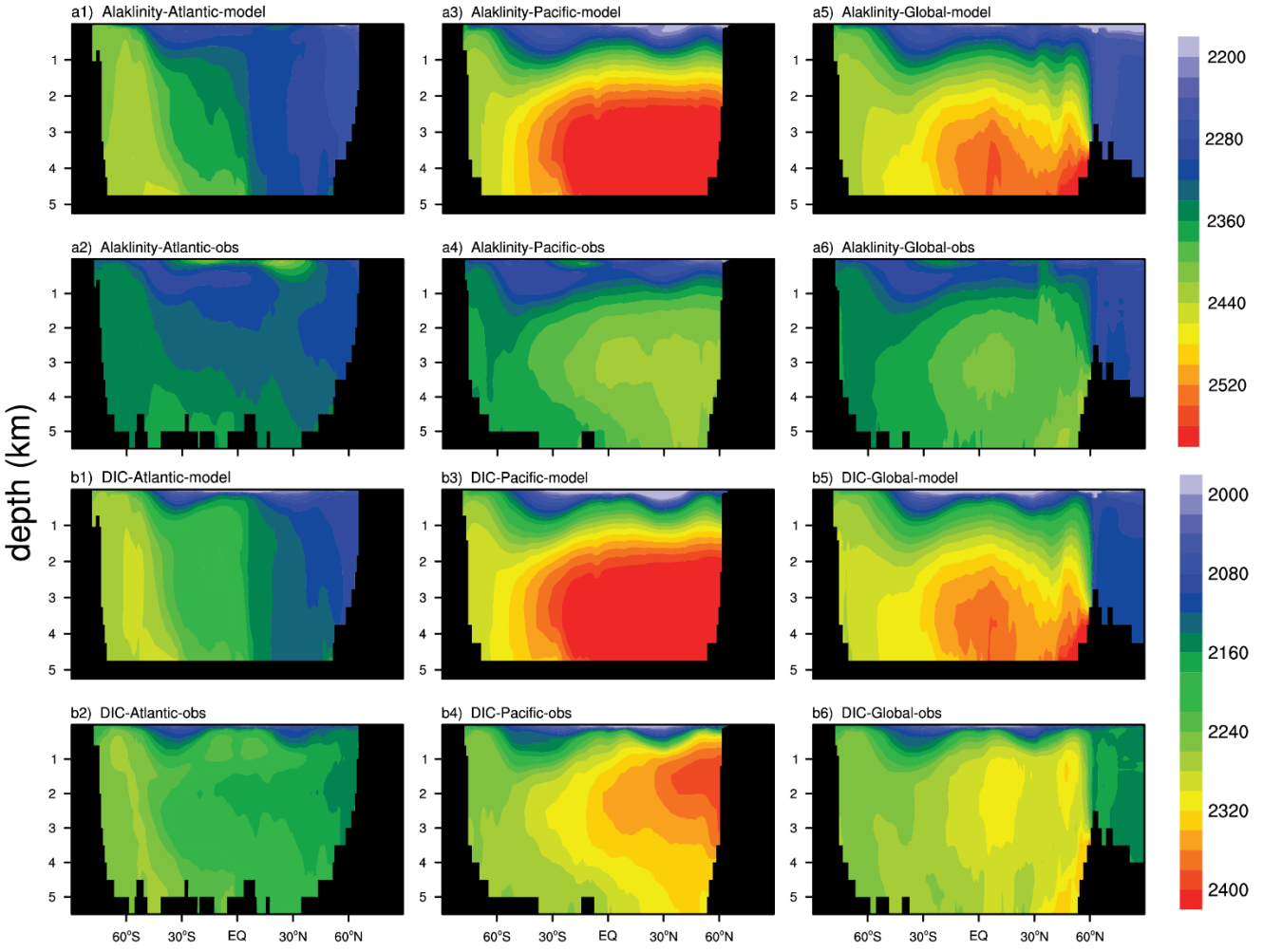
a1) Alaklinity-Atlantic-model
a3) Alaklinity-Pacific-model
a5) Alaklinity-Global-model
a2) Alaklinity-Atlantic-obs
a4) Alaklinity-Pacific-obs
a6) Alaklinity-Global-obs
b1) DIC-Atlantic-model
b3) DIC-Pacific-model
b5) DIC-Global-model
b2) DIC-Atlantic-obs
b4) DIC-Pacific-obs
b6) DIC-Global-obs
depth (km)
1
2
3
4
5
60°S
30°S
EQ
30°N
60°N
2200
2280
2360
2440
2520
2000
2080
2160
2240
2320
2400

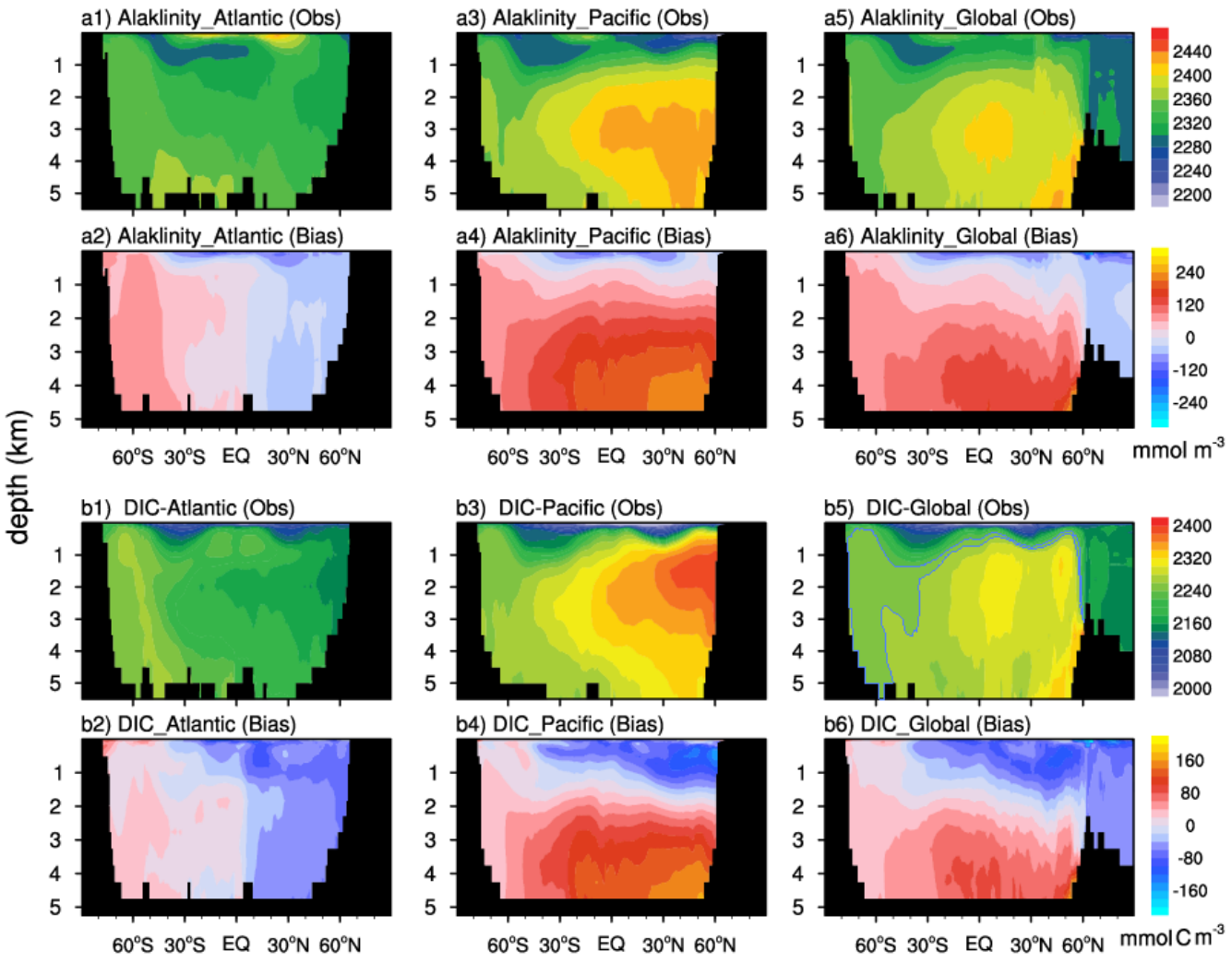

Figure 8. The latitude-depth distributions of the alkalinity (a, in the unit of mmol m^{-3}) and DIC (b, in the unit of mmol C m^{-3}) averaged from 1985 to 2014 (from the FC) run are compared with GLODAP v2 observations (with a unit of mmol m^{-3};. The observations are shown in the first and the third rows (a1, a2, b1, and b2: over the Atlantic Ocean; a3, a5, b1, b3, b5), whereas the bias (model minus observation) are shown in the second and the last rows (a2, a4, b3, and b4: over the Pacific Ocean; a5, a6, b5b2, b4, and b6: over the global).

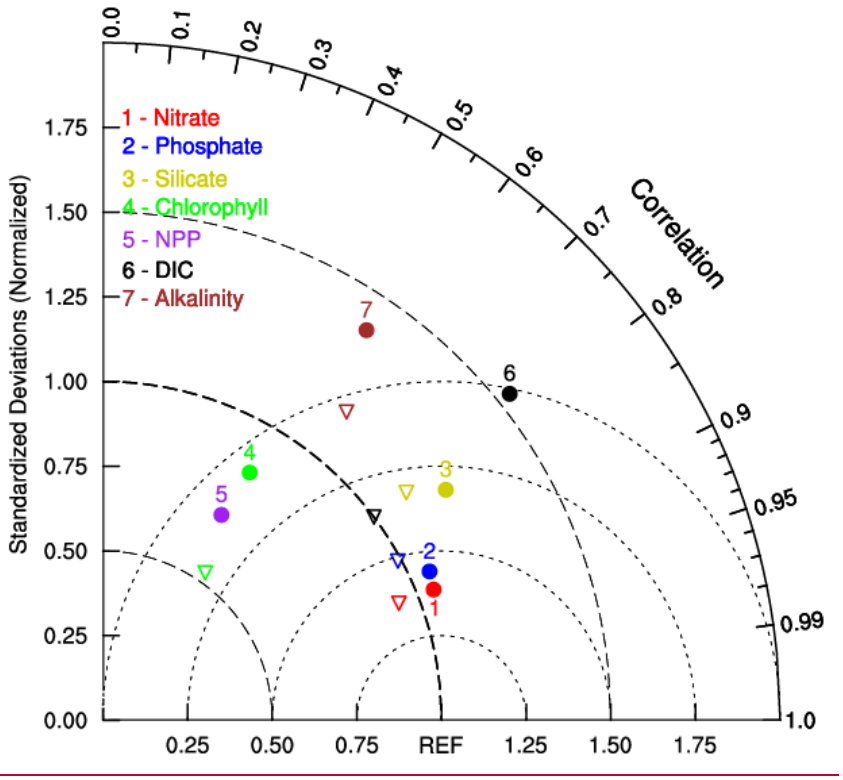

Figure 9. Taylor diagram comparing statistical patterns of annual mean biogeochemical fields between the NESM v3 simulation (FC) and corresponding observations, including upper 100-m ocean nitrate, phosphate, silicate, alkalinity, chlorophyll concentration, and vertically-integrated net primary production. Nutrient concentrations are compared with WOA 18, DIC and alkalinity concentration are compared with GLODAP v2, NPP is compared with the CbPM, and chlorophyll is compared with SeaWiFS. All fields are normalized by the standard deviation of corresponding observations. Thus, observation fields have a standard deviation of one, which is represented by REF. ~~).~~ The distance between the model points and the reference point indicates the root-mean-square (RMS) difference between model simulation and observations. The solid cycle represents the results diagnosed from the NESM v3, and the triangle represents the results from the IPSL. The NPP of IPSL is not shown here.

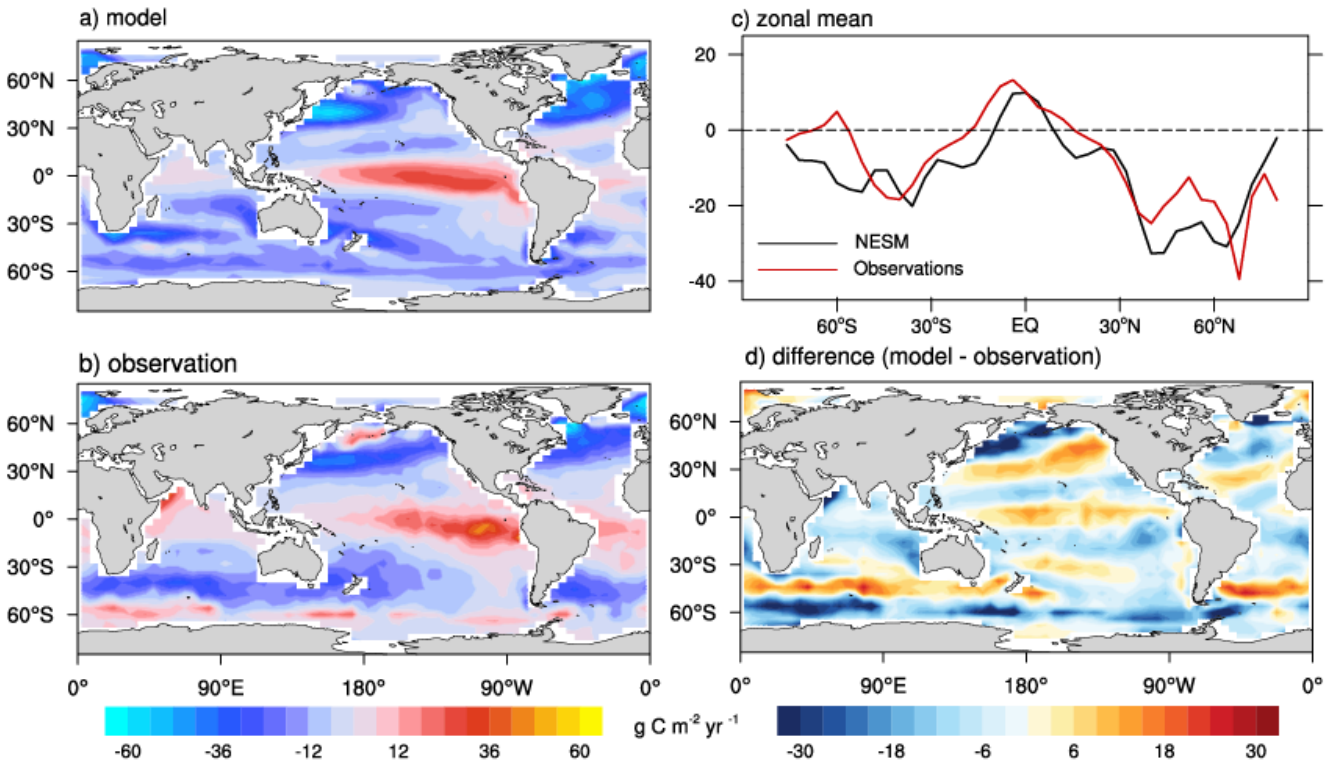
a) model
60°N
30°N
0°
30°S
60°S
c) zonal mean
20
0
-20
-40
NESM
Observations
60°S
30°S
EQ
30°N
60°N
b) observation
d) difference (model - observation)
0°
90°E
180°
90°W
-60
-36
-12
12
36
60
g C m-2 yr-1
-30
-18
-6
6
18
30

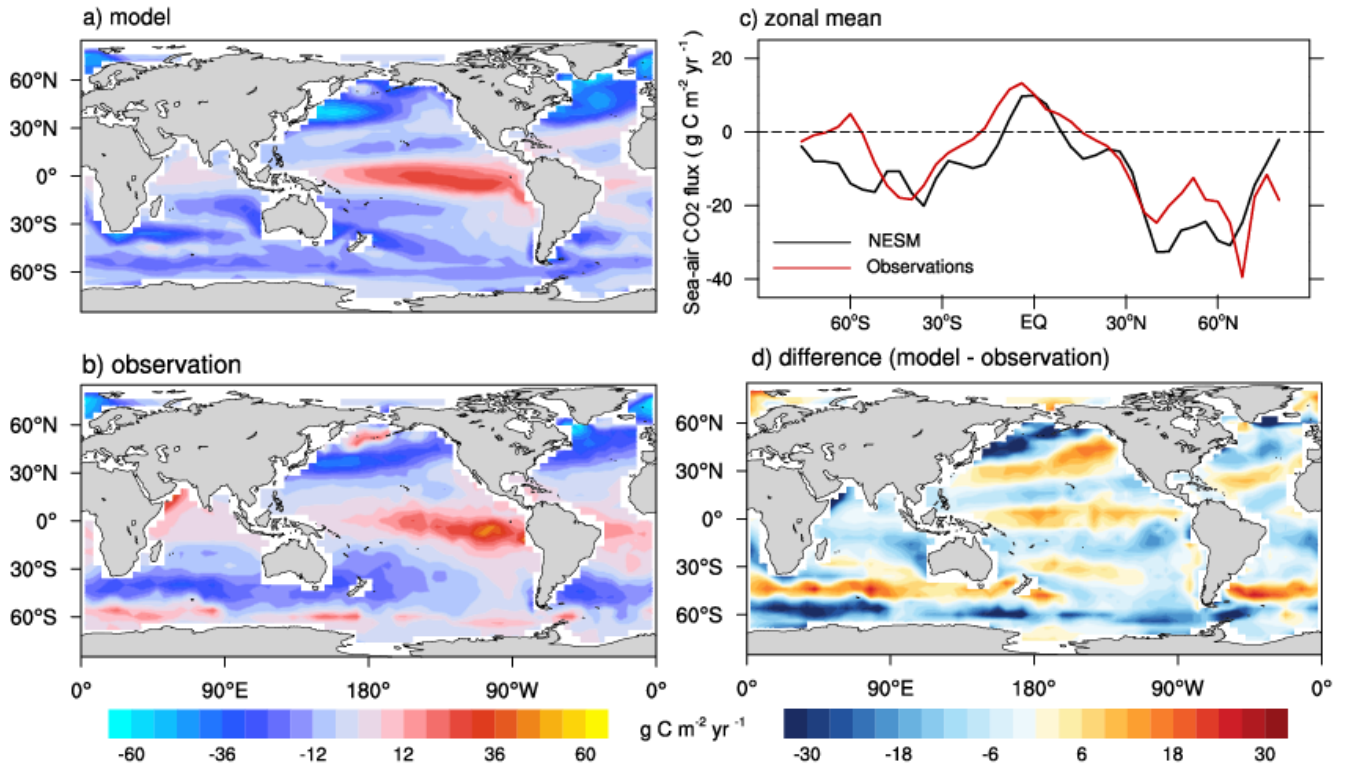

Figure 9~~10~~. Model-simulated sea-air CO_2 flux (g C m^{-2} yr^{-1}) in the year 2000 compared with data-based observational estimates (Takahashi.et al., 2009). Spatial distributions of model simulation (a), observation (b), the difference between model and observation (d), and zonal mean pattern of model simulation and observation (c). Positive values represent CO_2 flux out of the ocean, and negative values represent CO_2 flux into the ocean.

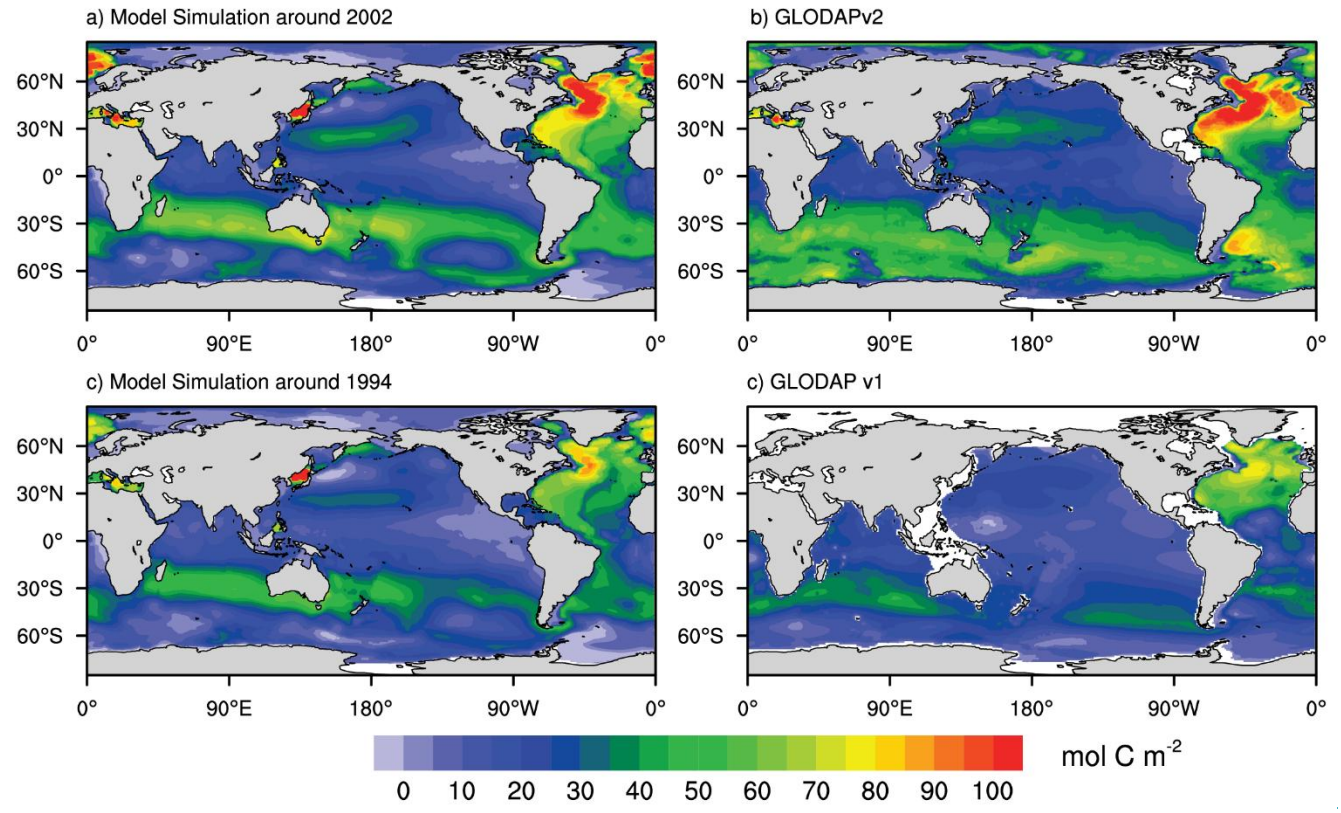
a) Model Simulation around 2002
b) GLODAPv2
c) Model Simulation around 1994
c) GLODAP v1
60°N
30°N
0°
30°S
60°S
0°
90°E
180°
90°W
0°
0
10
20
30
40
50
60
70
80
90
100
mol C m-2

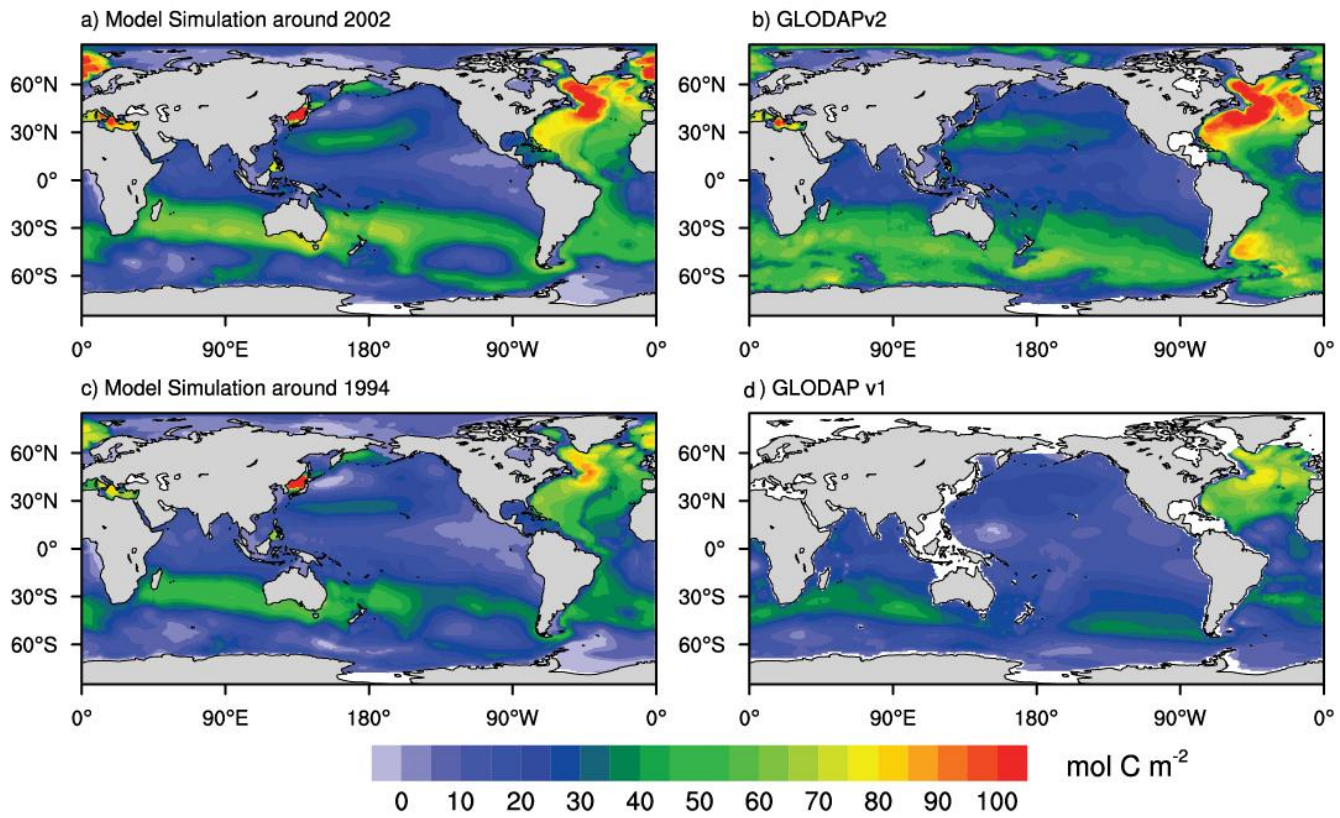
a) Model Simulation around 2002
b) GLODAPv2
c) Model Simulation around 1994
d) GLODAP v1
60°N
30°N
0°
30°S
60°S
0°
90°E
180°
90°W
0°
0
10
20
30
40
50
60
70
80
90
100
mol C m-2

Figure ~~10~~11. Vertically integrated column inventory of anthropogenic DIC (mol C m^{-2}) from the ~~FC~~ simulation (a, c) and GLODAP v1 and GLODAP v2 observation (b, d). Model simulation results are averaged from 2000 to 2004 (a) and from 1992 to 1996 (c), while the observation is normalized to the year ~~of~~ 2002 (b) and 1994 (d).

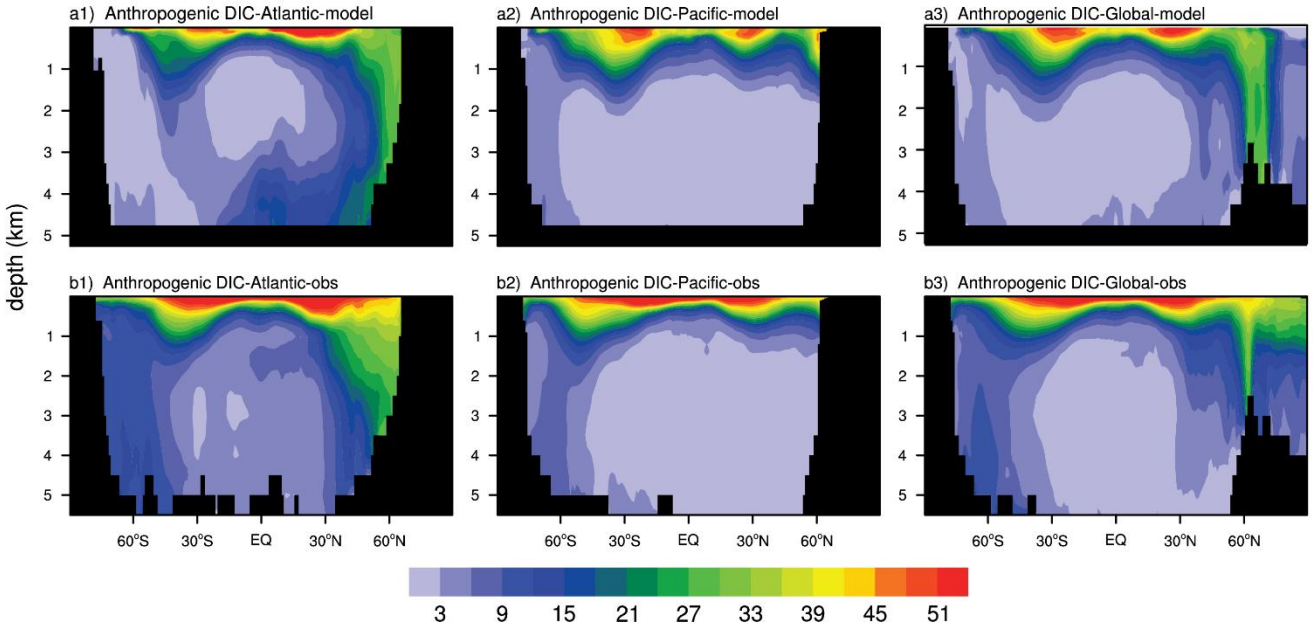

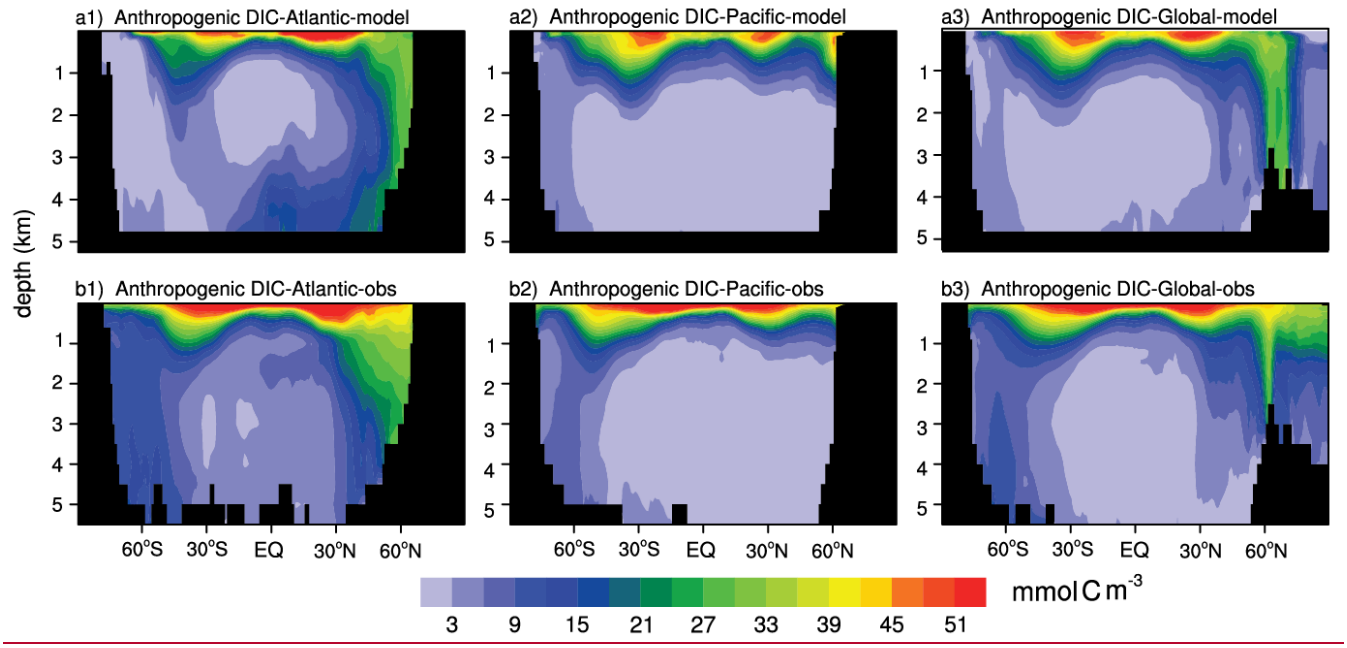

Figure ~~11~~12. Zonal mean latitude-depth distribution of anthropogenic DIC (mmol C m^{-3}) ~~distribution~~ from the ~~FC~~model simulation (a1: Atlantic, a2: Pacific, and a3: Global) and data-based estimates (GLODAP v2) (b1: Atlantic, b2: Pacific, and b3: Global).

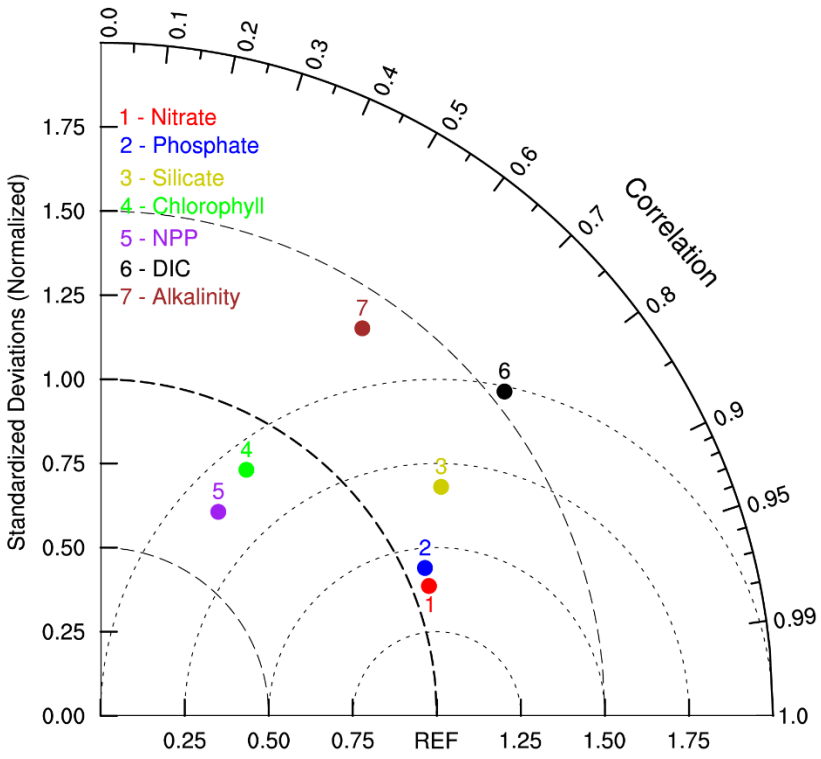

Figure 12. Taylor diagram comparing statistical patterns of annual mean carbon-related fields between the NESM v3Model simulation (FC) and corresponding observations, including upper ocean nitrate, phosphate, silicate, alkalinity, chlorophyll concentration, and vertically-integrated net primary production. NPPresults are averaged from 2000 to 2004 (a), while the observation is compared withnormalized to the CbPM, and chlorophyll is compared with SeaWiFS. All fields are normalized by the standard deviation of corresponding observations. Thus, observation fields have a standard deviation of one, which is represented by REF. The distance between the model points and the reference point indicate the root-mean-square (RMS) difference between model simulation and observations.year 2002 (b).

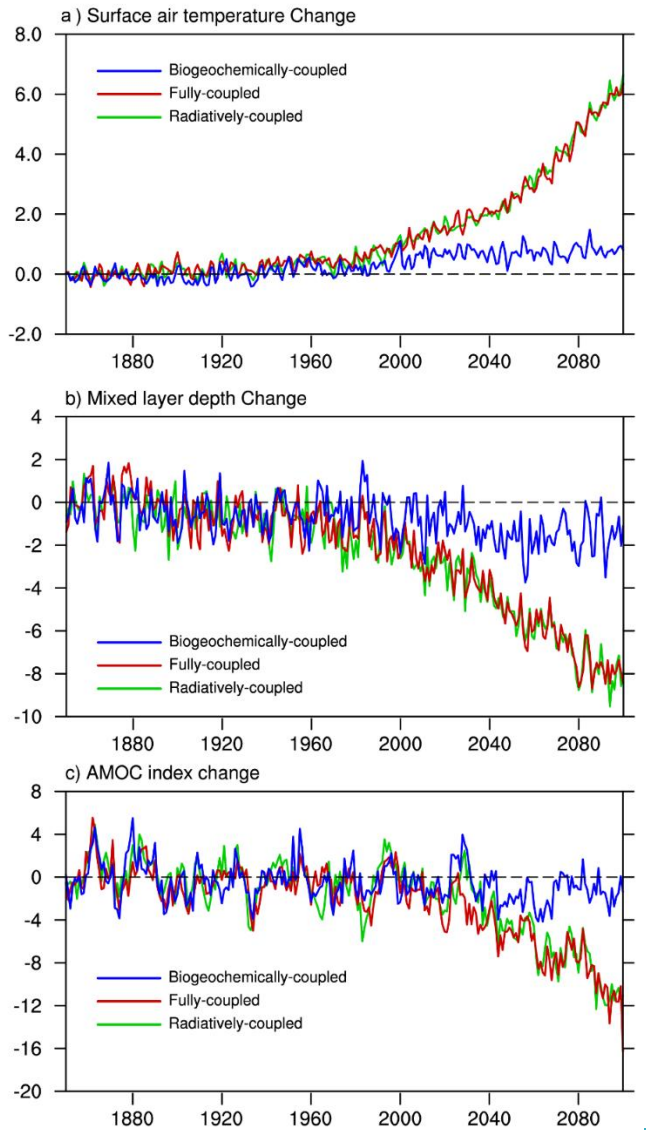
a) Surface air temperature Change
8.0
6.0
4.0
2.0
0.0
-2.0
Biogeochemically-coupled
Fully-coupled
Radiatively-coupled
1880
1920
1960
2000
2040
2080
b) Mixed layer depth Change
4
2
0
-2
-4
-6
-8
-10
Biogeochemically-coupled
Fully-coupled
Radiatively-coupled
1880
1920
1960
2000
2040
2080
c) AMOC index change
8
4
0
-4
-8
-12
-16
-20
Biogeochemically-coupled
Fully-coupled
Radiatively-coupled
1880
1920
1960
2000
2040
2080

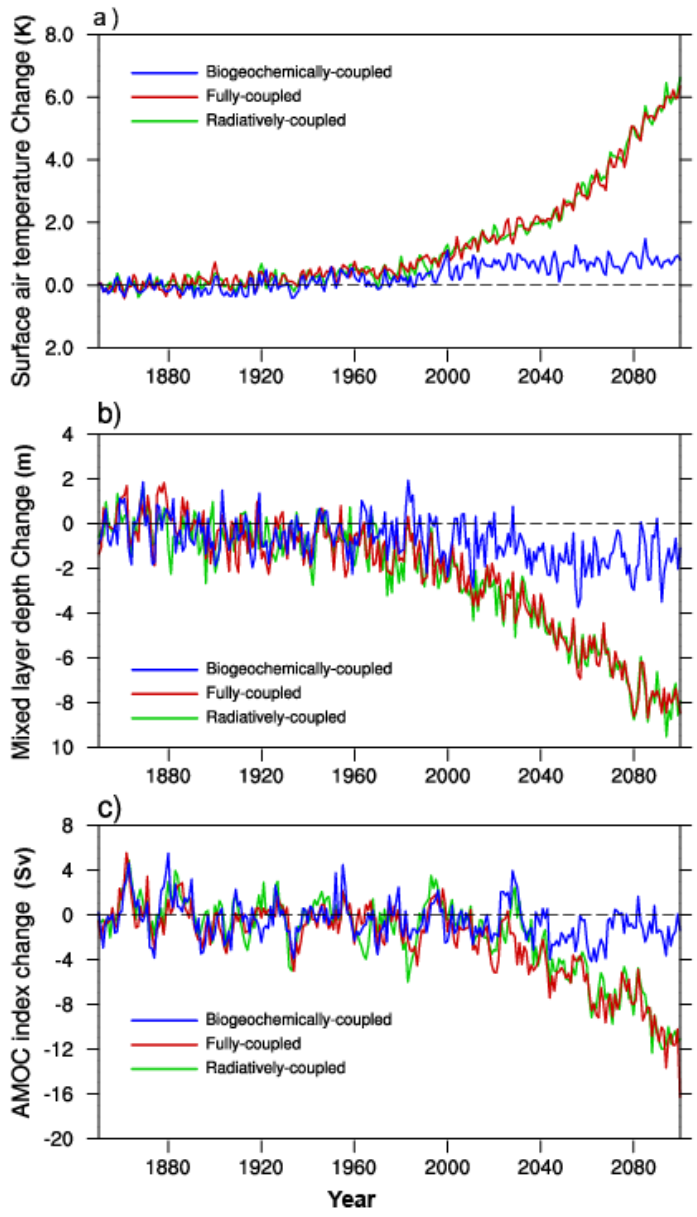

Figure 13. Time series of climate changes (~~minus~~relative to control simulation) from 1850 to 2100 for the simulation of fully-coupled, biogeochemically-coupled, and radiatively-coupled simulations. (a) global and annual mean surface air temperature~~,~~ (in the unit of K), (b) global and annual mean mixed layer depth (in the unit of meter, the depth where the difference in potential density is 0.01 kg m^{-3} relative to the sea surface) and (c) Atlantic meridional overturning circulation index (in the unit of Sv, maximum zonal mean stream function in the Atlantic Ocean at 30 ℃N).

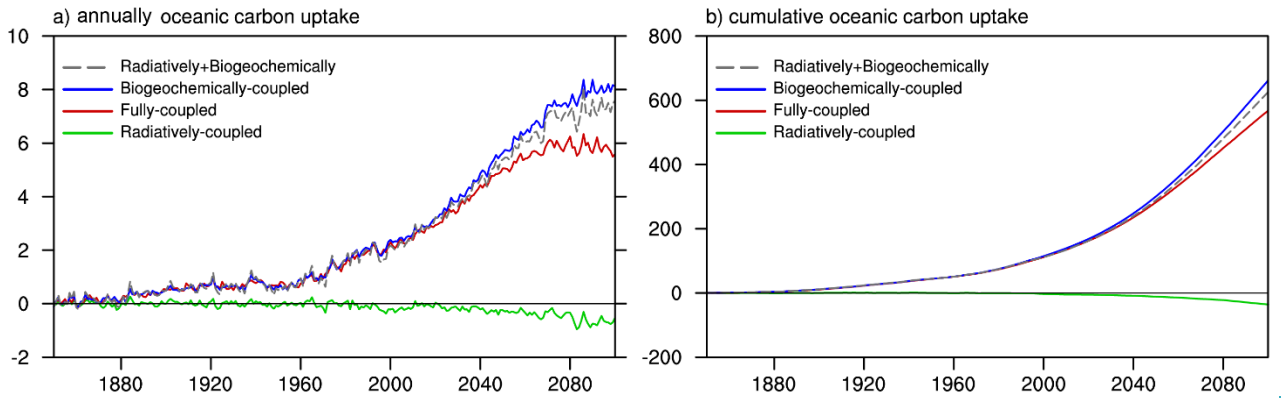

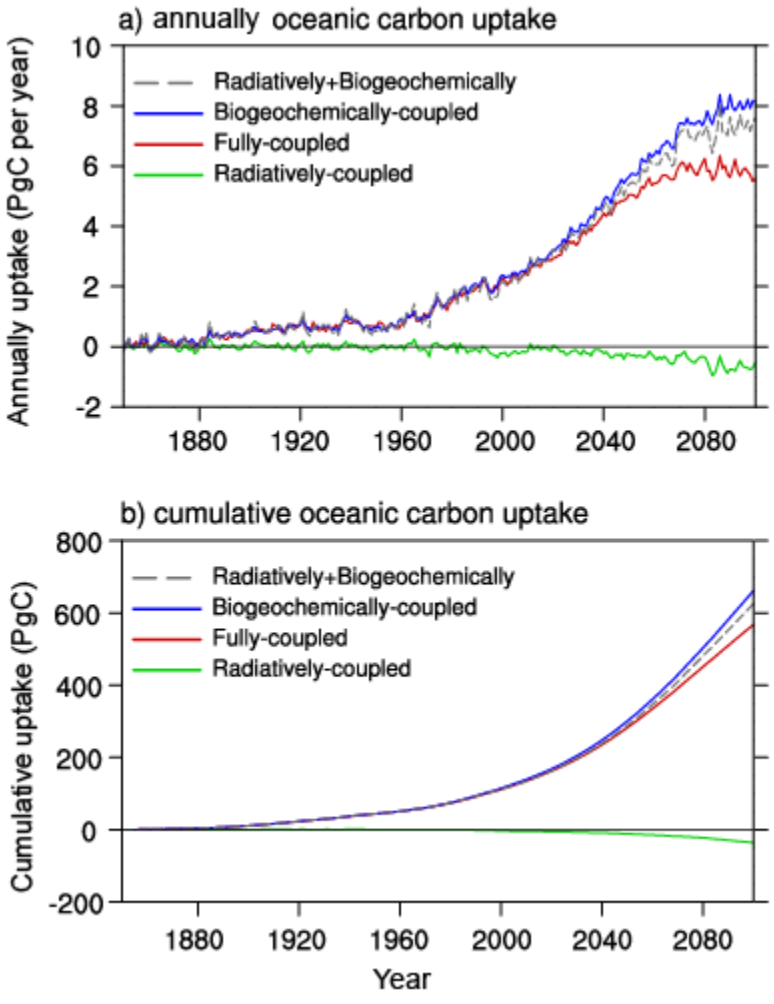

Figure 14. The NESM v3 simulated (a, in the unit of PgC yr^{-1}) annually anthropogenic oceanic CO_2 uptake change ~~(minus control simulation)~~ and (b, in the unit of PgC) cumulative oceanic CO_2 uptake for the simulations RC, BC, FC, and the linear sum of BC and RC from 1850 to 2100 ~~(in unit of Pg C).~~ .

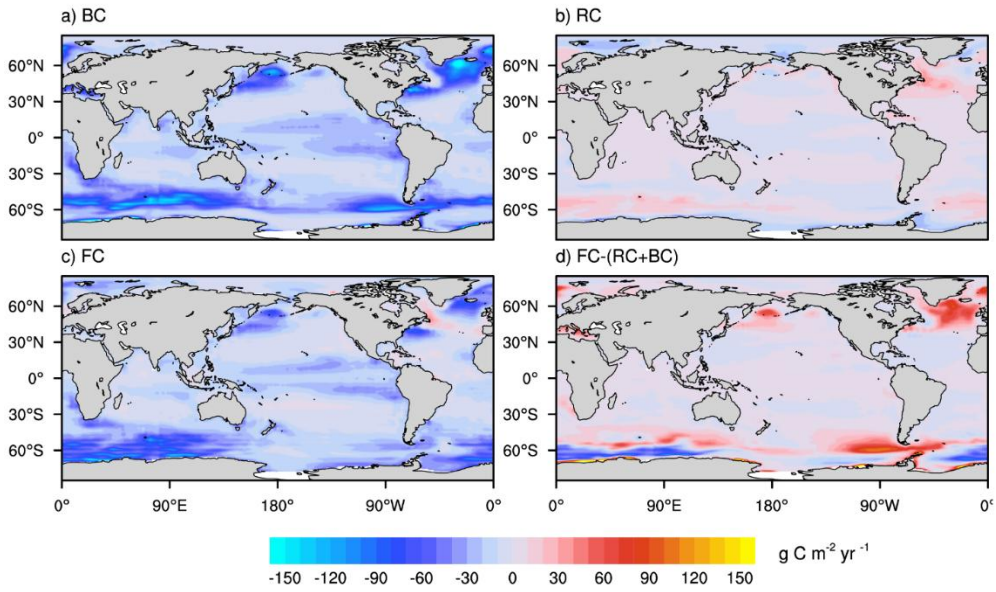
a) BC
b) RC
c) FC
d) FC-(RC+BC)
60°N
30°N
0°
30°S
60°S
0°
90°E
180°
90°W
-150 -120 -90 -60 -30 0 30 60 90 120 150
g C m-2 yr-1

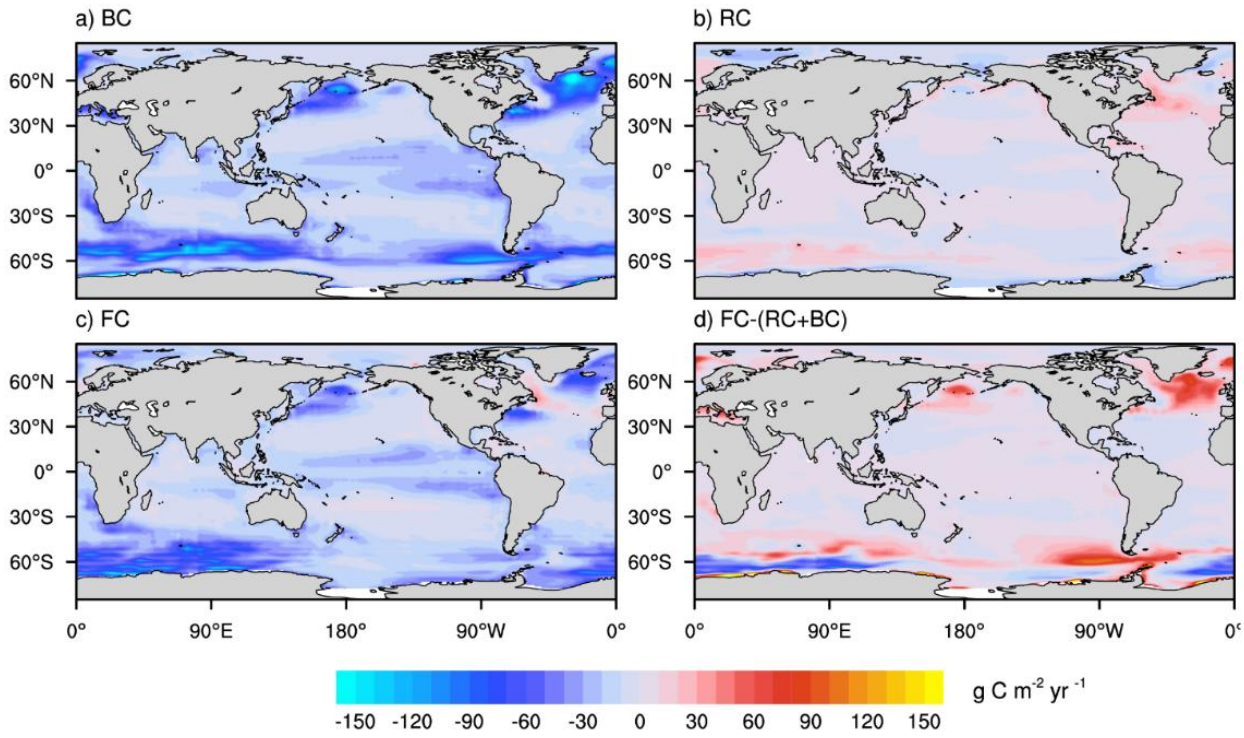

Figure 15. Spatial distribution of anthropogenic sea-air CO_2 flux (in the unit of g C m^{-2} yr^{-1}) at the end of the 21st century (mean of 2091-2100 ~~minus control simulation~~) from the (a) BC, (b) RC, and (c) FC, respectively. Also shown is the difference between FC simulation and the sum of RC and BC simulations (FC-RC-BC). Positive values represent CO_2 flux out of the ocean, and negative values represent CO_2 flux into the ocean.

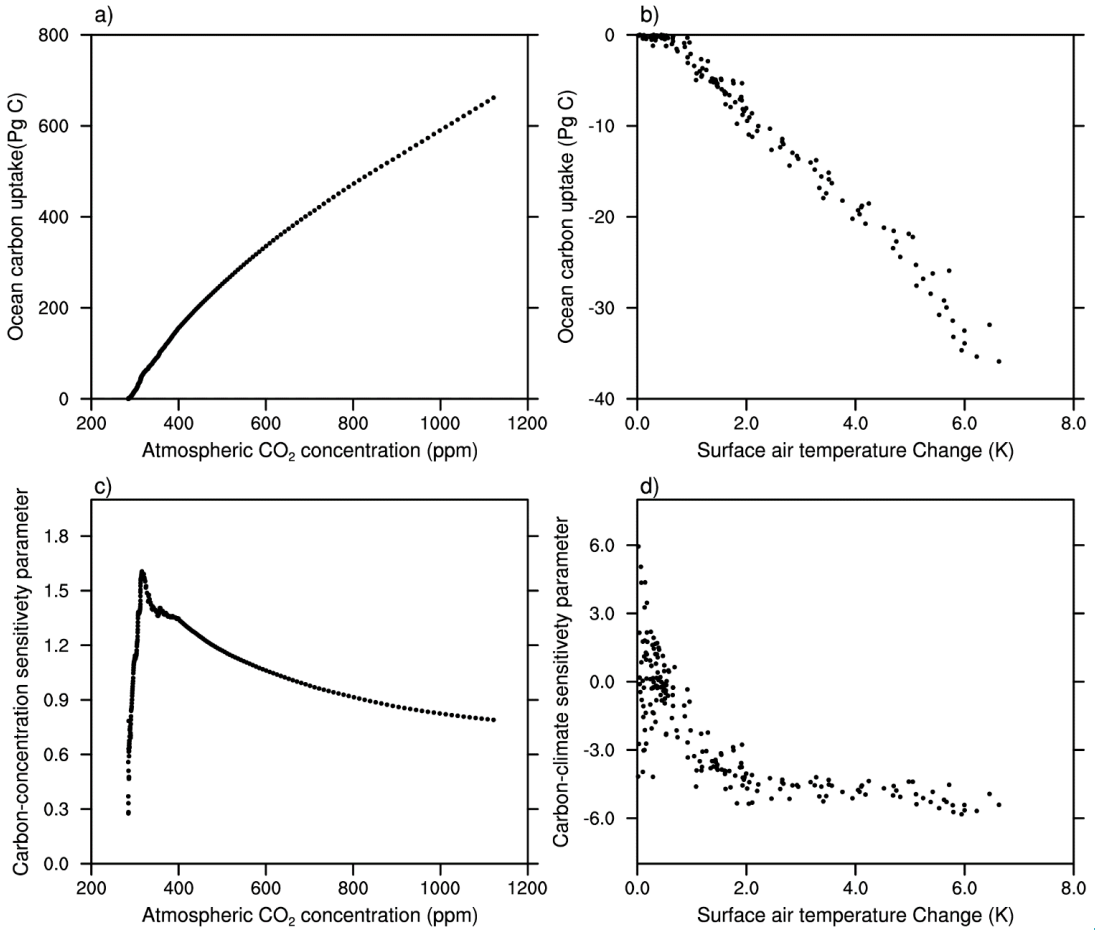
a)
Ocean carbon uptake(Pg C)
800
600
400
200
0
200
400
600
800
1000
1200
Atmospheric CO_2 concentration (ppm)
b)
Ocean carbon uptake (Pg C)
0
-10
-20
-30
-40
0.0
2.0
4.0
6.0
8.0
Surface air temperature Change (K)
c)
Carbon-concentration sensitivety parameter
1.8
1.5
1.2
0.9
0.6
0.3
0.0
200
400
600
800
1000
1200
Atmospheric CO_2 concentration (ppm)
d)
Carbon-climate sensitivety parameter
6.0
3.0
0.0
-3.0
-6.0
0.0
2.0
4.0
6.0
8.0
Surface air temperature Change (K)

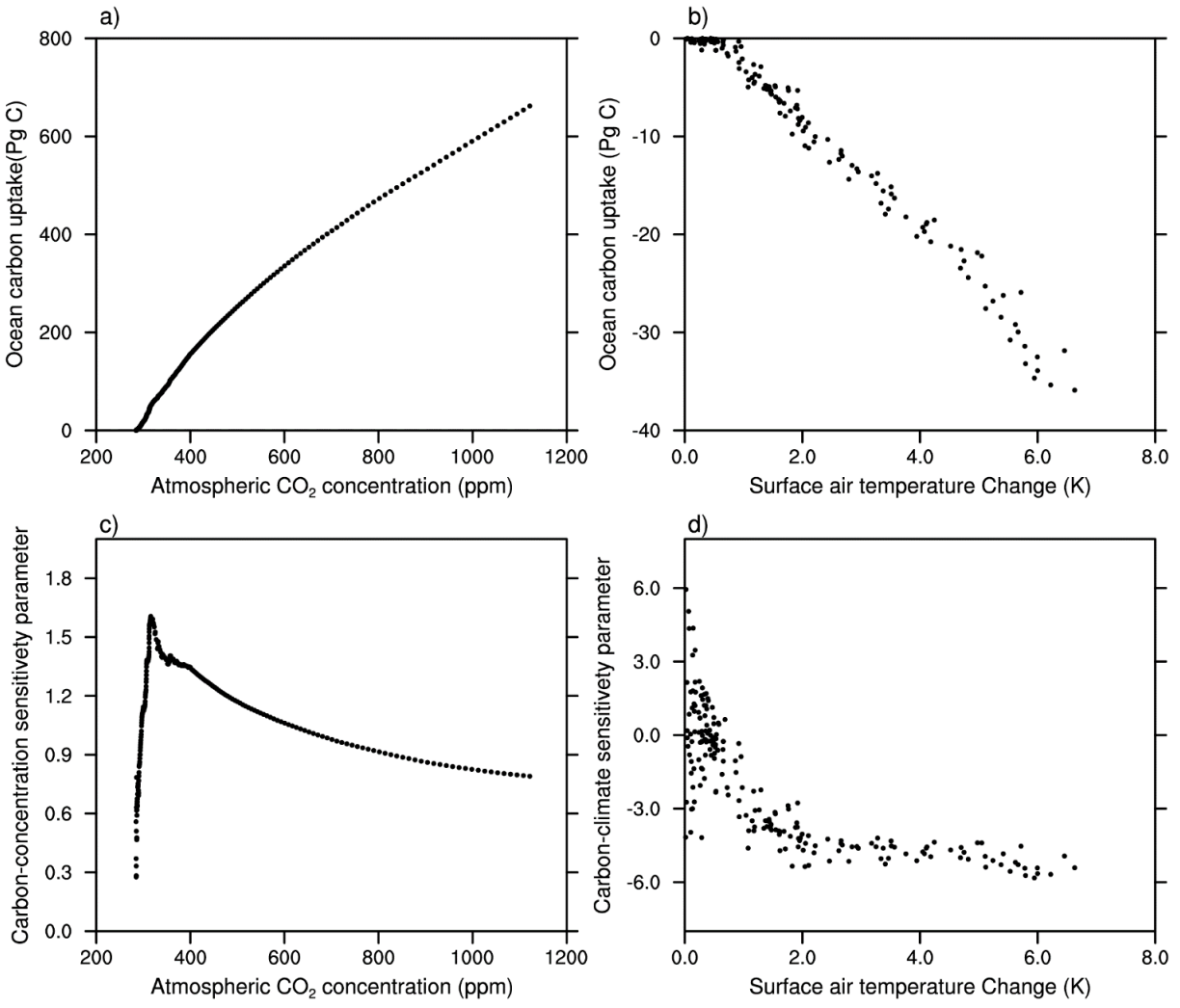

Figure 16. The ~~cumulated~~cumulative oceanic CO_2 uptake against (a) the atmospheric CO_2 in the BC simulation and (b) the global mean surface air temperature change in the RC simulation. Also shown is the time evolution of diagnosed (c) carbon-concentration sensitivity parameter as a function of atmospheric CO_2 ~~(c)~~ and (d) carbon-climate sensitivity parameter as a function of global mean surface air temperature change ~~(d).~~.

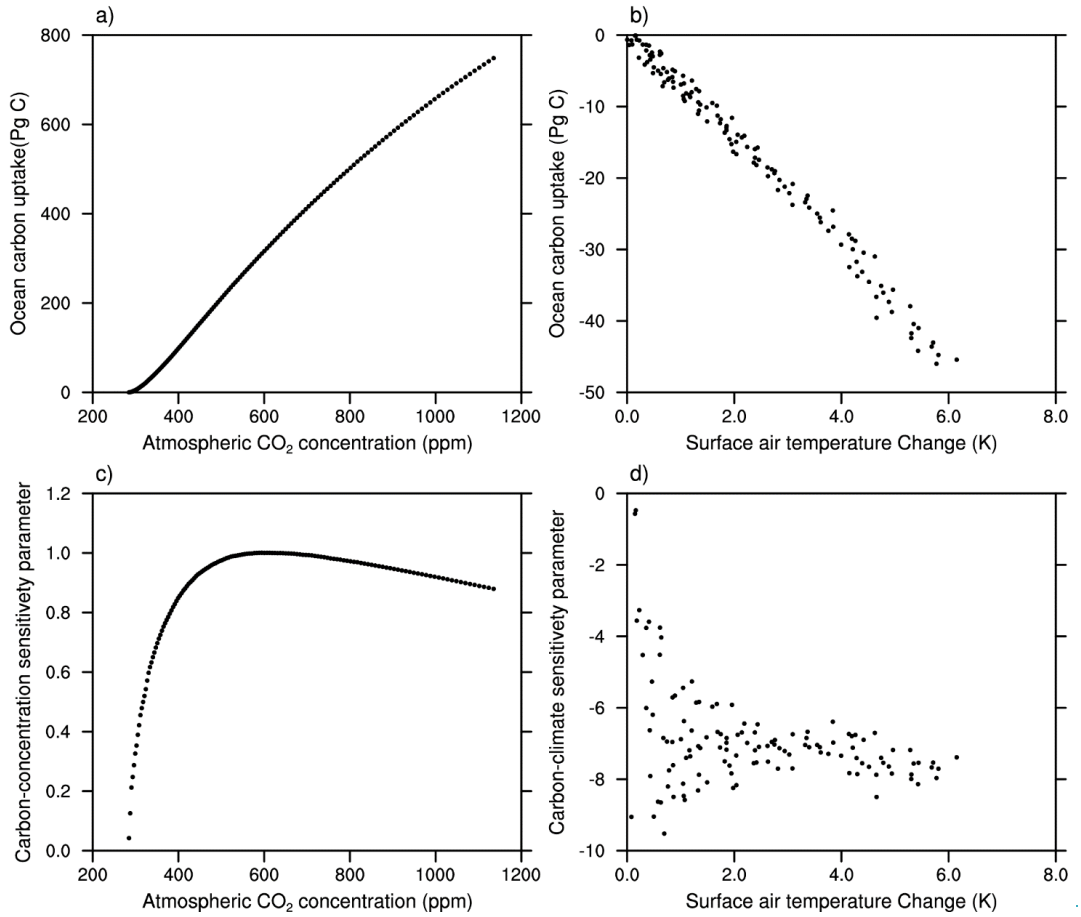
a)
b)
c)
d)
Ocean carbon uptake(Pg C)
Ocean carbon uptake (Pg C)
Carbon-concentration sensitivity parameter
Carbon-climate sensitivity parameter
Atmospheric CO2 concentration (ppm)
Surface air temperature Change (K)
0
200
400
600
800
1000
1200
-10
-20
-30
-40
-50
2.0
4.0
6.0
8.0
0.0
0.2
0.4
0.6
0.8
1.0
1.2
-2
-4
-6
-8

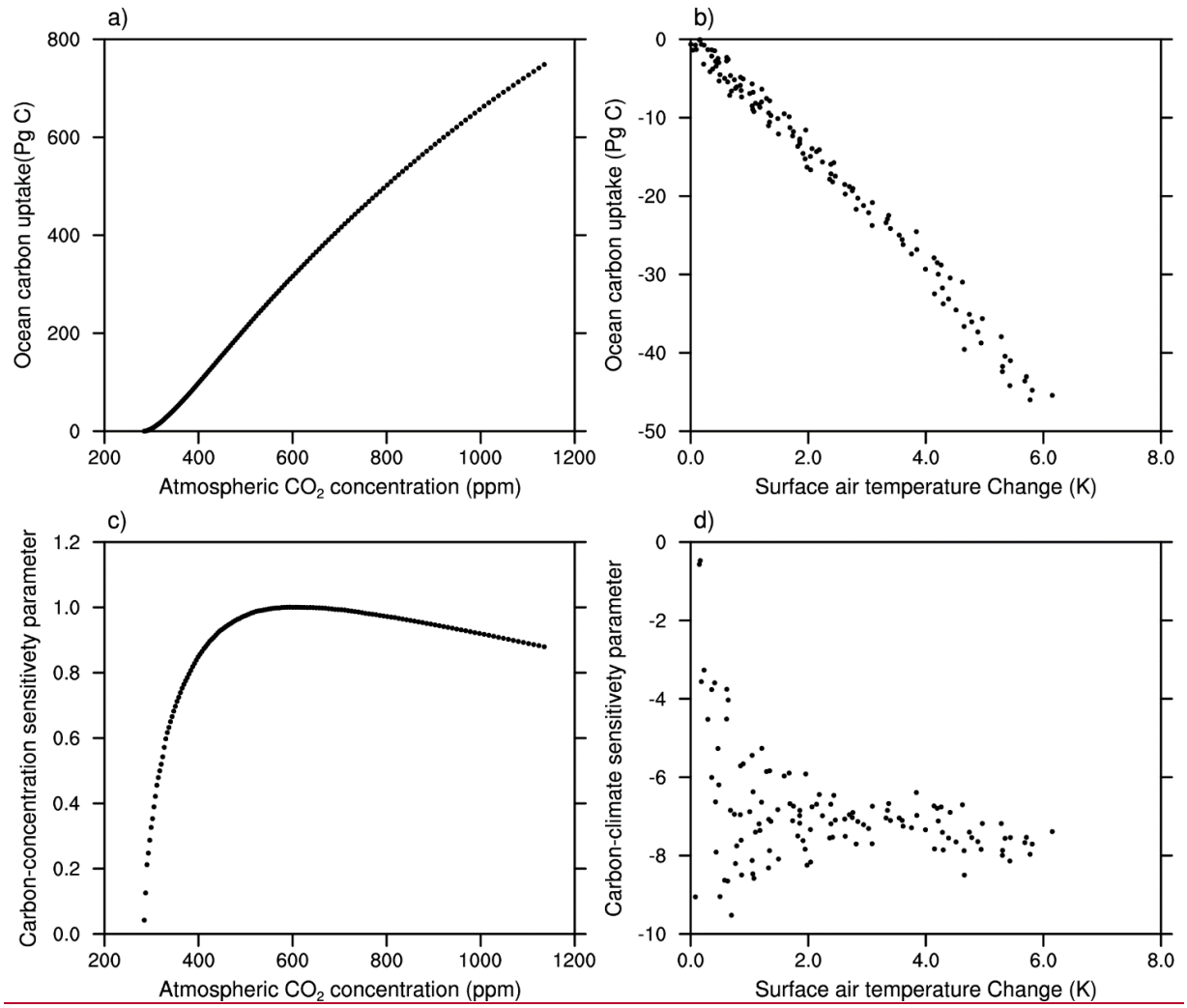

Figure 17. Same as Figure 16, but for the ~~1pt CO2~~1ptCO_2 runs.